

Mathematical Modelling of Oxygen and Glucose Conditions for Mesenchymal Stem
Cells in Culture and Bone Marrow

Kimberley Paige Green

Doctor of Engineering

School of Engineering

March 2021

Abstract

The prevalence of 3D tissue culture systems is increasing in order to overcome the perceived limitations of 2D culture in terms of providing a biomimetic niche for cells. However, the move to 3D systems requires that the availability of nutrients and oxygen within a 3D system is understood. The aim of this project was to develop mathematical models which would allow conditions in 2D and 3D culture and *in vivo* to be better understood. A mass transfer model was developed using physical data from experiments, the conservation of mass and Fick's law of diffusion, using the 2D and 3D culture of mesenchymal stromal cells as an exemplar system.

The model was then used to create oxygen and glucose profiles in 2D and 3D (spheroids and suspension) culture to provide a basis for comparison between the different systems. Predicted mass transfer of oxygen was found not to be affected by spheroid culture when compared to 2D culture, however mass transfer of glucose was restricted creating significant glucose concentration gradients through the spheroids. The predicted profiles in spheroid culture were applied to other culture systems with the aim of inducing the changes observed in the mesenchymal stromal cells in spheroid culture. Altered glucose concentrations were not sufficient to induce dedifferentiation in 2D adherent mesenchymal stromal cells nor result in the same cell size decrease as seen in 3D spheroid culture. Using suspension cultures, a comparable size decrease to 3D spheroid culture was observed. Mass transfer modelling of the *in vivo* mesenchymal stromal cells environment in bone marrow was also developed to compare the *in vitro* culture conditions to the natural environment.

It is concluded that oxygen concentrations within cell culture are lower than in bone marrow but relatively stable in the culture systems modelled. Glucose concentrations are significantly reduced within spheroid culture.

Acknowledgments

I would like to thank my supervisors Kenny Dalgarno (Newcastle University) and Paul Genever (University of York) for all their guidance and support throughout this project. Paul and his lab in the University of York's biology department have taught me cellular biology and cell culture techniques, with particular thanks going to Rebecca Pennock, Amanda Barnes and James Fox. I would also like to thank the staff within the technology facility at University of York for their assistance using equipment based in the department.

Additionally, I would like to thank my family and friends for the support and encouragement I really could not have done it without them. My husband Mark has been there through all the ups and downs and a constant source of encouragement. My children Thea and Francis have given me a smiles on even the hardest days and always a cuddle and my daughter Seren who although no longer with us has given me strength to continue my studies and will always be my shining star.

Contents

Abstract.....	i
Acknowledgments.....	ii
List of figures	vi
Nomenclature	vii
Chapter 1 Introduction	1
Chapter 2 Literature Survey.....	3
2.1 Introduction	3
2.2 Osteoarthritis.....	3
2.3 Mesenchymal Stem Cells.....	6
2.3.1 Definition.....	7
2.3.2 Function.....	9
2.3.3 Role as a treatment	9
2.3.4 Metabolism and control of cell function.....	11
2.4 Oxygen and Glucose Levels <i>In vitro</i> and <i>In vivo</i>	11
2.5 Previous work on modelling cell culture conditions	14
2.6 Summary.....	16
Chapter 3 Cell Culture Methods.....	18
3.1 Basic cell culture	18
3.2 Spheroid culture	19
3.3 Size measurement	19
3.4 Transmission Electron Microscopy (TEM).....	19
3.5 Colony forming unit assay (CFU-F).....	19
3.6 MTT (3-[4,5-dimethylthiazol-2-yl]-2,5 diphenyl tetrazolium bromide) assay	20
3.7 Osteogenic differentiation.....	20
3.7.1 <i>Alkaline Phosphatase Assay</i>	20
3.8 Adipogenic differentiation	21
3.8.1 <i>Oil red O staining of liquid droplets</i>	21
3.9 Disaggregation of spheroids.....	21
Chapter 4 Monolayer Adherent Culture Studies	22
4.1 Introduction	22
4.2 Monolayer Adherent Culture Model Development.....	22
4.2.1 <i>Oxygen</i>	22
4.2.2 <i>Glucose</i>	26
4.3 Monolayer Adherent Culture Model Predictions	26
4.3.1 <i>Input Data</i>	26

4.3.2 <i>Model Predictions</i>	27
4.4 Qualitative Validation against Existing Literature	31
4.5 Discussion	33
Chapter 5 Cell Spheroid Studies and Bone Tissue Models.....	34
5.1 Introduction	34
5.2 Extension of 2D Model to Cell Spheroids.....	35
5.2.1 <i>Oxygen</i>	35
5.2.2 <i>Glucose</i>	36
5.3 Cell Spheroid Model Input Data	36
5.4 Spheroid Model Predictions	44
5.5 Experimental Glucose Concentration Studies in 2D and Suspension Cultures.....	63
5.6 Qualitative Evaluation of Model Predictions from Experimental Studies.....	77
5.7 Extension of Model to Idealised Bone Tissue Geometry.....	78
5.8 Idealised Bone Tissue Model Input Data	89
5.9 Idealised Bone Tissue Model Predictions	91
5.10 Recreation of Bone Marrow Conditions	94
5.11 Discussion	100
Chapter 6 Discussion	104
6.1 Novelty and Validity of the Model.....	104
6.2 Implications of Results	107
References	111

List of figures

Figure 2-1 - MSC differentiation showing the differentiation of osteoblasts, chondrocytes and adipocytes	8
Figure 2-2 – Outline of macro autophagy.....	14
Figure 4-1 – Schematic of oxygen mass transfer during monolayer culture.	22
Figure 4-2 – Predicted oxygen concentration in media.....	28
Figure 4-3 – Predicted glucose concentrations in 2D culture calculated from a mass balance at 5mM and 25mM.	30
Figure 5-1 – Schematic of spheroid mass transfer	35
Figure 5-2 – Size change analysis of spheroids during 3D culture.	38
Figure 5-3 – Voidage and diffusion coefficient changes for Y201, HDF, K139 and Y202 spheroids throughout culture.	41
Figure 5-4 – Oxygen and glucose consumption rates measured in primary MSCs. .	43
Figure 5-5 – Predicted oxygen concentrations in the centre of MSC spheroids.....	45
Figure 5-6 – Predicted oxygen concentrations throughout the MSC spheroid.	47
Figure 5-7 – Predicted oxygen concentrations in the centre of Y201, Y202 and HDF spheroids.	48
Figure 5-8 – Predicted oxygen concentrations throughout the Y202 spheroid.....	50
Figure 5-9 – Predicted glucose concentrations in media for MSCs.	52
Figure 5-10 – Predicted glucose concentration in MSC spheroids calculated using mass transfer equations derived using Fick’s law.	54
Figure 5-11 – Predicted glucose concentrations throughout the MSC spheroid with a 2/3 media change on days 3 and 6.	56
Figure 5-12 – Predicted glucose concentrations throughout the MSC spheroid with no media change during the culture.....	57
Figure 5-13 – Glucose concentrations throughout Y201, Y202 and HDF spheroids with a 2/3 media change on day 3.	59
Figure 5-14 – Predicted glucose concentrations in Y201, Y202 and HDF spheroids.	62
Figure 5-15 – Effect of glucose and FBS concentrations on the growth of Y201 and Y201.5 cells.	64
Figure 5-16 – Effect of glucose concentrations on the colony forming ability of primary MSCs.....	65
Figure 5-17 – Optimisation of glucose and FBS for osteogenic differentiation of Y201s.....	67
Figure 5-18 – Optimisation of glucose and FBS for osteogenic differentiation of Y201 with a narrowed down glucose range.	68
Figure 5-19 – Optimisation of glucose and FBS using smaller range of glucose and FBS concentrations for osteogenic differentiation of Y201.5s.....	69
Figure 5-20 – Optimisation of glucose and FBS for adipogenic differentiation of Y201s.....	71
Figure 5-21 – Optimisation of seeding density, glucose and FBS in suspension cultures with Y201s, osteogenic differentiation post suspension culture in Y201s and size change analysis following suspension cultures of primary MSCs.....	74
Figure 5-22 – Osteogenic differentiation of Y201s and Y202s after pre - treatment in spheroid culture.	76
Figure 5-23 – Stained bone marrow section.	78
Figure 5-24 – Idealised 2D bone marrow schematic.....	79

Figure 5-25 – Schematic of diffusion between two vessels	80
Figure 5-26 – Schematic of arteriole and sinusoid model.....	83
Figure 5-27 – Schematic of diffusion between two arterioles and two sinusoids	85
Figure 5-28 – Schematic of diffusion from two arterioles and one sinusoid.....	87
Figure 5-29 – Model of bone marrow for oxygen transport.....	92
Figure 5-30 – Model of bone marrow for glucose transport.....	93
Figure 5-31 – 24-hour viability analysis of Y201s exposed to perfluoro-octane.....	95
Figure 5-32 – 72-hour viability analysis of Y201s exposed to perfluoro-octane.....	96
Figure 5-33 – 7-day viability analysis of Y201s exposed to perfluoro-octane.....	97
Figure 5-34 – Metabolic activity and osteogenic differentiation in Y201s with various concentrations of perfluoro-octane with PBS controls.....	99

List of tables

Table 0-1 – Nomenclature used with models.	vii
Table 2.1 – Comparison of oxygen concentrations in the body.....	12
Table 4-1 – Input data for monolayer adherent culture models	26
Table 4-2 – Concentration of Oxygen in media	27
Table 4-3 – Validation of 2D model against other modelled systems.....	32
Table 5-1 – Oxygen consumption rates for cells within bone marrow	90

Nomenclature

Table 0-1 – Nomenclature used with models.

Parameter	Units	Description
A_s	m^2	Spheroid surface area
C_A	mol/m^3	Concentration of O_2 in vessel A
C_{A1}	mol/m^3	Concentration in arteriole 1
C_{A2}	mol/m^3	Concentration in arteriole 2
C_{air}	mol/m^3	Concentration of O_2 in air
C_B	mol/m^3	Concentration of O_2 in vessel B
C_{cells}	mol/m^3	Concentration of O_2 at cell layer
C_{media}	mol/m^3	Concentration of O_2 in media
C_{O_2}	mol/m^3	Concentration of O_2 in liquid phase
C_s	mol/m^3	Concentration of O_2 at centre of spheroid
C_{s1}	mol/m^3	Concentration in sinusoid 1
C_{s2}	mol/m^3	Concentration in sinusoid 2
CSA	m^2	Cross sectional area of well
C_x	mol/m^3	Concentration of O_2 at point x
d	m	Depth of media
D_c	m^2/s	Diffusion coefficient for O_2 through cell membranes

D_G	m^2/s	Diffusion coefficient for glucose through water
D_m	m^2/s	Diffusion coefficient for O_2 through media
D_s/l_s	m/s	Diffusion coefficient for O_2 through the surface layer divided by the thickness of the surface layer
G	mol/s	Glucose consumption rate
PO_2		Partial pressure of oxygen in air
r_s	m	Spheroid radius
S_A	m^2	Surface area of blood vessel being evaluated
S_B	m^2	Surface area of blood vessel B being evaluated
U	mol/s	Oxygen consumption rate
U_{cell}	$mol/s.cell$	Oxygen consumption rate per cell
V_{cell}	m^3	Volume of a cell
x	m	Distance from vessel A
x_A	m	x co-ordinate of arteriole
x_a	m	Distance from arteriole
x_{A1}	m	x co-ordinate of arteriole 1
x_{a1}	m	Distance from arteriole 1
x_{A2}	m	x co-ordinate of arteriole 2
x_{a2}	m	Distance from arteriole 2
x_p	m	x co-ordinate of point being evaluated
x_t	m	Distance between vessel A and vessel B
y_A	m	y co-ordinate of arteriole
y_{A1}	m	y co-ordinate of arteriole 1
y_{A2}	m	y co-ordinate of arteriole 2
y_p	m	y co-ordinate of point being evaluated

Chapter 1 Introduction

The study of human cell behaviour using *in vitro* culture systems allows for research into the function and activity of these cells and also for the exploitation of these cells to provide treatment for diseases and injury. However, it is readily recognised that these culture methods incorporate a number of compromises when compared to *in vivo* conditions, which is known to have implications for the resulting cell phenotype. One of the big issues is the lack of transport system for the delivery of nutrients and removal of waste products, this becomes a bigger problem as these systems are scaled up and where 3D cultures are performed. Fundamental to these processes is mass transfer which is the mechanism of moving substances from one place to another. Within *in vitro* culture the mechanism of transfer is diffusion, the governing principle of this is that molecules move from areas of high concentration to areas of low concentration.

The use of 3D tissue culture systems to either grow tissues or in a step towards biomimicking the *in vivo* environment introduces more limitations to mass transfer than traditional 2D culture systems. Therefore, in both cases it is important to understand the way the availability of oxygen and nutrients are affected by the structure of the 3D culture system in use. In studies aiming to achieve biomimicry it is also important to understand the mass transfer profiles in the *in vivo* environment in order to understand the differences and to replicate these conditions. The predominant method of mass transfer within 3D cell culture is diffusion, within the *in vivo* environment there are additional mechanisms such as blood vessels to aid the distribution of oxygen and nutrients. It is generally considered that diffusion is a sufficient mass transfer mechanism within small 3D cell culture systems however without assessment of the mass transfer profiles this cannot be guaranteed.

Enhancing the understanding of how different culture systems affect the availability of oxygen and glucose at a cellular level is important in establishing new culture techniques for growing tissues. The process of tissue engineering using stem or progenitor cells to create new functional tissue is complicated with respect to providing the right cues for differentiation into the correct type of tissue. These cues which influence cell behaviour include chemical and mechanical stimuli and the use of 3D culture systems affects the availability of chemical stimuli and changes the mechanical stimuli the cells experience; therefore, these culture environments have

the potential to change the way stem cells differentiate into new tissue. Additionally, the process of growing tissue relies upon the balance of progenitor cells expanding and differentiating, both of these processes are affected by the metabolic activity of the cell which in turn is dependent on the nutrient availability. Understanding this relationship and balance provides the ability to shape the cell activity to achieve a specific purpose.

Tissue Engineering is a promising option for the regeneration of tissue damaged by osteoarthritis and mainly comprises of using stem cells in a supporting construct to produce new tissue. The stem cells in use by the Versus Arthritis Tissue Engineering and Regenerative Therapies Centre are mesenchymal stromal cells (MSCs) these cells which can be isolated from bone marrow and are capable of undergoing osteogenic, adipogenic and chondrogenic differentiation. There is potential for these cells to be isolated from the patient then implanted with a scaffold to generate new tissue. However, MSCs from patients with osteoarthritis tend not to differentiate or proliferate as well as cells from younger healthy people (Murphy, et al., 2002). Research within the centre has developed a technique which encourages the cells to de-differentiate into an earlier mesenchymal state which is then capable of proliferating and differentiating with greater efficiency (Pennock, et al., 2015).

This process has been found to occur through autophagy, which may be caused by nutrient deprivation in the 3D culture system. Autophagy is a cell survival mechanism which aims to preserve the cell in adverse conditions, changes within the cell allow for oxygen and glucose to be used more efficiently. In order to recreate the conditions on a scaffold the system needs to be modelled to find the nutrient concentration profile which can then be recreated on a scaffold or *in vivo* to encourage new tissue formation.

The main aim of this project is to identify the conditions of spheroid culture which induce the changes observed. This is done by creating oxygen and glucose profiles throughout the spheroids using modelling techniques developed from fundamental mass transfer principles. Once these conditions were identified they were recreated in other culture systems such as 2D and suspension culture.

Chapter 2 Literature Survey

2.1 Introduction

This chapter covers the background of this project and includes, osteoarthritis, stem cells, oxygen and glucose levels *in vitro* and *in vivo* and previous work on modelling in cell culture.

This project was conducted within the Tissue Engineering and Regenerative Therapies Centre Versus Arthritis as part of ongoing work to develop new treatments and understanding of how mesenchymal stromal cells can be affected by osteoarthritis and their potential for use in tissue engineering applications. The properties of stem cells are discussed and in particular the routes of differentiation for mesenchymal stromal cells into skeletal tissue are described. Previous work within the centre has identified a 3D culture system which induces autophagy to drive a restructuring of the MSCs, the main aim for this project was to identify the specific cause(s) of this process and so the mechanisms of autophagy are discussed.

The focus of this research was on the oxygen and glucose levels within the 3D culture system and how these levels compared to the concentrations *in vivo* and in other culture systems, current knowledge of oxygen and glucose levels *in vivo* and culture are included in this chapter.

Mathematical modelling was used to predict the oxygen and glucose concentrations in the different culture systems and *in vivo*, previous work present in the literature utilising mathematical modelling techniques is evaluated.

2.2 Osteoarthritis

Osteoarthritis is caused by the deterioration of cartilage in joints, which can eventually cause deformation of the surrounding bone and affects 4% of the over 45s in the UK (Edwards, et al., 2015) causing pain, discomfort and mobility issues. The development of osteoarthritis is not widely understood and can be triggered by a variety of factors including age, gender, weight, injury and genetics. There is currently little treatment available for the progression of osteoarthritis, current treatment methods revolve around pain relief and anti-inflammatory methods, once the pain becomes unmanageable the other option is joint replacement. Between 1st April 2003 and 31st December 2017, 2,526,601 joint replacement procedures took

place in the UK which includes 992,090 hip replacement and 1,087,611 knee replacements (National Joint Registry, 2018).

Osteoarthritis can affect any joint in the body but mainly occurs in the knees, hips, hands, feet and spine. Worldwide it is estimated that 9.6% of men and 18% of women over 60 have symptomatic osteoarthritis, the total number of people affected is only likely to rise as lifespans are increasing. The current treatments commonly available do not prevent the progression of the disease (Woolf & Pfleger, 2003).

The standard treatment for osteoarthritis in the early stages is to give pain killers and non-steroidal anti-inflammatory medication along with encouraging weight loss and appropriate exercise. The use of pain killers may relieve symptoms but they do not treat the osteoarthritis, there have also been concerns about the use of some medications including naproxen which has been shown to affect cell-mediated repair of subchondral repair in osteoarthritis patients (Salem, et al., 2014). Once these treatments are no longer satisfactory normally the next option is to have the joint replaced.

Osteoarthritis is a major cause of joint replacements; during 2012 it was responsible for 92% of primary hip replacements, 98% of primary knee replacements, 84% of ankle replacements, 32% of elbow replacements and 61% of shoulder replacements (National Joint Registry, 2013). This shows a dependence on joint replacement for treatment for most of the joints listed, the total number of joint replacements has also been increasing. Joint replacements can provide a considerable reduction in pain and return of mobility to the joint; however, there are also problems associated with joint replacement. In 2012, 12% of all hip replacements were revision surgeries and 6.5% of all knee replacements were revision surgeries (National Joint Registry, 2013) while these percentages are not huge they are far from the ideal case and show the need for an alternative technique. A joint replacement is normally expected to last 15-20 years depending on use, weight and age (NHS, 2015 and Losina, et al., 2015), research conducted between April 2003 and December 2014 showed that the average life of a hip replacement was 11.75 years and the average person having their first hip replacement is female and 69 years old (National Joint Registry, 2015), while this may not be a problem for older patients, younger patients could face one or multiple revisions.

As osteoarthritis is not a condition that can currently be cured (even with joint replacement) the cost of the treatment is not to be neglected. These costs not only arise from medical cost but also the costs associated with everyday life. A study in Italy (Leardini, et al., 2004) explored the costs per patient per year and has given the direct costs of the disease which include medical costs such as appointments, medication and transportation to and from treatment as €934/yr. The same study found the indirect costs which include loss of earnings, care costs and informal care given by family, totalled €1236/yr. This study also stated the economic impact can be between 1 and 2.5% of countries GDP. Another study this time in Canada (Gupta, et al., 2005) has found the average annual costs to each individual with osteoarthritis were \$12,200 (Canadian dollars) where the average direct and indirect costs are \$2,300 and \$12,990 respectively. In an American study (Losina, et al., 2015) the costs were evaluated depending on the treatment regime, this found that during the first year of diagnosis which included medication and doctor visits was \$684 USD subsequent years using medication would then cost \$520 if then the patient moved on to injections as part of their treatment this would cost \$494 per year, if these failed to be effective and they were eligible for a total knee replacement during the year of treatment this would cost \$20,293 and follow up costs would be \$95 per year. If the first replacement is not satisfactory or wears out the cost of revision is \$26,388 for that year and then \$95 for the following years. As all of these studies show osteoarthritis is a costly disease and with the occurrences of the disease increasing its impact is not to be ignored, additionally costs of medical conditions which may be linked to or exasperated by osteoarthritis are not easily quantified which could increase the cost of osteoarthritis. If there was the possibility to treat the disease prior to requiring joint replacement and full functionality restored, the ongoing costs could be reduced to zero.

Other alternatives that have been researched include intra-articular injections (corticosteroid, hyaluronic acid and platelet rich plasma). Corticosteroid injections can be effective in the reduction of pain, hyaluronic acid has mixed reviews over effectiveness and is not a cost effective option, and platelet rich plasma can be effective pain relief and has shown regenerative potential. Platelet rich plasma delivers growth factors and bioactive molecules which in younger patients and mild osteoarthritis cases has shown promising results however there are no data to show that platelet rich plasma will cause osteophytes (abnormal bony growths often

associated with the disease) to regress or that cartilage and meniscus will regenerate in patients with substantial damage (Ayhan, et al., 2014).

There is the potential to use cellular treatments to repair or aid repair of joints in the early stages of osteoarthritis, various trials and studies have been or are being conducted investigating the possible methods of using implanted stem cells and/or chondrocytes as a viable treatment method. Injection of mesenchymal stem cells (MSCs) into arthritic knees has been shown to improve pain and knee function (Lopa, et al., 2019), but the extent of these improvements is however variable and more studies are required to fully evaluate the effectiveness of using unexpanded or expanded cell populations. Adipose derived stem cells have also been used as a potential treatment and studies have shown improvements, however more investigation is required (Biazzo, et al., 2020). Cartilage injuries have been treated by autologous chondrocyte implantation (ACI) with improvements for 80% of patients and long-term effects (Richardson, et al., 2017), the use of stem cells on their own or in conjunction with chondrocytes is being investigated in a large study(ASCOT trial) to determine if using MSCs gives different functional results to chondrocytes and whether the two cell types together achieve a better outcome (Richardson, et al., 2017). These studies show the use of stem cell therapies for osteoarthritis is a feasible treatment option which could reduce the need for joint replacements and treat joints which cannot be replaced.

2.3 Mesenchymal Stem Cells

Stem cells are cells that can develop into many different types of cells, these cells also divide in such a way that each new cell can differentiate into another type of cell or remain as a stem cell. These cells are present in early life and growth; they also exist in many tissues to serve as an internal repair system (Alvarez, et al., 2012). There are two main categories of stem cells, embryonic and adult (or somatic). Stem cells are also classified according to their differentiation potential. Totipotent cells are the zygote and first daughter cells which are capable of creating a whole organism, pluripotent cells from the inner cell mass of the blastocyst can form all three of the germ layers, multipotent cells are present in foetal and postnatal tissues and can differentiate into multiple cell types but are limited, unipotent cells can only produce one cell type but they can self-renew, finally there are also progenitor cells which can only produce one cell type but can only renew a limited number of times (Xian & Jevnikar, 2015).

Embryonic stem cells (ESCs) are from embryos and are fundamental to foetal development. These cells can differentiate into any type of cell. Due to these properties embryonic stem cells have great potential to be used to treat many diseases; however, there are two problems with embryonic stem cells, ethical issues and immune rejection. There are ethical issues surrounding embryonic stem cells due to their source. Using embryonic stem cells in clinical treatments could cause immune rejection as the cells would not be from the patient, they were given to (Swijnenburg, et al., 2008).

Adult stem cells are undifferentiated cells which are present in the body and carry out roles in tissue maintenance and repair. These cells can be found in many tissues including bone marrow, skin, and brain (Hipp & Atala, 2008). There is great potential for adult stem cells to be used as they have multiple advantages over ESCs, they are easily accessible for the patient, free from ethical concern, retain a reduced risk of tumour formation and they do not require immunosuppression treatments to prevent rejection (Muscarelli, et al., 2013).

Induced pluripotent stem cells (iPSCs) are somatic cells which have been exposed to four factors (Oct 4, Sox2, c-Myc and Klf4) which reverts the cells to an embryonic stem cell-like state (Takahashi, et al., 2007). This offers promising routes for cell therapy as iPSCs would avoid the ethical and immunological issues that are encountered with embryonic cells, however there are still problems with iPSCs, efficiency of reprogramming is low and they still have the potential to produce teratomas (Romeo, et al., 2012 and Bai, et al., 2013).

Other techniques of inducing pluripotency have also been investigated including using small molecule modifiers, fewer factors and chemical induction, these have increased the efficiency. However these techniques focus on nuclear reprogramming and do not address the metabolic or cytoplasmic reprogramming as somatic cells use mitochondrial oxidative phosphorylation instead of glycolytic ATP-generating pathways used by ESCs and iPSCs (Pennock, et al., 2015).

2.3.1 Definition

Mesenchymal Stromal Cells (MSCs) are found in bone marrow (but not exclusively) and can form all skeletal tissues including bone, cartilage, fibroblasts, adipocytes and haematopoiesis-supporting stroma (Bianco, et al., 2013) (Figure 2-1). Within bone

marrow, MSCs are found around the sinusoids (blood vessels in bone marrow) and replace differentiated osteoblasts and adipocytes during tissue growth and turnover and generate cartilage under conditions including trauma, additionally MSCs maintain a niche environment for haematopoietic stem cells and support haematopoiesis (Bianco, et al., 2013).

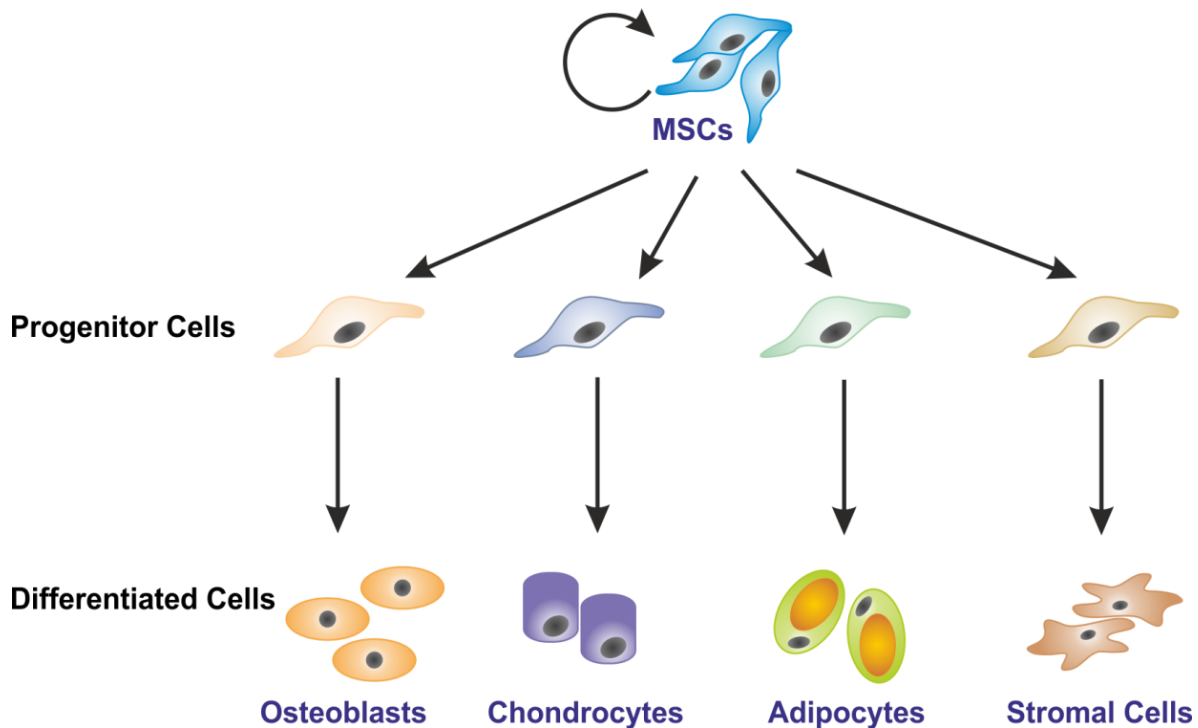


Figure 2-1 - MSC differentiation showing the differentiation of osteoblasts, chondrocytes and adipocytes

The characteristics used by the International Society for Cell and Gene Therapy to identify multipotent mesenchymal stromal cells are; plastic adherence, surface antigens CD73, CD15 and CD90 $\geq 98\%$ positive, surface antigens CD34, CD45, CD14 or CD11b, CD79 α or CD19 and HLA-DR $\leq 2\%$ negative and differentiation potential *in vitro* into osteocytes, chondrocytes and adipocytes (Wilson, et al., 2019). None of these criteria are specific to MSC's and so must be used together to identify MSCs correctly. MSCs are a heterogeneous population, clonal lines from one donor can contain tri-, bi-, uni-, and nulli-potent cells expressing a variety of the expected markers, this makes identification difficult. Within literature the term MSC is used to describe cells from this population with some described as stromal cells, others stem cells and different surface markers and criteria may have been used.

2.3.2 Function

MSCs differentiate to form new tissue as bone, cartilage and fat, differentiation can be induced *in vitro* by providing the right combination of conditions and chemical factors. MSCs also have other functions within the bone marrow such as hematopoietic support and immunoregulation (James, et al., 2015).

Osteogenic differentiation can be initiated in culture by the addition of dexamethasone, ascorbic acid and beta-glycerophosphate, during the early stages of differentiation (MSC to pre-osteoblast) the expression of Runx2 and osterix increases along with an increase in alkaline phosphatase, later in differentiation the expression of these genes decrease with an increase in Msx2, Dlx3 and Dlx5/6 (Frith & Genever, 2008).

Adipogenic differentiation can be induced by adding dexamethasone, isobutylmethylxanthine, indomethacin and insulin. Early during the differentiation process C/EBP β and C/EBP δ expression increases and initiates adipogenic differentiation and are expressed during commitment and mitotic clonal expansion. Expression levels of CHOP- 10 decrease at the end of mitotic clonal expansion, and allow expression of C/EBP α . C/EBP α and PPAR γ as well as SREBP1 during lipid accumulation and into mature adipocytes (Frith & Genever, 2008).

MSCs differentiate into cartilage through a series of stages and also require environmental cues to follow this path. The first step is commitment and condensation which increases the transcription factor Sox9, then the cells become proliferating chondroblasts, which involves Sox9, activating L-Sox5 and Sox6. The next stage is the formation of columnar chondroblasts which still requires L-Sox5 and Sox6; pre-hypertrophic chondrocytes are then differentiated with another increase in Sox9. Finally, hypertrophic chondrocytes form from differentiation driven by Sox9 and Runx2 (Frith & Genever, 2008).

Cartilage has limited self-renewal ability due to its avascular and hypocellular nature. This also makes it difficult for MSCs to relocate to the damaged site (Carstairs & Genever, 2014).

2.3.3 Role as a treatment

Stem cells are already being used clinically to benefit many patients; one of the most recognisable treatments is a bone marrow transplant. Other current treatments include skin grafts and treating corneal injury (Main, et al., 2014). Stem cells are a

highly researched area with studies into how they can help cardiovascular disease, Huntington's disease, Alzheimer's disease, pregnancy disorders, cerebral ischemia and many more (Reed, et al., 2013, Crane, et al., 2014, Chen & Blurton-Jones, 2012, James, et al., 2014 and Chen, et al., 2013).

Using autologous or allogeneic stem cells come with different advantages and disadvantages. Autologous cells come from the patient so less risk of rejection and cross infection but involves harvesting and transplantation which depending on the treatment the cells require could leave quite a bit of time between isolation and implantation. If cells which have been harvested do not survive culture, then harvesting needs to be repeated. Allogeneic cells can be prepared in advance from other patients or donors and have more predictability however have a higher risk of rejection and incompatibility.

Cell therapy is also currently being used within orthopaedics for repairing cartilage damage, autologous discs have been formed by removing cells from patients and culturing them prior to re-implantation, they can then be injected or directly applied to the joint and can also be applied via a scaffold (Roberts, et al., 2011).

Mesenchymal stromal cells are being used in many clinical trials to treat a wide range of areas including immunology, skeletal, wound healing and cardiovascular (Wilson, et al., 2019).

Other research being conducted using stem cells to regenerate cartilage includes a trial (The Robert Jones and Agnes Hunt Orthopaedic Hospital NHS Foundation Trust, 2019) where bone marrow is removed from the patients hip, centrifuged to concentrate then mixed with hyaluronic acid and surgical glue before being injected into damaged cartilage sites in the patients knee, the aim of this is to allow the cartilage to repair and prevent osteoarthritis from developing from the injury.

As it is desirable to use stem cells from the patient to treat osteoarthritis it is therefore important to determine how osteoarthritis affects the stem cells of that patient. Age has been thought to impact stem cells, this was investigated in a study (Diekman & Guilak, 2013) which used cells from people aged 5-80, this study found that proliferation of the MSCs decreased with age but showed no significant effect on the differentiation. It was also noted that donors which had low proliferation failed to produce sufficient type II collagen, this was not correlated with age but highlights the increased risk that age has on cartilage formation. The same study also found that

obesity (one of the risk factors of osteoarthritis) also affects the quality of stem cells. Another factor that this study has shown to affect stem cells is inflammation, which is also a factor in the development of osteoarthritis. Inflammation has been shown to reduce the differentiation potential of stem cells, so this also needs to be considered in tissue engineering.

2.3.4 Metabolism and control of cell function

Metabolic pathways within cells to generate energy to perform cellular functions are regulated to respond to the energy demand and the availability of substrates. Stem cells in quiescence predominantly use anaerobic glycolysis but switch to mitochondrial oxidative phosphorylation for differentiation, stem cells adapt their metabolism in response to the environment and need to proliferate and differentiate (Ito, 2016).

A technique has been developed within Paul Genever's laboratory (University of York) which uses a 3D culture technique to restrict nutrient availability inducing autophagy (Pennock, et al., 2015). This 3D system reduces the nutrients to a level low enough to induce autophagy while avoiding apoptosis, during this process restructuring within the cell returns the cell to a more primitive state. The mitochondria were observed to become more rounded and loss of expression of genes connected to oxidative phosphorylation occurred. After de-differentiation cells from aged patients exhibited increased replicative capacity, reversal of senescence and the cells can form organised tissue *in vivo*. The resulting cells are also not pluripotent and do not form teratomas.

2.4 Oxygen and Glucose Levels *In vitro* and *In vivo*

Energy production in cells is achieved by degrading glucose to create adenosine triphosphate (ATP) either by using oxygen in oxidative phosphorylation or without oxygen in anaerobic glycolysis. Oxidative phosphorylation yields more ATP per glucose molecule than anaerobic glycolysis (Demirel, 2002), therefore the supply of oxygen and glucose are key to culturing cells *in vitro*.

Standard incubator conditions used for cell culture use humidified atmospheric air supplemented with 5% CO₂. Cells within culture are however exposed to the oxygen levels dissolved in the culture media and not in direct contact with the air. Culture media is largely comprised of water, the solubility of oxygen in water is well documented as a function of temperature and partial pressure of oxygen in the

atmosphere, using Henry's law constants and solubility data for incubator conditions gives a range of oxygen concentrations from 0.19 mol/m³ to 0.218 mol/m³ (Moore J, 2010, Sanders R, 2014 and Engineering Toolbox, 2005). The oxygen concentration in media has been measured as 0.214 mol/m³ (Heimburg, et al., 2005), more detail on these is included in chapter 4.3.1.

The concentration of oxygen in blood and other tissues is commonly expressed as partial pressure of oxygen present, another common form of representation is volume %, the partial pressure of oxygen in atmospheric air is 0.21 atm or 21%. The percentage of oxygen that is in arterial blood drops to 13% and venous blood to 5.3% (Carreau, et al., 2011).

Reported values of oxygen concentration in the bone marrow vary, the values in (Carreau, et al., 2011) were taken by using a blood gas analyser on bone marrow aspirate and the range of values found by Spencer et al 2014 were taken using 2-photon phosphorescence lifetime microscopy (Table 2). Another study also (Spencer, et al., 2014) reported that the average value in the sinusoids within the bone marrow is 0.025 atm (1 mol/m³, 2.5%).

Table 2.1 – Comparison of oxygen concentrations in the body

	Partial Pressure atm	Concentration mol/m ³
Arterial Blood (Carreau, et al., 2011)	0.13	5.173
Bone marrow (Carreau, et al., 2011)	0.06	2.529
Bone marrow (Spencer, et al., 2014)	0.015 - 0.04	0.6 -1.6

The differences between oxygen transport *in vivo* and cell culture are discussed in the publication by Place, et al., 2017 this paper highlights the adaptability of *in vivo* tissue to adjust the oxygen supply compared to cell culture where the oxygen concentration is dependent on the balance between the oxygen consumption rate and the rate of diffusion of oxygen from the air into the media and through the media. The oxygen availability in cell culture is dependent on many factors including, oxygen consumption rate, cell density, incubator conditions (temperature, pressure, partial pressure of oxygen) and media depth. Therefore, there is the need to assess cell culture systems individually and not make assumptions about the oxygen availability in one culture based on the assessment of another system.

Glucose concentrations are less well recorded within literature both *in vitro* and *in vivo*. The glucose concentration within the body is generally assumed to be the same as the level in blood which averages 5mM (Tankasala & Linnes, 2019). Glucose is present in cell culture media and commonly used concentrations are 5mM and 25mM, these concentrations will only be present in fresh media and will reduce over time in culture.

Within cells low oxygen levels stabilise HIF α which induces a number of changes including, lowering oxygen consumption by shifting to glycolysis instead of oxidative phosphorylation and reducing energy intensive activities such as cell division (Choudhry & Harris, 2018). Hypoxia increases the amount of reactive oxygen species (ROS) which can lead to damage to proteins, lipids and DNA particularly in mitochondria, recycling of damaged organelles is part of the survival response utilising autophagy (Benson Ham III & Raju, 2017).

The first response to glucose starvation is to use lipids as an alternative energy source, the secondary response is to induce autophagy (Singh, et al., 2009).

Autophagy means 'eating of self' and is a survival mechanism employed by cells which involves the degradation of cytosolic components via a lysosome. There are three types of autophagy: macro, micro and chaperone mediated. Macro autophagy uses an intermediary double membrane bound vesicle called an autophagosome to transport cytoplasmic cargo to the lysosome creating an autolysosome, in micro autophagy the cytosolic components are taken up directly by the lysosome, both of these mechanisms are capable of engulfing large structures selectively and non – selectively. Chaperone mediated autophagy uses targeted proteins translocated in the lysosome membrane along with chaperone proteins which are recognised by the lysosomal receptor which results in their un-folding and degradation (Glick, et al., 2010). An outline of the mechanisms involved in macro autophagy is shown in Figure 2-2, autophagy can be induced by different factors but the main inducer is nutrient starvation this can be starvation of essential nutrients such as glucose but can also be caused by amino acid deprivation (Mizushima, 2007). This deprivation does not need to be a direct reflection of the immediate environment as in a multicellular organism the nutrient consumption needs to be regulated for the whole organism (Mizushima, 2007).

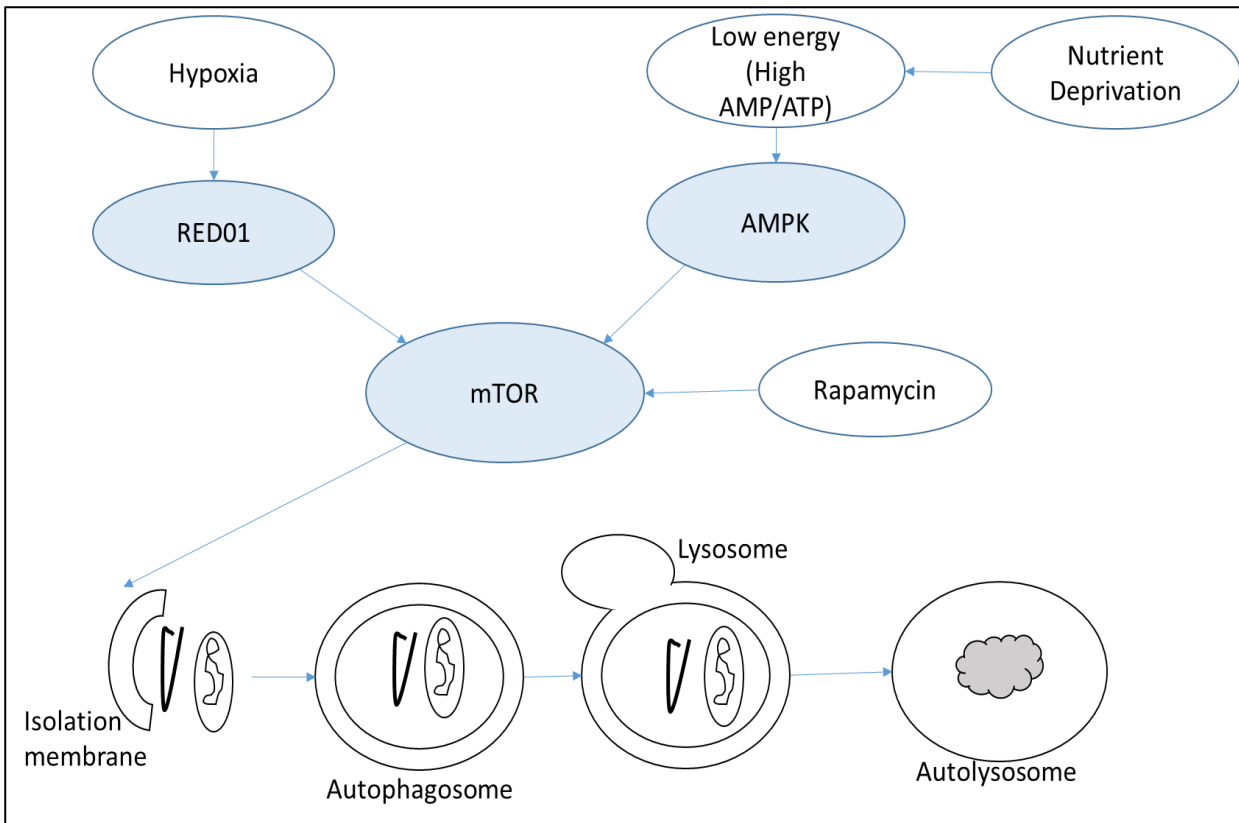


Figure 2-2 – Outline of macro autophagy.

Nutrient deprivation and hypoxia can both induce autophagy through the activation of mTOR, which can also be activated by the addition of rapamycin, this activation then allows the isolation membrane to isolate components for degradation, a lysosome then breaks down the cytosolic components

2.5 Previous work on modelling cell culture conditions

Optimisation of cell culture protocols is a time and labour-intensive process often requiring large numbers of cells and consumables. Mathematical modelling allows prospective culture systems to be provisionally refined to give a better starting point for physical experiments, without being as intensive as computational 3D modelling, which makes it feasible to investigate several options. The availability of oxygen, glucose and other nutrients are essential for cell survival, therefore if the culture system doesn't allow for adequate mass transfer for these nutrients to reach the cells the culture system will not be successful. In addition to physical experiments being cell and time intensive it is difficult to measure the oxygen and glucose concentrations with the spatial resolution required to accurately assess the concentrations available at a cellular level.

Predictive modelling is a routine aspect of most chemical engineering design, using this approach in tissue engineering also helps to predict how an implant will behave

in the body and if any areas of the construct are going to suffer from lack of oxygen or nutrient availability. These modelling principles are also relevant to developing more representative 2D and 3D cell culture models as discussed below.

Synthetic scaffolds pose a problem during implantation as they are prone to creating oxygen mass transfer limitations which then forms the limiting factor for cell survival. Mathematical modelling of these constructs can offer a substantial contribution to understanding how the structure will affect cell growth (Curico, et al., 2014). To assess how oxygen concentration would affect the growth of cells in a tissue engineered trachea, (Curico, et al., 2014) modelled the scaffold and tested the behaviour of the cells which would be seeded on to the polymer scaffold at different oxygen concentrations. This model incorporates Henry's law, Michaelis Menten and diffusion laws in a finite element method using computerised fluid dynamics. The model created is not included in the paper and no validation techniques were stated.

The effect of oxygen concentration on cell growth in a spiral collagen scaffold was also assessed experimentally by (Ardakani, et al., 2014) which found that a spiral scaffold of 4mm diameter causes significantly different oxygen concentrations within the scaffold causing more cell death within the centre. The scaffold was a nylon mesh set in collagen, seeded with HDFs (human dermal fibroblasts), oxygen concentration was measured across the scaffold using fibre optic probes.

Mass transfer limitations are not confined to scaffold structures but can also occur in 3D culture such as the 3D MSC spheroids. Spheroid culture systems are generally a multicellular mass of cells suspended in medium and up to 1mm in diameter, the mechanism of transport for nutrients and waste products for these systems relies upon diffusion with no active transport system. Oxygen and glucose concentrations and transfer in embryoid bodies has also been modelled by Winkle, et al., 2012 to help understand the cues for differentiation within the embryoid body. Embryoid bodies are 3D cell aggregates similar to spheroids. This model represents mass transfer in a spinner flask at equilibrium. The spheroid system for dedifferentiation uses static culture and has changing consumption rates and size over time so concentration needs to be considered as a function of time (Winkle, et al., 2012). This model was developed using Fick's law for mass transfer through the media using a modified mass transfer coefficient for spinner flask. A mass balance was then used over the embryonic body and the equations were structured to be a function of the radius as the focus of the modelling was to analyse how size affected mass

transfer. Validation of this model was achieved by literature comparison.

Mathematical modelling of oxygen concentration in hepatocyte spheroids has been done by Glicklis, et al., 2004; however, this model cannot be applied to the spheroid system for dedifferentiation as it does not use concentration as a function of time, it is based upon a proliferating culture and it is also not as adaptable to nutrients in the media. The hepatocyte spheroids were up to 600µm in spinning cultures, the model is based upon Monod kinetics and relies on growth kinetics, the model also directly links cell viability to oxygen concentration and uses this relationship to validate the model.

To appreciate the results of modelling a 3D system they need to be compared to the natural and 2D culture environment. Modelling 2D culture conditions can also give an insight into how heterogeneous the conditions are. Oxygen concentrations for rat cardiac cells in a petri dish have been monitored in laboratory experiments (Kagawa, et al., 2015), and oxygen gradients were found through the depth of the media (2mm) and along the radial distance from the centre of the dish, these cells have a higher oxygen consumption rate than MSCs (0.8 pmol/cell.hour maximum uptake for rat cardiac cells compared to 0.007 pmol/cell.hour measured for 2D MSCs (Pennock, et al., 2015)) which causes the balance between diffusive rate to be smaller than the cell uptake rate in some areas.

2.6 Summary

There is a need to provide improvement treatment for osteoarthritis which allows repair of damaged joints, with the aim of ensuring a long-term effect for patients. The use of 3D culture systems to investigate these treatments requires an understanding of how the transport of oxygen and other nutrients is influenced in 3D culture.

Existing models and assessments cannot be applied to the 3D culture system in use and there is little information available on the native *in vivo* environment.

The specific aims of this research are to;

- Develop a model to predict oxygen and glucose availability in,
 - Monolayer adherent culture
 - Spheroid culture
 - Bone marrow
- Assess whether difference in availability of nutrients across the different environments effects the proliferation, size and differentiation of the cells.
- To validate the outcomes of the model predictions for mono-layer adherent culture and spheroid culture against laboratory experiments.

Chapter 3 Cell Culture Methods

3.1 Basic cell culture

Cell culture media and reagents were purchased from Invitrogen and chemicals were from Sigma unless otherwise stated.

Primary mesenchymal stromal cells (MSCs), Y201s, Y202s, Y201.5s and human dermal fibroblasts (HDFs) were all cultured prior to conducting experiments. These cells were adhered to plastic during culture in high glucose Dulbecco's modified eagles medium (DMEM) with Penicillin streptomycin (final concentrations 100 units/ml and 100µg/ml respectively) and varying concentrations of foetal bovine serum (FBS). Primary cells were cultured in 15% batch tested FBS, Y201s, Y202s and HDFs were cultured in 10% FBS and Y201.5s were cultured in 0.5% FBS. Cells were cultured to confluency and periodically tested for mycoplasma. Unless otherwise stated media was changed every 3-4 days. Incubators were set at 37°C, 5%CO₂ and 95% humidity.

Primary MSCs used were extracted from knee bone fragments donated by an osteoarthritis patient (sample labelled as K139), the bone was broken into fragments and placed in petri dish with medium described above, MSCs migrated from the bone and adhered to the surface of the petri dish. Cells from the first five passages were used in these experiments. Primary cells used in these experiments were characterised by plastic adherence and visual morphology, further analysis has been conducted on cells isolated using the same methods. Y201s and Y202s are MSCs which have been immortalised as detailed in (James, et al., 2015) and passages used ranged from 70-110. Y201.5s were Y201s which had been acclimatised to be cultured in 0.5% FBS media and used from passage 83-96. HDFs used were a commercial cell line and used from passage 7-25.

Once confluency was reached or the cells were required for use, the cells were detached from the flasks by washing with phosphate buffered saline (PBS) followed by 10 minutes incubation in 0.025% trypsin and 0.01% ethylenediamine tetraacetic acid (EDTA) in PBS.

For storage the cells were stored in liquid nitrogen at -80°C, cells were detached from flasks using trypsin/EDTA pelleted using centrifugation (5 min at 12,000g) and re-suspended in 10% (v/v) dimethyl sulphoxide (DMSO) in FBS and placed in cryovials.

The cryovials were then placed in containers surrounded by isopropanol to control the rate of temperature decrease in a -80°C freezer, after 24 hours the cryovials were then transferred to liquid nitrogen storage.

3.2 Spheroid culture

For spheroid culture normal culture media was supplemented with 0.25% methylcellulose to make a viscous media. Spheroids were formed by resuspending cells in the 3D media and culturing in u-bottom 96 well plates which were not tissue culture treated to prevent cell attachment as previously described (Pennock, et al., 2015). Unless otherwise stated a 2/3 media change was conducted every 3 days. MSC, Y201 and Y202 spheroids contained 60,000 cells, HDF spheroids contained 30,000 cells.

3.3 Size measurement

Spheroid size was measured using brightfield microscopy and Image J (Open Source) analysis, spheroids were imaged within the well plate which allowed the monitoring of individual spheroids over the time course. Minimum of 10 spheroids were used per condition, 4 diameters were taken per spheroid and averaged, measurements were validated using a calibration image.

Cell size was measured using a VICELL coulter counter which also measured viability using trypan blue, circularity and cell number. Single cell suspensions were created from the spheroids as detailed in 3.9.

3.4 Transmission Electron Microscopy (TEM)

Spheroids were isolated and then fixed and processed for TEM by Technology Facility, University of York. Spheroids were fixed in formaldehyde and glutaraldehyde in phosphate buffer, the secondary fix was osmium tetroxide, dehydration was done using ethanol and epoxypropane before embedding in Epon Araldite. Sections were then stained in uranyl acetate in ethanol and Reynold's lead citrate. Imaging was performed using a FEI Tecnai G transmission microscope.

3.5 Colony forming unit assay (CFU-F)

During CFU-Fs assays cells were cultured in media with 20% hyclone FBS. Cells were seeded at a density of 10cells/cm² in a 6 well plate and cultured for 2 weeks or

until colonies were about to merge. Plates were then stained with crystal violet (0.05% w/v crystal violet, 0.1%v/v formaldehyde, 1xPBS, 1% methanol, and 79% distilled water), media was removed, and wells were covered in staining solution for 20 minutes at room temperature, the stain was then washed off under running water. Plates were then left to air dry prior to analysis.

3.6 MTT (3-[4,5-dimethylthiazol-2-yl]-2,5 diphenyl tetrazolium bromide) assay

Cells were seeded into a 96 well plate at a density of 1200 cells per well with 100µl culture media and left in incubator at 37°C for 24 hours. The media was then removed and replaced with media at the different experimental conditions. At the chosen time point 25µl MTT solution (5mg/ml in PBS) was added to each well and incubated for 3 hours. The media and MTT solution were then removed from wells and 70µl 0.04M isopropanol in hydrochloric acid added to each well. The plate was then analysed on a plate reader at 570nm.

3.7 Osteogenic differentiation

Cells were seeded at a density (3×10^4 cells/m²) which allowed confluency to be reached 24 hours after seeding in 96 well plate in normal culture media. Media was changed after 24 hours. Osteogenic media contained normal culture media supplemented with 50µg/ml L- ascorbic acid 2 phosphate, 5mM β-Glycerophosphate and 10 nM dexamethasone.

3.7.1 Alkaline Phosphatase Assay

Osteogenic differentiation was measured using an alkaline phosphatase assay at appropriate time points of day 3,6 and 9. Wells were washed with 0.2M carbonate buffer, lysis buffer (0.1% triton-X in 0.2M carbonate buffer) was added to each well, 3 freeze thaw cycles were performed from -80°C to 37°C. The lysate was then split equally for para-Nitrophenyl phosphate (pNPP) alkaline phosphatase assay and picogreen DNA quantification assay.

Standard solutions of para-nitrophenyl (pNP) were prepared at 0.5, 0.3, 0.2, 0.1, 0.05, 0.025, 0.0125 and 0 µmol/ml pNP in 0.2M carbonate buffer. pNPP solution (0.33mg/ml pNPP 0.06 M carbonate buffer and 3.3 mM magnesium chloride in distilled water) was added to standards and samples and incubated at 37°C until a colour change was seen (up to an hour), length of time was recorded and used with

the DNA quantification to calculate the $\mu\text{mol pNP}$ produced per $\mu\text{g DNA}$ per minute. Absorbance was measured at 405nm to quantify colour change, standards were used to set up a standard curve.

For DNA quantification standards were made using salmon sperm DNA at 8, 4, 2, 1, 0.5, 0.25 and 0 $\mu\text{g/ml}$ in 0.1% triton X in 0.2M carbonate buffer. Standards and samples were placed into a black 96 well plate. Picogreen (2% picogreen reagent in 10 mM tris, 1mM EDTA in water pH 7.5 buffer) (Invitrogen) solution was added to each well. Fluorescence was measured at 485 nm excitation and 538nm emission, standards were used to set up a standard curve. Results were used to standardise the alkaline phosphatase activity to amount of DNA.

3.8 Adipogenic differentiation

Cells were seeded at a density (3×10^4 cells/ m^2) which allowed confluency to be reached 24 hours after seeding in 96 well plate in normal culture media. Media was changed after 24 hours. Separate plates were seeded for analysis on days 7, 14 and 21. Adipogenic media contained normal culture media supplemented with 1 μM dexamethasone, 500 μM IBMX (3-Isobutyl-1-methylxanthine), 1 $\mu\text{g/ml}$ insulin and 100 μM indomethacin.

3.8.1 Oil red O staining of liquid droplets

Oil red O was used to stain liquid droplets formed in cells undergoing adipogenic differentiation. Cells were washed with PBS then fixed in 4% paraformaldehyde in PBS pH 7.4 for 10 minutes, washed with water, 60% isopropanol added for 5 minutes, and incubated with 0.3% oil red O solution in 60% isopropanol for 10 minutes. Samples were then washed with 60% isopropanol and water. Wells were then imaged prior to elution of the stain. Elution of Oil Red O was performed by adding isopropanol for 15 minutes and transferring to a new plate, absorbance was then read at 490 nm.

3.9 Disaggregation of spheroids

Spheroids were disaggregated using liberase TL (Roche) working solution at 1.3 Wunsh units per ml in PBS, spheroids were incubated for 20 minutes at 37°C covered in liberase solution. After incubation the spheroids were pipetted and passed through a needle to form a single cell suspension.

Chapter 4 Monolayer Adherent Culture Studies

4.1 Introduction

Current mathematical models of nutrients in tissue culture are mainly based on 3D models, direct measurement of nutrients is more common in 2D culture. The data presented here develops a predictive model for a 2D culture system that is based on mass transfer principles and which can be adapted for 3D culture systems. The specific aims were to develop a model to predict the oxygen and glucose concentrations within 2D culture where the inputs and outputs were the same format as the models being developed for 3D and bone marrow.

4.2 Monolayer Adherent Culture Model Development

4.2.1 Oxygen

Commonly MSCs are cultured in monolayers adhered to plastic, therefore the mass transfer process for oxygen to reach the cells is in two-stages: transfer from the air into media followed by transfer through the media to the cell surface (Figure 4-1).

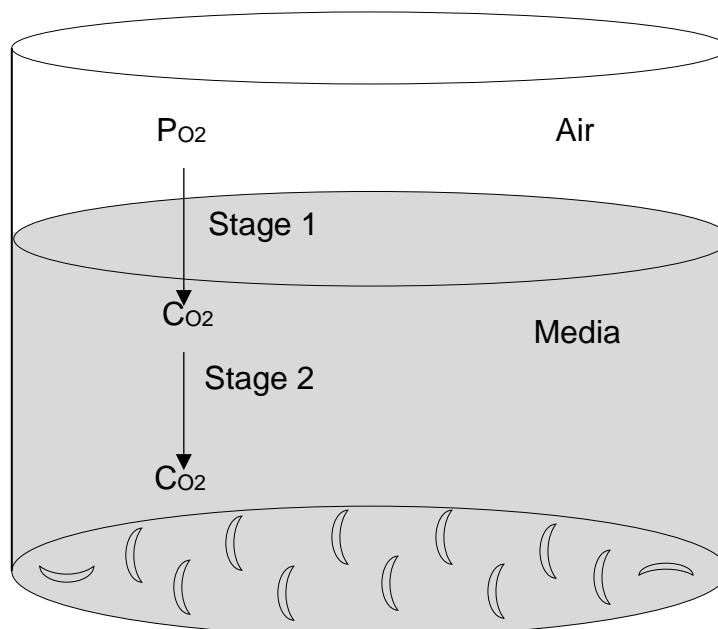


Figure 4-1 – Schematic of oxygen mass transfer during monolayer culture.

Oxygen transfers from the air into the media then through the media to the cell layer at the bottom of the well. PO_2 is the partial pressure of oxygen in air, CO_2 is the

concentration of oxygen in the liquid phase. Stage one transfer is governed by Henry's law and stage two transfer is governed by Fick's law.

The relationship between the partial pressure of a gas in air and the concentration which dissolves in a liquid phase beneath it is described by Henry's law (Coulson, et al., 2008):

$$P_A = \frac{H}{x_A} \quad (4.1)$$

Where;

P_A is the partial pressure of A in the gaseous phase

H is Henry's constant

x_A is the amount of A dissolved in the liquid phase

During cell culture the oxygen concentration will not only be in equilibrium with the partial pressure it will be also be dependent on the rate of consumption by the cultured cells and the rate of transfer from the air into the liquid to replace the used oxygen. Starting with a basic mass balance over the well (equation 4.2).

$$\text{Oxygen in} - \text{Uptake} \pm \text{Accumulation} = 0 \quad (4.2)$$

The oxygen will transfer into the media via diffusion, the rate of diffusion across the phase boundary is described by (Molder, et al., 2005) (equation 4.3)

$$N_A = \left(\frac{D_s}{l_s} \right) (C_{air} - C_{media}) CSA \quad (4.3)$$

Where;

N_A = Mass transfer rate of O_2 (mol/s)

D_s = Diffusion coefficient for O_2 in the surface layer (m^2/s)

l_s = Thickness of the diffusion layer (m)

C_{air} = Concentration of O_2 in the air (mol/m^3)

C_{media} = Concentration of O_2 in the media (mol/m^3)

CSA = Cross sectional area of well surface (m^2)

This equation is based on Fick's law, the rate of diffusion into the media is dependent on the concentration gradient between the air and liquid phases, the area available for mass transfer, distance through the boundary and speed at which oxygen can diffuse. Inserting equation (4.3) into equation 4.2 gives equation 4.4, U is the update

rate of oxygen in the well (mol/s), dC_{media}/dt is the change of oxygen concentration in the media over time (mol/s).

$$\left(\frac{D_s}{l_s}\right) (C_{air} - C_{media})(CSA) - U = \frac{dC_{media}}{dt} \quad (4.4)$$

As D_s , l_s and CSA are constants,

Let;

$$a = \left(\frac{D_s}{l_s}\right) CSA$$

Therefore,

$$\frac{dC_{media}}{dt} = a(C_{air} - C_{media}) - U$$

$$\frac{dC_{media}}{dt} = aC_{air} - aC_{media} - U$$

Let;

$$b = aC_{air} - U$$

Therefore,

$$\frac{dC_{media}}{dt} = b - aC_{media}$$

$$\frac{dC_{media}}{b - aC_{media}} = dt$$

$$\int \frac{1}{b - aC_{media}} dC_{media} = \int dt$$

$$\frac{\ln(b - aC_{media})}{-a} = t + K \quad (4.5)$$

K = integration constant

The integration constant can be found by setting equation 4.5 to initial conditions (starting media concentration) equation 4.6 can then be used to find the concentration of oxygen in media throughout a culture.

$$C_{media} = \frac{e^{-\alpha(t+k)} - b}{-a}$$

$$C_{media} = \frac{e^{-\left(\frac{D_s}{l_s}\right)CSA(t+k)} - \left(\frac{D_s}{l_s}\right)CSA C_{air} - U}{-\left(\frac{D_s}{l_s}\right)CSA} \quad (4.6)$$

The concentration in the media can then be used to model the diffusion within the media by constructing a mass balance within the well as the transfer into the well has been quantified above.

Diffusion through media

$$N_m = \frac{D_m CSA}{d} (C_{media} - C_{cells})$$

Where;

d = depth of media (m)

C_{cells} = concentration at cell layer (mol/m³)

D_m = diffusion coefficient of O₂ through media (m²/s)

The uptake rate is the same as above

$$\frac{D_m CSA}{d} (C_{media} - C_{cells}) - U = \frac{dC_{cells}}{dt}$$

Let;

$$a = \frac{D_m CSA}{d}$$

Therefore,

$$aC_{media} - aC_{cells} - U = \frac{dC_{cells}}{dt}$$

Let;

$$b = aC_{media} - U$$

Therefore;

$$b - aC_{cells} = \frac{dC_{cells}}{dt}$$

$$\frac{dC_{cells}}{b - aC_{cells}} = dt$$

$$\int \frac{1}{b - aC_{cells}} dC_{cells} = \int dt$$

$$\frac{\ln(b - aC_{cells})}{-\alpha} = t + K$$

Integration constant K can be found at initial conditions.

$$C_{cells} = \frac{e^{-\alpha(t+K)} - b}{-a}$$

$$C_{cells} = \frac{e^{-\frac{D_m CSA}{d}(t+K)} - \frac{D_m CSA}{d} C_{media} - U}{-\frac{D_m CSA}{d}} \quad (4.7)$$

4.2.2 Glucose

Glucose is present in the cell culture media and does not diffuse into the well, therefore the concentration of glucose in the well is dependent on the starting concentration (C_{start} , mol/m³), consumption rate (G , mol/s) and time in culture (t , s) as shown in equation 4.8.

$$C_{media} = C_{start} - Gt \quad (4.8)$$

4.3 Monolayer Adherent Culture Model Predictions

4.3.1 Input Data

Input values for the monolayer culture models are detailed in Table 4-1 and Table 4-2.

Table 4-1 – Input data for monolayer adherent culture models

Parameter	Units	Value	Description	Source
C_{air}	mol/m ³	7.67	Concentration of O ₂ in air	
CSA	m ²	3.85E-5	Cross sectional area of well	Measured
d	m	3.90E-3	Depth of media	
D_m	m ² /s	3.8E-9	Diffusion coefficient for O ₂ through media	(Curico, et al., 2014)
D_s/l_s	m/s	1.3E-6	Diffusion coefficient for O ₂ through the surface layer divided by the thickness of the surface layer	(Molder, et al., 2005)

The concentration of oxygen in the incubator is calculated from an ambient air concentration of 21 vol%, as the air intake in the incubator is supplemented by the addition of 5% CO₂ the volume percent of oxygen drops to 19.5%, therefore applying equation 4.9 gives the concentration of oxygen in air shown in Table 4-1.

$$P V = n R T$$

Equation 4.9 – Ideal gas law (Coulson, et al., 2008)

Where;

P is the pressure (Pa)

V is the volume occupied (m³)

n is the amount of substance (mol)

R is the universal gas constant 8.314 (J/mol.K)

T is the absolute temperature (K)

Oxygen concentrations in the media as calculated by two Henry's law constants and two oxygen concentrations based on solubility data are shown in Table 4-2, Henry's constants are applicable at 37°C, and atmospheric pressure, the partial pressure of O₂ is 0.195 atm (incubator conditions).

Table 4-2 – Concentration of Oxygen in media

Method	H	O ₂ concentration (mol/m ³)
Henry's law (Moore J, 2010)	1.33 mol/L.mmHg	0.1972
Henry's law (Sanders R, 2014)	9.62 mol/m ³ .Pa	0.1901
Solubility (water 35°C) (Engineering Toolbox, 2005)		0.218
Solubility (media 37°C) (Heimburg, et al., 2005)		0.214

Oxygen consumption rates for monolayer and spheroid culture were obtained experimentally within the laboratory group prior to this project and the value used in the monolayer culture models is in section 5.2.

4.3.2 Model Predictions

The equations derived in 4.2 were used in conjunction with the data in section 5.2 and results were calculated using MATLAB software.

The oxygen and glucose concentrations in monolayer adherent culture (2D) are shown in Figure 4-2 and Figure 4-3 respectively.

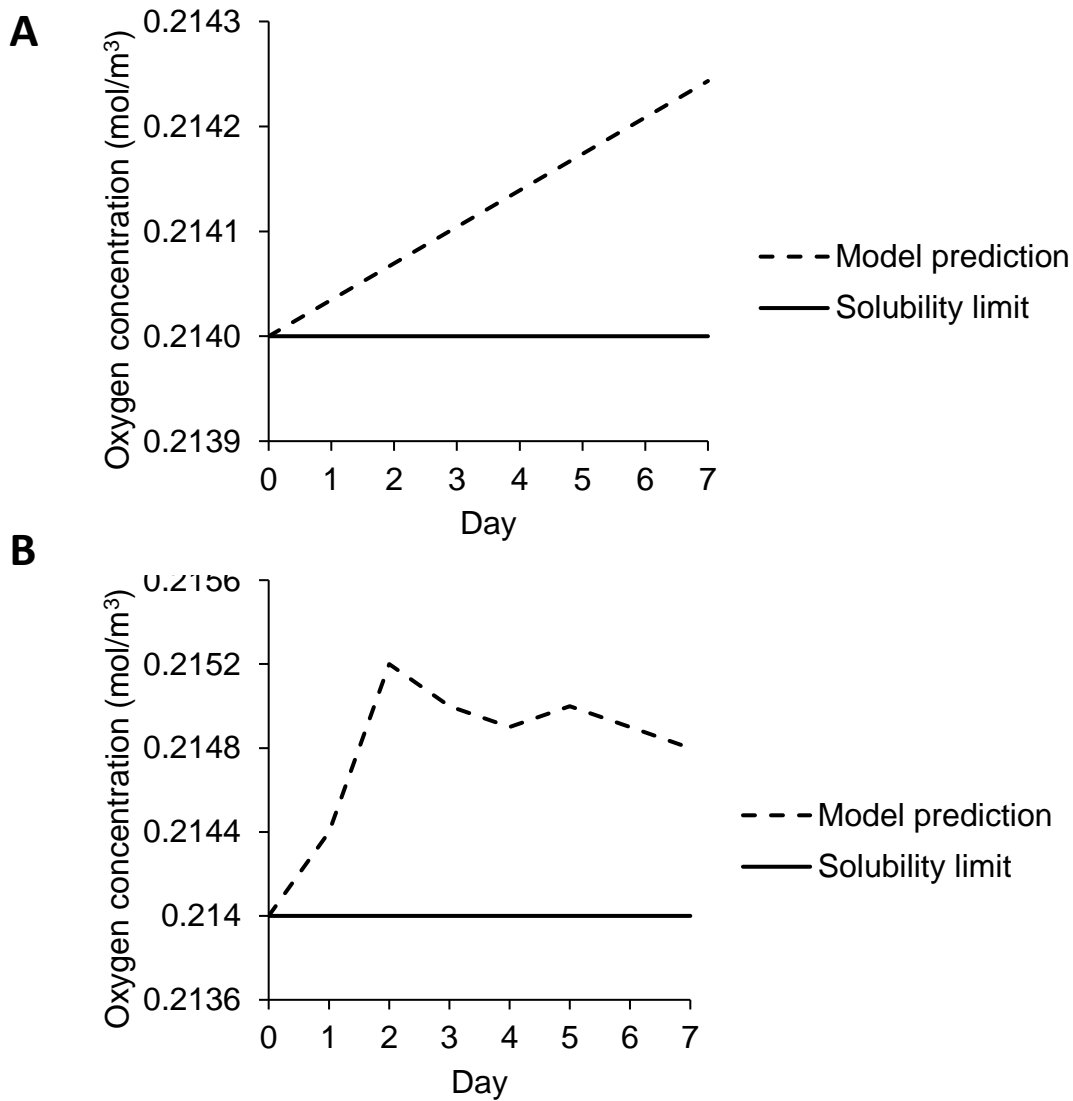
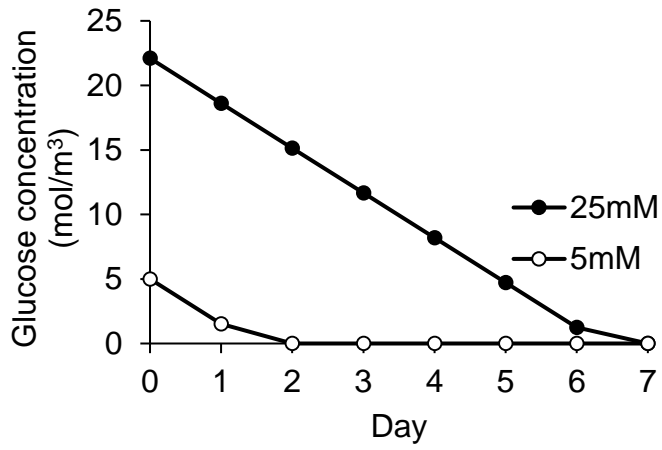


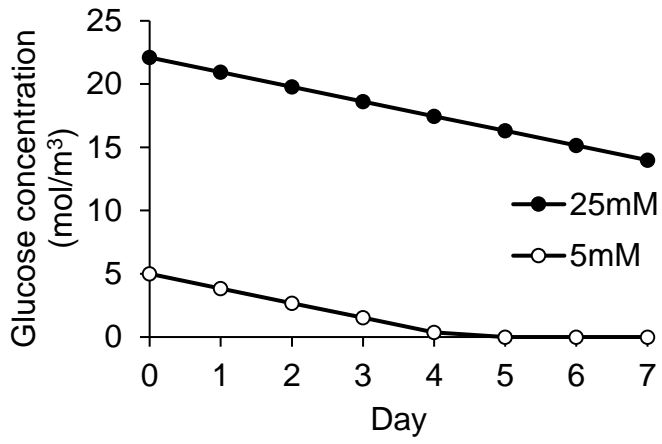
Figure 4-2 – Predicted oxygen concentration in media.
 A – Oxygen in media during conventional 2D culture, B – Concentration in media during spheroid culture.

As shown in Figure 4-2 graph A the oxygen concentration in 2D culture is not depleted during culture and remains stable at the solubility limit. Oxygen solubility is the limiting factor in oxygen availability for MSC monolayer cultures as the rate at which oxygen can diffuse into the media is greater than the consumption rate for this cell type.

A



B



C

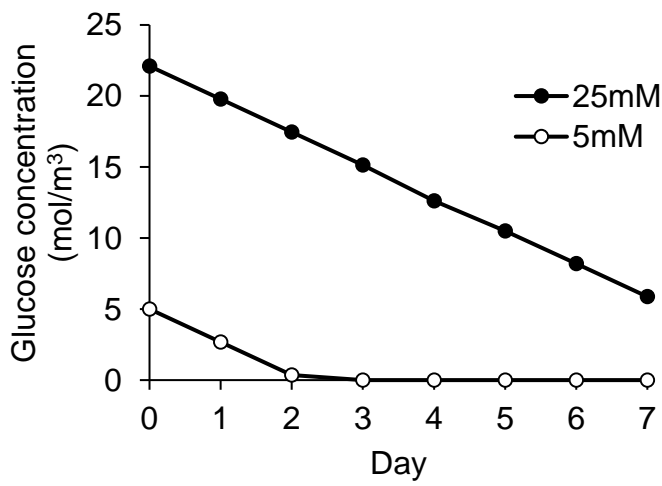


Figure continues next page.

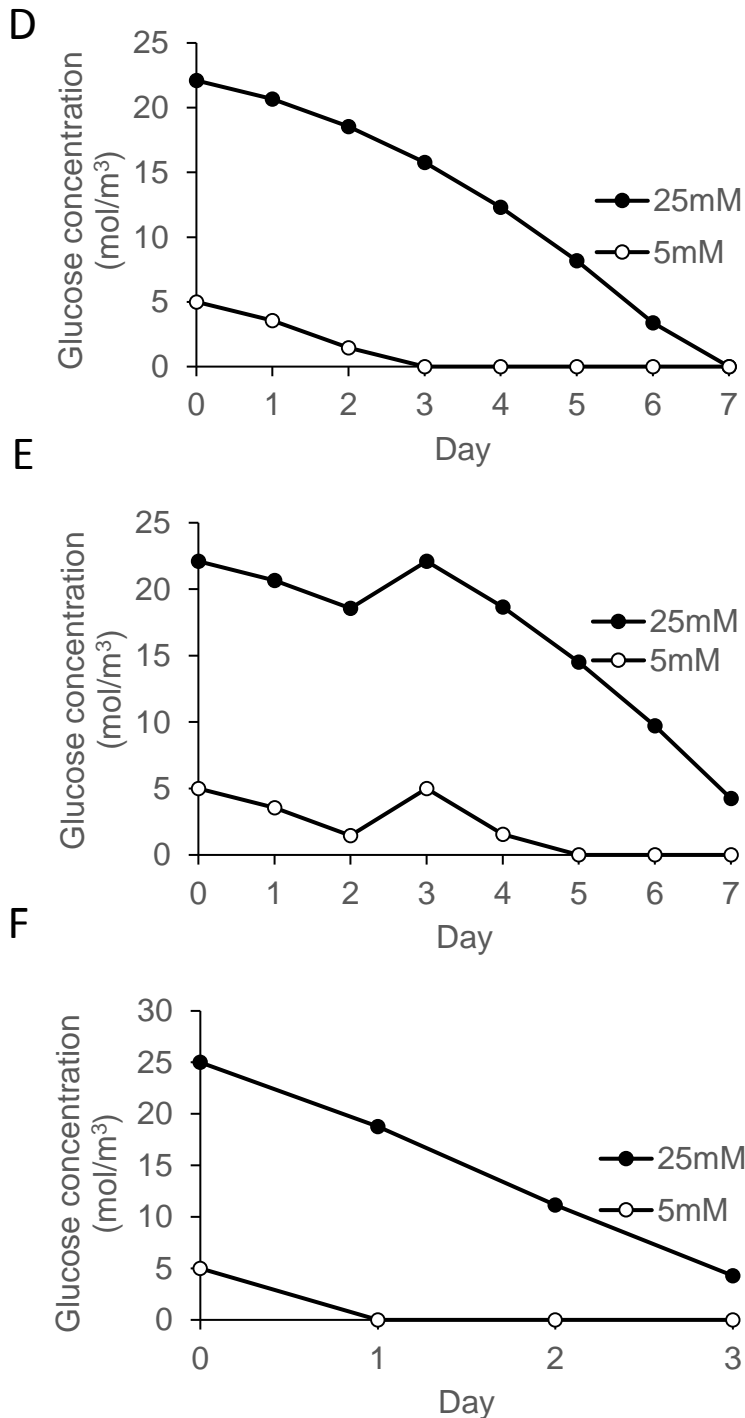


Figure 4-3 – Predicted glucose concentrations in 2D culture calculated from a mass balance at 5mM and 25mM.

A – 6×10^4 cells in 96 well plate (100 μ l media) no media change or proliferation, B – 1×10^6 cells in T75 (10ml media) no media change or proliferation, C – 2×10^6 cells in T75 (10ml media) no media change or proliferation, D – 5×10^5 cells in T25 (5ml media) proliferation included, no media change, E – 5×10^5 cells in T25 (5ml media) proliferation included, media changed on day 3, F – Suspension culture with 5×10^5 cells/ml no proliferation.

Glucose concentration in media was predicted in a variety of conditions as shown in Figure 4-3. The standard culture conditions for MSCs uses 25mM glucose media

which is then slightly lowered with the addition of FBS and antibiotics whereas 5mM glucose media is closer to *in vivo* concentrations. The conditions in graph A are the 2D equivalent of the spheroid culture discussed later and show depletion of glucose after 7 days (25mM) and 2 days (5mM) with no media changes. Graph B shows the glucose concentrations in a T75 flask at partial confluency but without proliferation and shows that depletion would occur after 5 days (5mM) and longer than a week (25mM), graph C shows the depletion at confluency would be considerably quicker at 2 days (5mM) and still over a week (25mM). Graphs D and E are both based on the standard seeding density into a T25 flask with proliferation then considered (measured by cell counts), D shows without media changes depletion would occur after 3 days (5mM) and 7 days (25mM) and in E with media changes on day 3 it would be 5 days (5mM) and then after 7 days (25mM). Graph F shows the concentrations predicted in suspension conditions discussed later and shows depletion after 1 day (5mM) and later then 3 days (25mM). Therefore, during normal culture procedures using 25mM glucose media should not result in glucose depletion and using 5mM glucose would require more frequent media changes than currently operated.

4.4 Qualitative Validation against Existing Literature

The model developed was also applied to other published culture systems where oxygen concentration was measured to validate the workings of this model. The literature search to find these publications was conducted by searching for 'oxygen concentration in 2D culture', papers which didn't include the input data required to use this model were excluded. Papers were selected where oxygen concentration had been measured in a 2D culture system, all systems evaluated used different cell types which also shows the versatility of the model. The results of these comparisons are shown in Table 4-3 below.

Table 4-3 – Validation of 2D model against other modelled systems

Cell Type	Oxygen Consumption rate (mol/s.Cell)	Seeding Density (cells/mm ²)	Oxygen Concentration (mol/m ³)
MSC	2.16243E-18	1.56E+01	0.214
		3.74E+03	0
rat-CMs	8.05556E-17	1.56E+01	0.214
		3.74E+03	0
hiPSC-CMs	1.52778E-16	1.56E+01	0.214
MIN6	1.06667E-14	1.56E+01	0

A study using a pancreatic β cell line (MIN6) found hypoxia evidenced by HIF-1 α and pimonidazole (Sato, et al., 2011). These cells have a higher oxygen consumption rate than MSCs at 1.07×10^{-14} mol/s compared to 2.16×10^{-18} mol/s for MSCs, this then translates into oxygen depletion being predicted by the 2D model (Table 4-3).

The spatial distribution of oxygen within 2D culture was measured (Kagawa, et al., 2015) using neonatal rat cardiomyocytes (rat-CMs) and human induced pluripotent stem cell derived cardiomyocytes (hiPSC-CMs). This paper found oxygen gradients within petri dish culture but did not find complete depletion. The oxygen consumption rates of rat-CMs and hiPSC-CMs are both higher than MSCs at 8.06×10^{-17} mol/s and 1.53×10^{-16} mol/s but not as high as the MIN6 cells above. The cardiomyocytes were also seeded and cultured more densely than the MSCs, the rat-CMs are seeded at 3.74×10^3 cells/mm² whereas the MSCs were seeded at 1.56×10^1 cells/mm². The oxygen consumption and more dense culture are both the cause of the gradient observed in this paper. The model derived in this section predicts that if the cardiomyocytes were seeded at the same density as the MSCs then the gradients would not be present (Table 4-3).

4.5 Discussion

Standard culture for MSCs is monolayer culture, oxygen concentration during these cultures is stable at the solubility limit. Other 2D culture systems using denser and/or cells with higher oxygen consumption rates can experience hypoxia which can also be predicted using this mathematical model. High glucose (25 mM) media poses no risk of glucose depletion in normal media change regimes but does obviously reduce in concentration over time, whereas a low (5mM, body concentration) glucose starting concentration would encounter depletion in normal media change regimes.

The findings presented in this chapter show that:

- A mathematical model can be successfully developed to represent the nutrient availability in 2D culture.
- This model is applicable to a range of different cell types in 2D culture and can be used to compare different cell types.
- This model can be used a predictive tool for 2D culture systems to analyse the effect of cell number, media concentrations of nutrients and media change regimes.
- This model can be used in conjunction with the 3D models also developed to compare culture conditions.

Chapter 5 Cell Spheroid Studies and Bone Tissue Models

5.1 Introduction

Existing mathematical models of nutrients in 3D tissue culture have included models of spheroids, scaffolds and other 3D constructs, these have shown that spatial modelling of these systems is possible and can provide information on the likelihood of nutrient depletion occurring within a structure. These models have shown that in some systems depletion can occur and in others there is no depletion. The models and data developed in this chapter build upon the 2D model (described in Chapter 4) to assess the availability of oxygen and glucose in 3D culture and in bone marrow.

The specific aims were to develop a mathematical model which predicted the oxygen and glucose concentration at different distances through the spheroid, incorporated the changing size of the spheroid and could be easily adapted for different cell types and nutrients. The second aim was to develop a model to predict the oxygen and glucose concentration in bone marrow and compare these concentrations to the culture conditions. Additionally, the impact of the different concentrations on the proliferation, size and differentiation capability of MSCs was assessed.

5.2 Extension of 2D Model to Cell Spheroids

Mass transfer in spheroid culture has another stage of transfer when compared to monolayer culture as the cells are aggregated into a ball which the oxygen and glucose need to diffuse through (Figure 5-1).

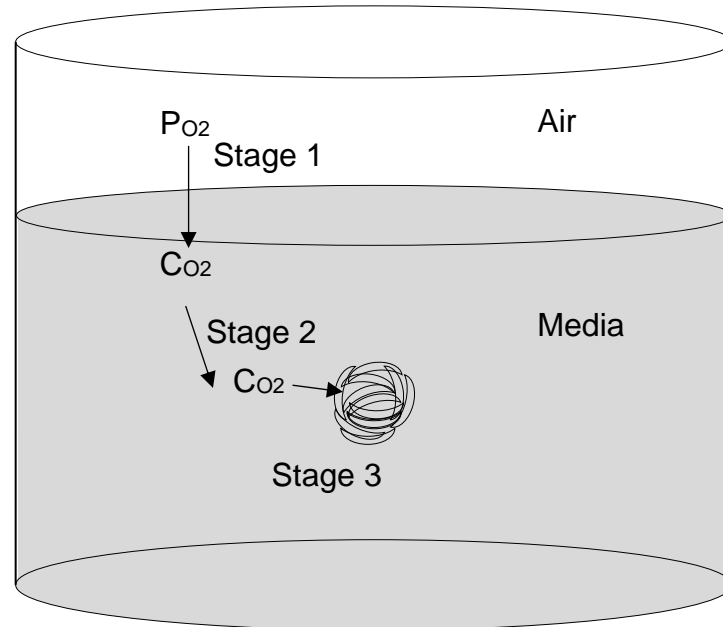


Figure 5-1 – Schematic of spheroid mass transfer

5.2.1 Oxygen

The oxygen concentration in the media can be found in the same way as for 2D culture (equation 4.6), the oxygen concentration in the spheroid then needs to be calculated. In the spheroid oxygen will diffuse from the media through the spheroid with cells using some along the way. Starting with equation 4.2 a similar process can be followed as in monolayer culture.

$$\text{Oxygen in} - \text{Uptake} \pm \text{Accumulation} = 0 \quad (4.2)$$

The diffusion rate through the spheroid is described by equation 5.1 which is again based on Fick's law.

$$N_A = \frac{D_c}{r_s} (C_{media} - C_s) A_s \quad (5.1)$$

Where;

D_c = Diffusion coefficient for oxygen through the spheroid (m^2/s)

r_s = Radius of spheroid (m)

C_{media} = Oxygen concentration in the media (mol/m³)

C_s = Concentration in middle of spheroid (mol/m³)

A_s = Surface area of the spheroid (m²)

Using a mass balance, the diffusion, uptake and accumulation terms are assembled.

$$\frac{D_c}{r_s}(C_{media} - C_s)A_s - U \pm \frac{dC_s}{dt} = 0$$

Let;

$$\alpha = \frac{D_c}{r_s} A_s$$

Therefore,

$$\alpha(C_{media} - C_s) - U = \frac{dC_s}{dt}$$

$$\alpha C_{media} - \alpha C_s - U = \frac{dC_s}{dt}$$

Let;

$$\beta = \alpha C_{media} - U$$

Therefore,

$$\beta - \alpha C_s = \frac{dC_s}{dt}$$

$$\int \frac{dC_s}{\beta - \alpha C_s} = \int dt$$

$$\frac{\ln(\beta - \alpha C_s)}{-\alpha} = t + K$$

K is the integration constant, this can be calculated at initial conditions of t=0, C=C_{media} (without cells).

$$C_s = \frac{\beta - e^{-\alpha(t+K)}}{\alpha}$$

$$C_s = \frac{\frac{D_c}{r_s} A_s C_{media} - U - e^{-\frac{D_c}{r_s} A_s (t+K)}}{\frac{D_c}{r_s} A_s} \quad (5.2)$$

5.2.2 Glucose

The mass transfer of glucose into the spheroid can be represented by the same equation as oxygen, changing the diffusion coefficient and uptake rate.

5.3 Cell Spheroid Model Input Data

The spheroids undergo a change in size as previously documented in (Pennock, et al., 2015), therefore the change in spheroid size needed to be measured for multiple

parameters in the spheroid model. Figure 5-2 shows the size change in spheroid and cell diameter for four cell types; Y201s an immortalised mesenchymal stromal cell line (MSC) as detailed in (James, et al., 2015), human dermal fibroblasts (HDFs), primary MSCs isolated from a knee (K139) and Y202s another immortalised MSC line.

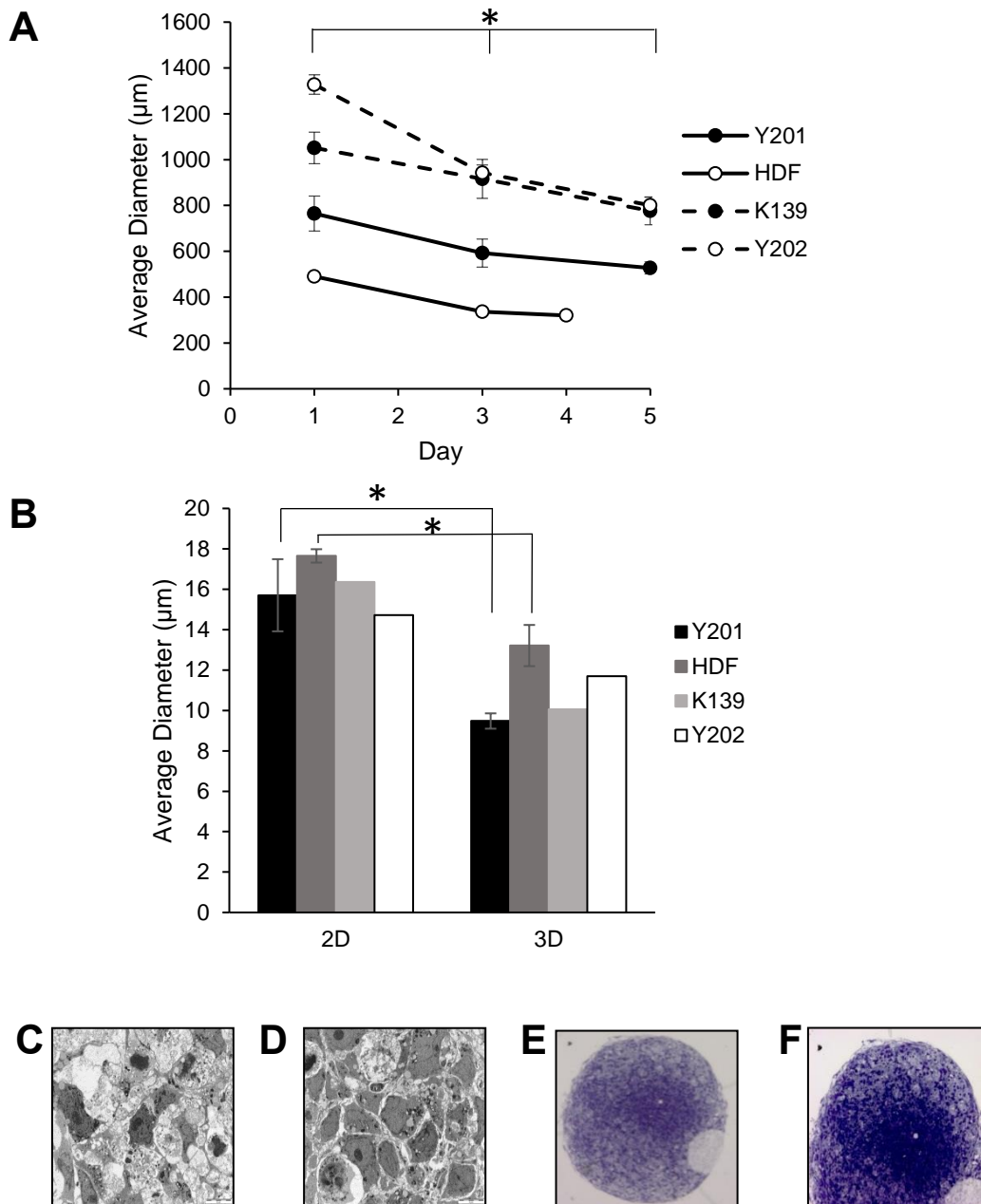


Figure 5-2 – Size change analysis of spheroids during 3D culture. A - size change of spheroids measured by bright field microscopy, Y201, Y202 and K139 spheroids containing 60,000 cells and HDF spheroids containing 30,000 cells, error bars represent SEM and are present for all cell lines however not visible for HDFs. B – Size change of cells during 3D spheroid culture after 5 days for Y201, Y202 and K139, and after four days for HDF spheroids, measured after disaggregation by vicell analysis. n too low for error or statistical analysis for K139 and Y202 cells. C – Transmission electron microscopy image of an outer section of a Y201 spheroid on Day 5 at 2.55K magnification, D – Transmission electron microscopy image of a centre section of a Y201 spheroid on Day 5 at 2.55K magnification, E – Toluidine blue stained image of a Y201 spheroid on Day 5 at 10x magnification, F – Toluidine blue stained image of a Y201 spheroid on Day 5 at 20x magnification. * signifies a P value < 0.005.

All cell types experienced a reduction in cell and spheroid size during the cultures (Figure 5-2). With Y202 spheroids being the largest spheroids but not the largest cells, Y201s are a similar size cell to the K139 primary MSCs however the spheroid size of the primary MSCs is closer to the size of the Y202 spheroids than the Y201s. The HDFs form the smallest spheroids with the largest cells as the number of cells in an HDF spheroid is half the amount used in the other spheroids. The cell numbers used in these spheroids were previously optimised for peak de-differentiation markers as in (Pennock, et al., 2015). TEM microscopy and toluidine blue staining shows the Y201 spheroid is denser in the middle and less dense towards the edge of the spheroid.

The relationship between cell size and spheroid size can be described by the voidage, which is the volume of the spheroid not occupied by the cell volume. This was calculated by deducting the volume of cells from the spheroid volume, the cell volume was calculated from the cell diameter measurements then multiplied by the cell density used to seed the spheroids, the spheroid volume was calculated from the spheroid diameter measurements taken. The same spheroids were used for spheroid and cell size measurements. Assumptions include, constant cell number and equal distribution of cells. The proportion of voidage affects diffusion through the spheroid and therefore alters the effective diffusion coefficient, the change in voidage during culture and the subsequent change in diffusion coefficient for the different cell types are shown in Figure 5-3.

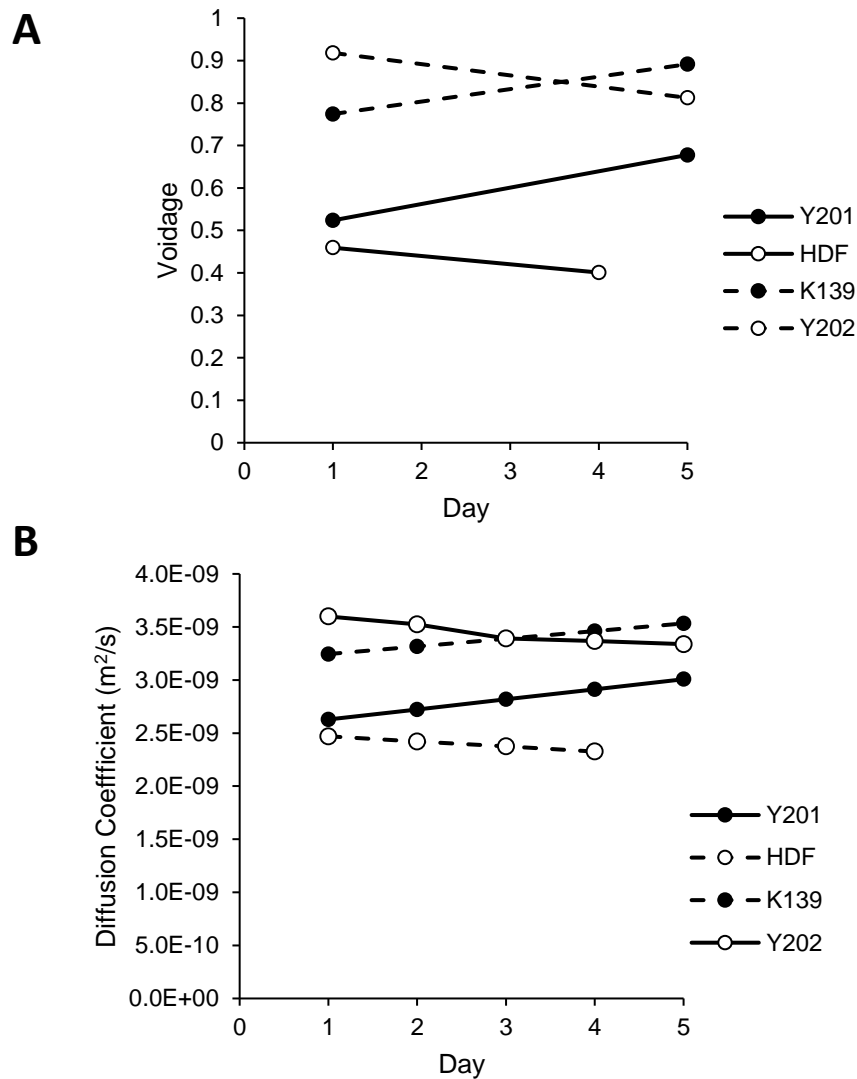


Figure 5-3 – Voidage and diffusion coefficient changes for Y201, HDF, K139 and Y202 spheroids throughout culture.

A – Voidage change over the spheroid culture calculated from spheroid and cell sizes. B – Diffusion coefficients calculated using voidage figures.

While the spheroid and cell size decrease for all the cell types the ratios at which they decrease show differences in voidage change patterns. The voidage for Y201 and K139 spheroids increases over the spheroid time course however the voidage for the Y202 and the HDF spheroids decreases, this then translates to the trends in the diffusion coefficients. Y201 and K139 spheroids become less dense over the culture whereas the Y202 and HDF spheroids become denser. Throughout the cultures the HDF are consistently the densest whereas the Y202 spheroids start as the least dense and the K139 spheroids finish the least dense.

The diffusion coefficients shown in Figure 5-3 are calculated using the voidage values to ratio the diffusion coefficient for oxygen through media and the diffusion coefficient for oxygen through cell membranes, the value for diffusion through media is $3.8 \times 10^{-9} \text{ m}^2/\text{s}$ (Curico, et al., 2014) and the value for diffusion through cell membranes is $1.34 \times 10^{-9} \text{ m}^2/\text{s}$ (Subczynski, et al., 1992). The smaller the diffusion coefficient the slower the rate of diffusion due to more resistance in the mass transfer, as the coefficient for transfer through membranes is lower than the coefficient for transfer through media the denser the spheroid the more resistance to oxygen transfer.

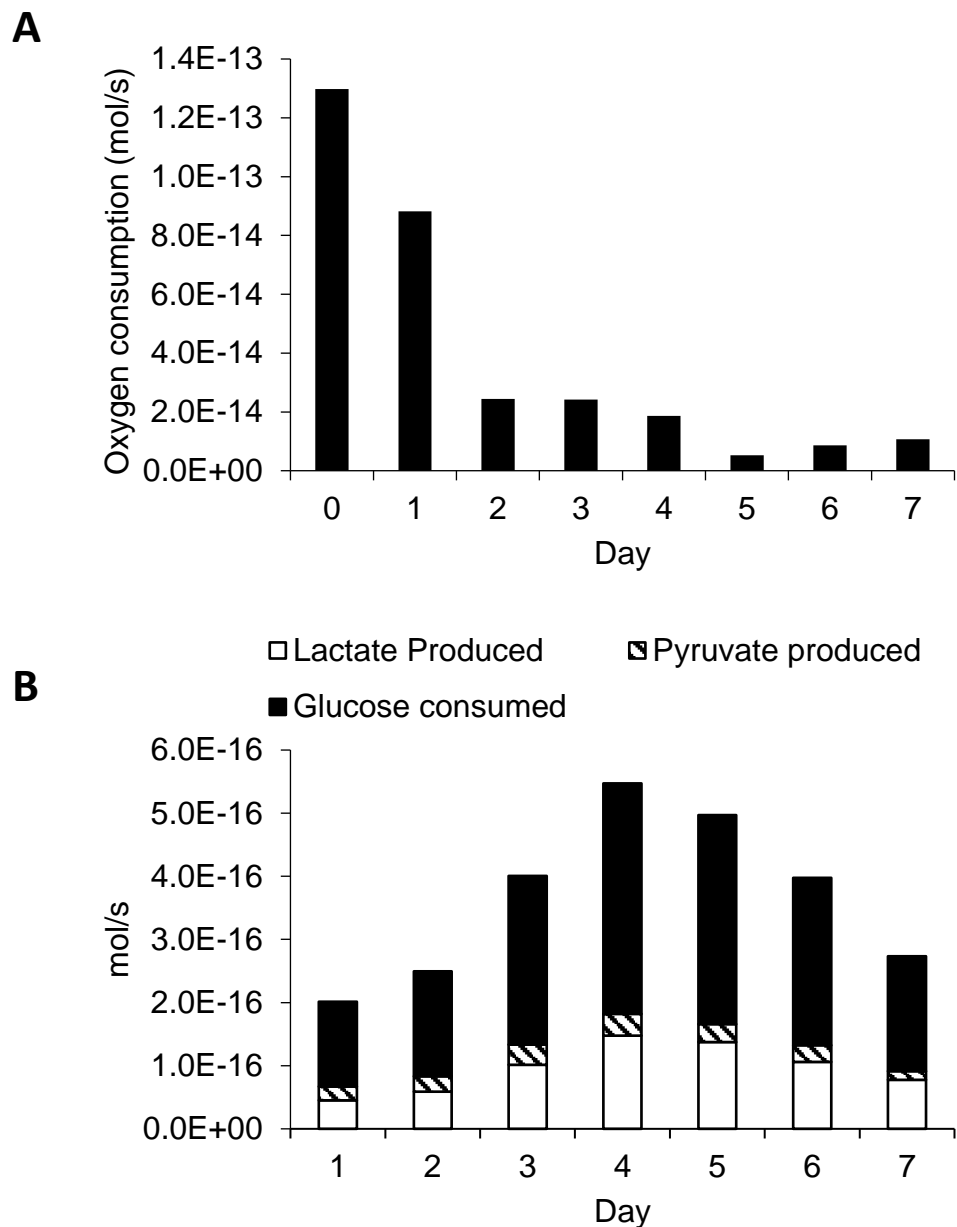


Figure 5-4 – Oxygen and glucose consumption rates measured in primary MSCs. A – Oxygen consumption rate. B – Glucose consumption rates as calculated from lactate and pyruvate production rates.

Oxygen and glucose consumption rates were measured previously (Pennock, et al., 2015 and unpublished data). The oxygen consumption decreases during the spheroid culture with the lowest consumption rate on day 5. Glucose consumption rates were based upon the production of lactate and pyruvate, each mole of lactate produced uses 2 moles of glucose similarly each mole of pyruvate produced also

uses 2 moles of glucose (Berg, et al., 2002). The glucose consumption increases towards the middle of the culture but then decreases after peaking on day 4.

5.4 Spheroid Model Predictions

The models from section 5.2 and the input data from section 5.3 were then used together to predict the oxygen and glucose concentration in spheroid culture. Initially the concentration in the centre of the spheroid was analysed followed by further analysis of the concentration throughout the spheroids. Oxygen and glucose concentrations were predicted for MSC, Y201, Y202 and HDF spheroids. The analysis of the oxygen concentration in the centre of MSC spheroids is shown in Figure 5-5.

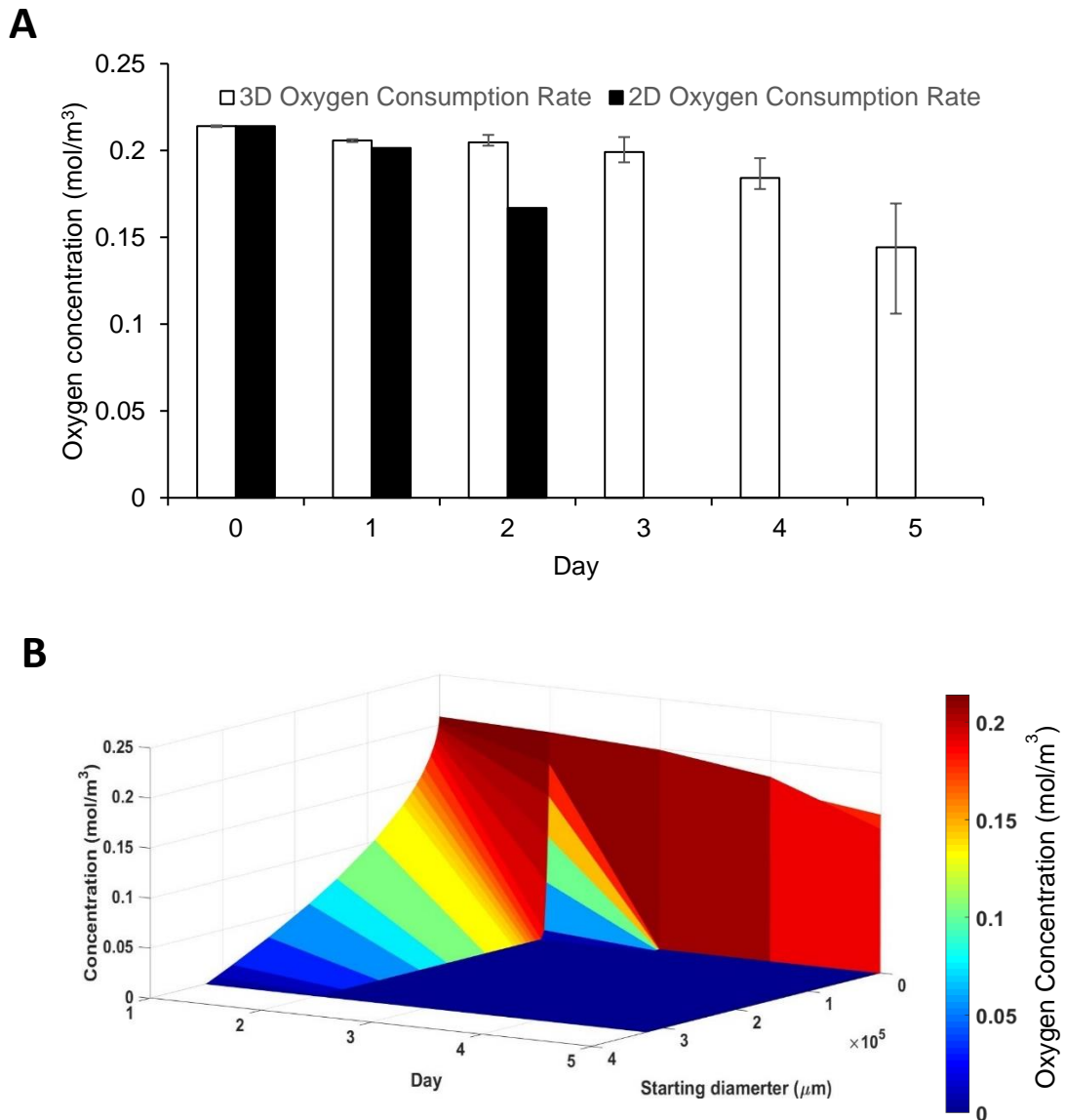


Figure 5-5 – Predicted oxygen concentrations in the centre of MSC spheroids. A – Concentration in the centre of MSC spheroids during culture with 3D oxygen consumption rates and if 2D oxygen consumption rates were maintained, error analysis is included for 3D oxygen consumption rates B – Analysis of how big a spheroid would need to be before oxygen concentration in the centre would become hypoxic, colour scale indicates oxygen concentration.

As shown in graph A on Figure 5-5 the predicted oxygen concentration in the centre of MSC spheroids does not show oxygen depletion, although the oxygen concentration is less than in 2D culture. As shown in Figure 5-4 the oxygen consumption rate in spheroid culture is less than in 2D culture, this is then reflected

in graph A of Figure 5-5 which shows that if 2D consumption rates were maintained during spheroid culture the centre of the MSC spheroid would experience oxygen depletion after day 2 of culture. The timescale for oxygen consumption reducing is similar to the timescale that oxygen concentration would decrease if the higher consumption rate was maintained, therefore it is not clear from this information alone whether the consumption rate reduces in response to the mass transfer restrictions to conserve oxygen or whether there is another cause. Graph A shows error analysis of the model using 3D oxygen consumption rates, the main causes of error in the model comes from error in the spheroid diameter especially as this measurement is used to calculate voidage volumes, the error is not a constant value as the model is not linear. Error was calculated by combining the error ranges in the input data using methodology described in (Pentz & Shott, 1989).

Graph B (Figure 5-5) depicts the analysis of how big a spheroid would need to be for depletion to occur, depletion after day 3 starts to occur once the spheroid is over 1.4mm, on day 2 at 13mm and day 1 at 323mm, the standard size used in spheroid culture is ~ 1mm, this analysis was done using the oxygen consumption for spheroid culture and as previously mentioned if 2D oxygen consumption was maintained the oxygen concentration would deplete at a much smaller sized spheroid.

Predicted oxygen concentration throughout MSC spheroids is shown in Figure 5-6.

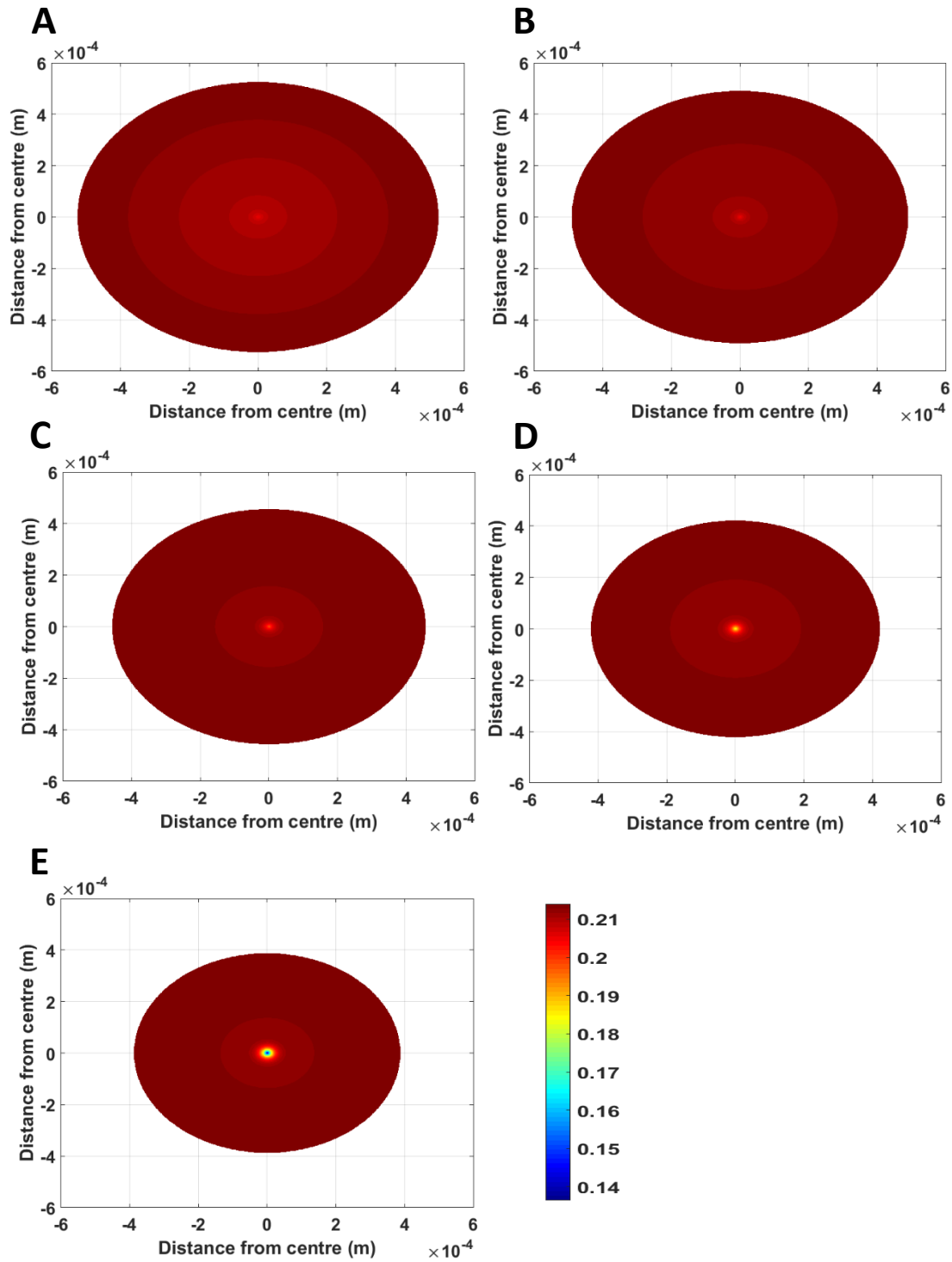


Figure 5-6 – Predicted oxygen concentrations throughout the MSC spheroid. Calculated by using derived mass transfer equations from Henry’s and Fick’s law. A – Day 1, B – Day 2, C – Day 3, D – Day 4, E – Day 5. Colour scale representing the oxygen concentration (mol/m³) set to the same scale for each graph.

Analysis of the oxygen concentration throughout the MSC spheroid shows that the oxygen concentration for most of the spheroid is close to levels in 2D culture and that only the centre sees the slight dip shown in Figure 5-5. Oxygen concentrations were

also predicted in spheroids of different cell lines; Y201s and Y202s both clonal immortalised MSC lines and HDFs (Human dermal fibroblasts), the results of which are shown in Figure 5-7.

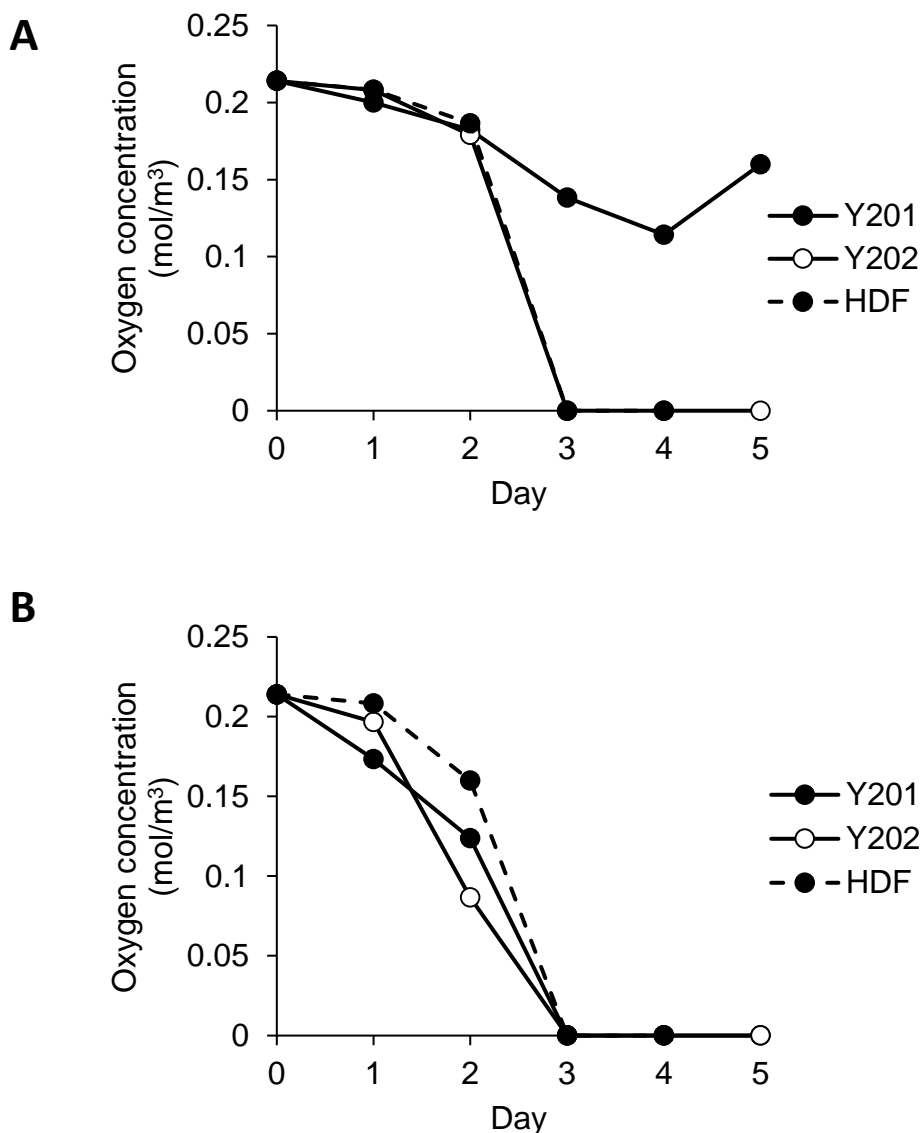


Figure 5-7 – Predicted oxygen concentrations in the centre of Y201, Y202 and HDF spheroids. Calculated using mass transfer equations derived from Henry’s and Fick’s Laws. A – Uses oxygen consumption of cells during 3D spheroid culture with voidage accounted for in the diffusion rates, B – Uses oxygen consumption of cells cultured in conventional 2D culture and voidage is accounted for in the diffusion rates.

The oxygen concentration in the centre of Y201 spheroids closely follows the concentration in primary MSC spheroids and shows no depletion during the spheroid culture. However the Y202 and HDF spheroids are predicted to experience oxygen depletion in the centre from day 3 onwards, all three cell lines would experience depletion from day 3 if 2D consumption rates were sustained during spheroid culture which is the same as the centre of MSC spheroids under 2D consumption rates. The concentrations throughout Y202 spheroids was predicted and shown in Figure 5-8 to analyse the extent of the oxygen deprivation.

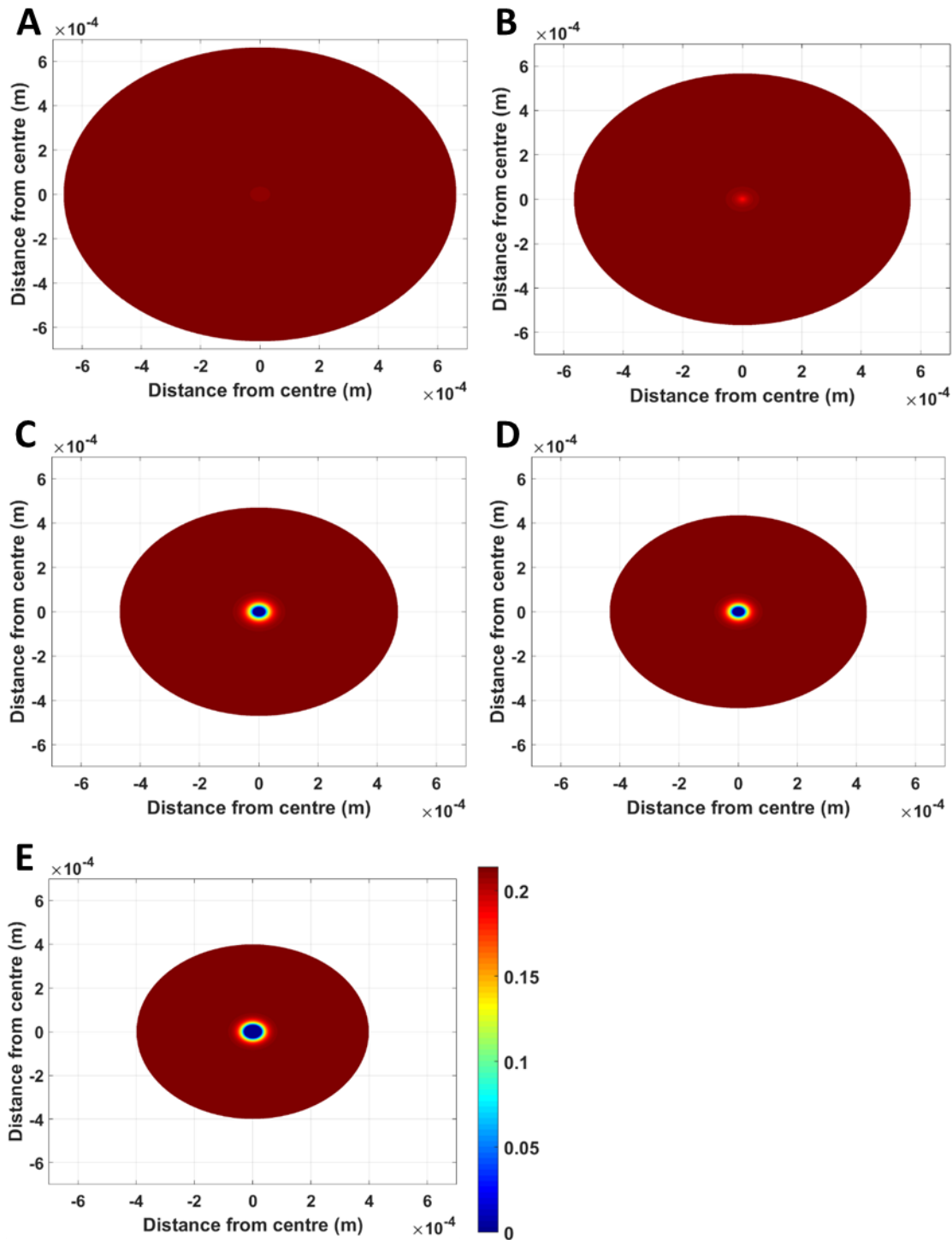


Figure 5-8 – Predicted oxygen concentrations throughout the Y202 spheroid. Calculated by using derived mass transfer equations from Henry’s and Fick’s law. A – Day 1, B – Day 2, C – Day 3, D – Day 4, E – Day 5. Colour scale representing the oxygen concentration (mol/m^3) set to the same scale for each graph.

Figure 5-8 shows the oxygen deprivation in Y202 spheroids only effects the very centre of the spheroid and most of the spheroid will not experience oxygen deprivation. This paints a different picture than just looking at centre concentrations alone as only a small percentage of cells will be experiencing oxygen deprivation, the

largest proportion of cells experiencing deprivation is on day 5 but the majority of a day 5 spheroid does not experience depletion. The Y202 spheroids are the largest spheroids which means the greatest distance for oxygen to travel, these spheroids also become more dense over the culture which also impedes oxygen transport, the other spheroids which experience deprivation in the centre are the HDFs, these spheroids are the densest spheroids with the most resistance to oxygen transfer. Whether depletion occurs is dependant on the cell type even for similar sized spheroids and similar types of cell, the supply of oxygen is very situation specific, this model provides a good resource to predict oxygen concentration in many different spheroids.

Glucose concentrations were also predicted for spheroid culture, starting with concentrations in the media, followed by the concentration in the centre of MSC spheroids then the concentration throughout MSC spheroids. Glucose concentration was also predicted for Y201, Y202 and HDF spheroids. The glucose concentration in media for spheroid culture under different media change routines was predicted and shown in Figure 5-9.

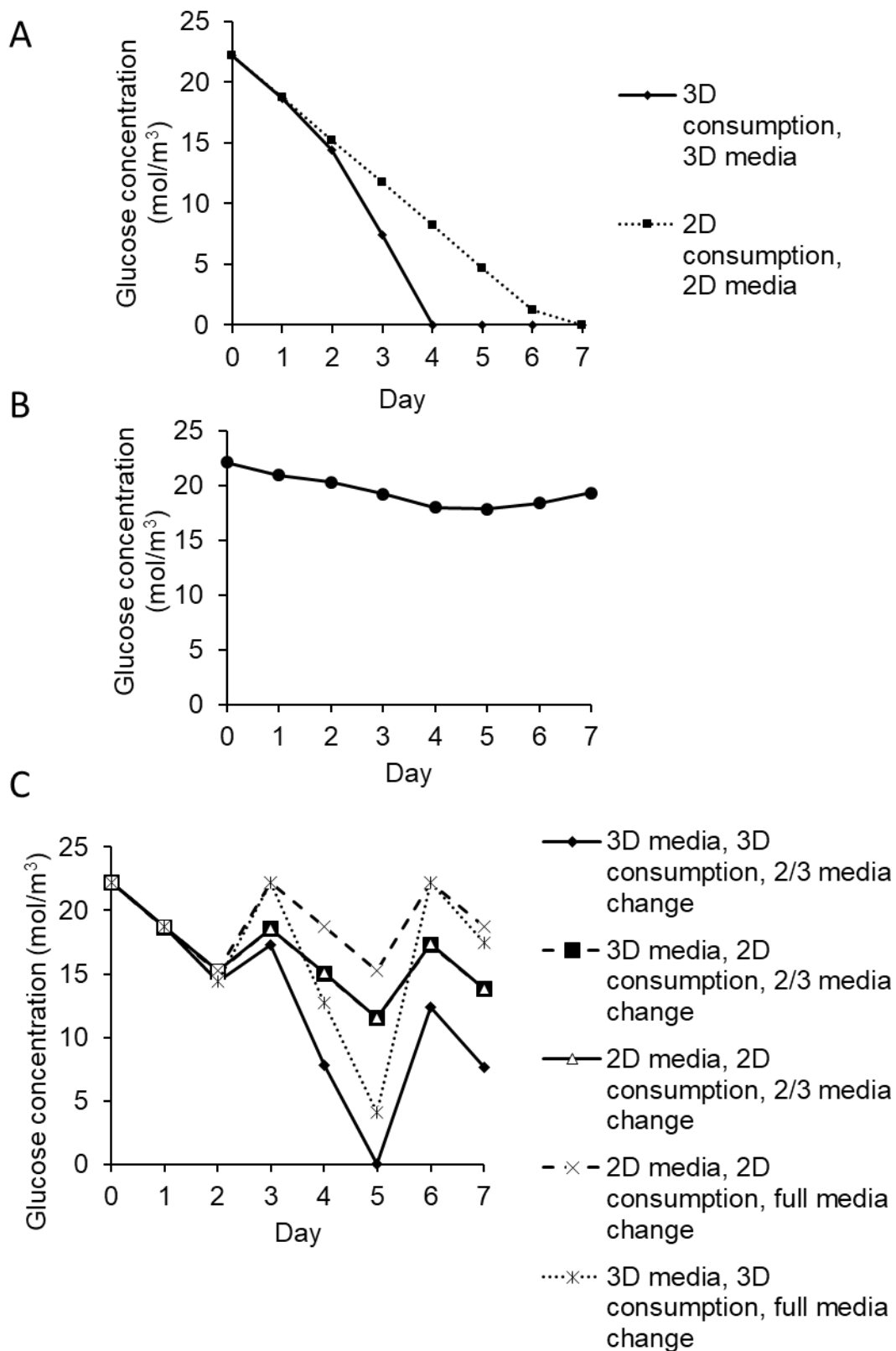


Figure 5-9 – Predicted glucose concentrations in media for MSCs.
 A – Concentration in the media with no media changes, B – Concentration in the media with partial media changes every day, C – Concentration in the media with media changes on days 3 and 6.

The concentration of glucose in the media was predicted in multiple scenarios as shown in Figure 5-9. The first graph (A) shows predicted concentrations when the media is not changed throughout the culture, this shows depletion in the spheroid (3D) case after 4 days whereas if 2D consumption rates were maintained it would be 7 days, this is due to the increase in glucose consumption which peaks on day 4 as shown in Figure 5-4. Graph B shows the media concentration can be kept stable if partial (2/3) media changes are performed every day. During normal culture conditions media is usually changed every 3-4 days, graph C shows the predicted concentrations when media is changed on day 3. The only scenario which predicted depletion was the conditions used most commonly which was a spheroid in 3D media with a 2/3 media change on day 3, a full media change would remove this however a full change can be difficult to achieve without damaging the spheroid. The media used in 2D culture has a slightly higher glucose concentration as methylcellulose is added to this media to create the 3D media.

Concentrations in the centre of the spheroids is shown in Figure 5-10.

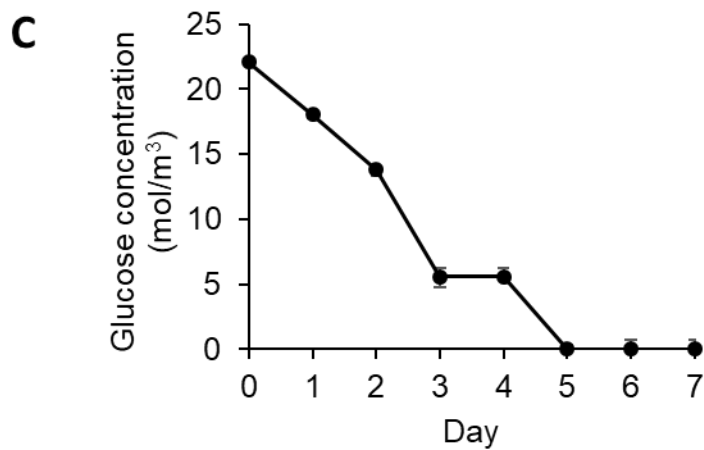
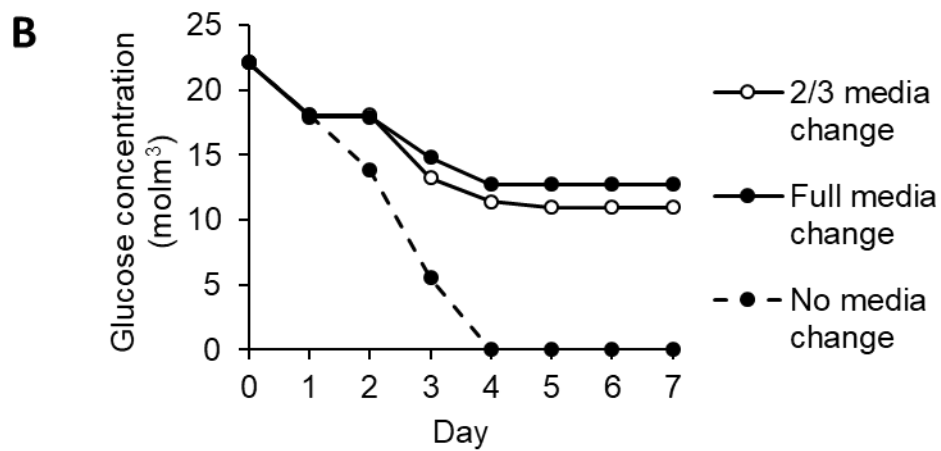
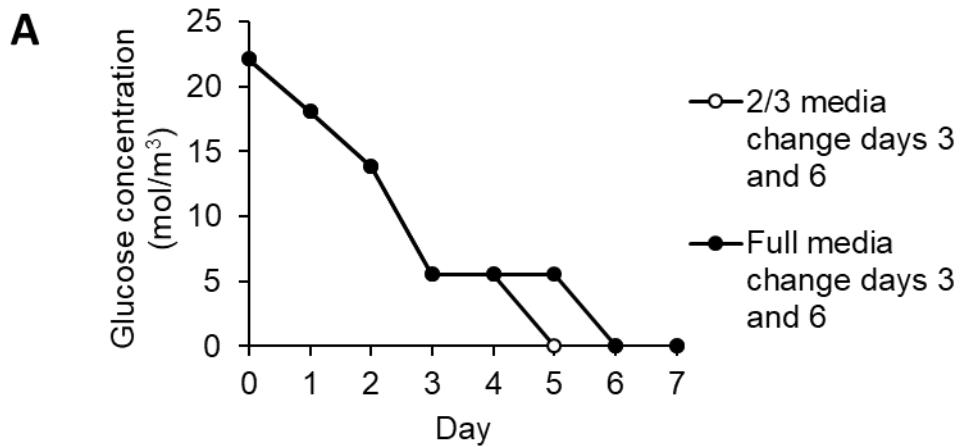


Figure 5-10 – Predicted glucose concentration in MSC spheroids calculated using mass transfer equations derived using Fick's law.
 A – Concentration in the centre of spheroids with media changes on days 3 and 6, B – Concentration in the centre of spheroids with either no media changes or media changes every day, C – Error analysis.

Concentrations in the centre of MSC spheroids as shown in Figure 5-10 are predicted to cause depletion whether the media is changed by 2/3 on days 3 and 6 (depletion from day 5) or full media changes on days 3 and 6 (depletion from day 6). As graph B shows this can be avoided by media changes every day and is exhausted to depletion from day 4 if no media changes are performed at all. Sensitivity analysis was carried out on the usual case of 2/3 media change on days 3 and 6 by using the accuracies of the input data and shows the error within this model is small, the percentage errors average 5.43% and increases over the time in culture due to the decreasing spheroid size (graph C). Further analysis was performed to assess the extent of the depletion as shown in Figure 5-11.

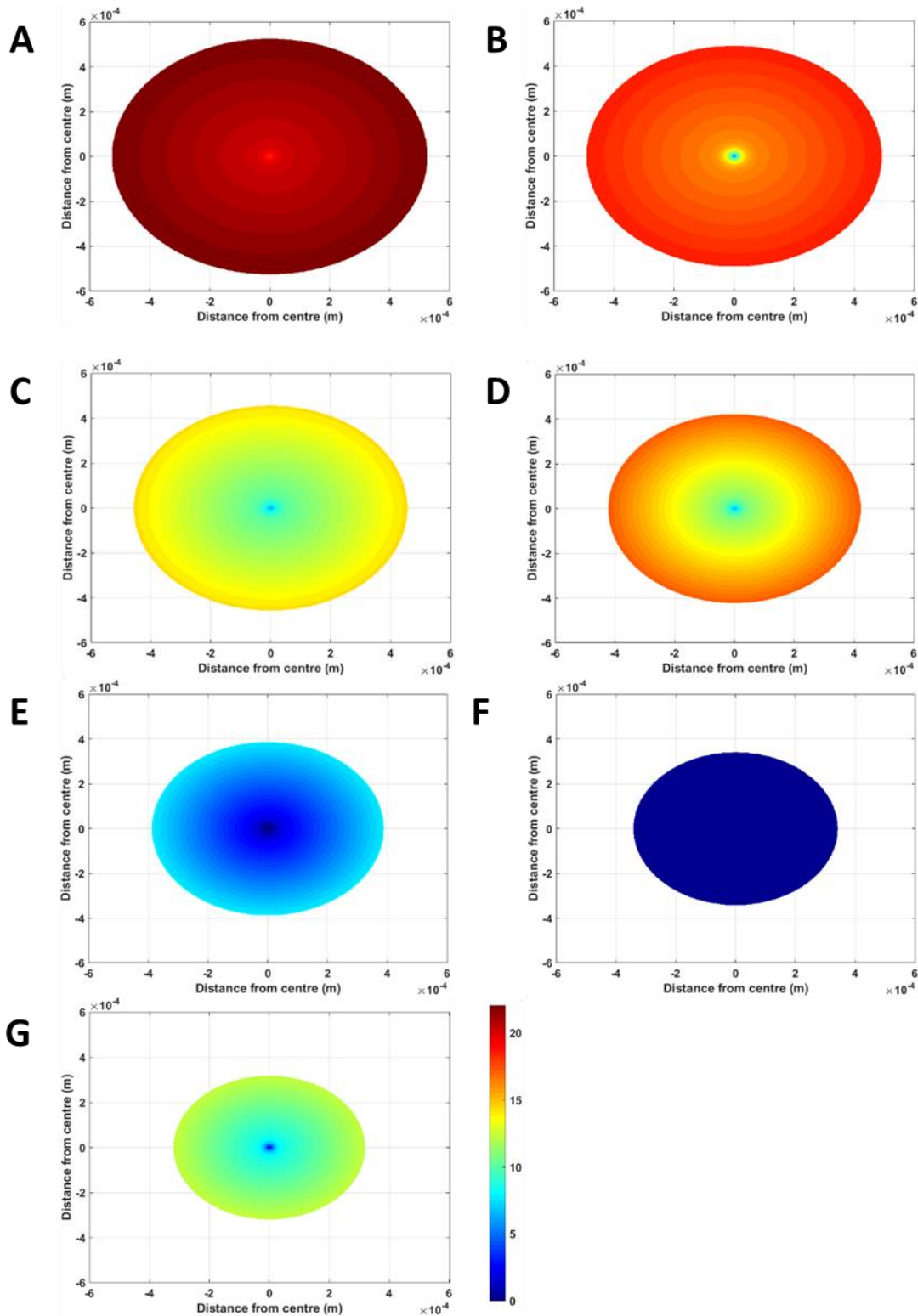


Figure 5-11 – Predicted glucose concentrations throughout the MSC spheroid with a 2/3 media change on days 3 and 6. Calculated using mass transfer equations derived from Fick’s law. A – Day 1, B – Day 2, C – Day 3, D – Day 4, E – Day 5, F – Day 6 and G – Day 7. Colour scale represents the glucose concentration set to the same scale for each graph.

The concentrations throughout the spheroid show that the concentration throughout the spheroid drops from day 1 and is low on day 5 before being completely depleted on day 6, then rising again on day 7 following the media change on day 6. Concentrations through the MSC spheroid were also calculated for the case of no media change, Figure 5-12.

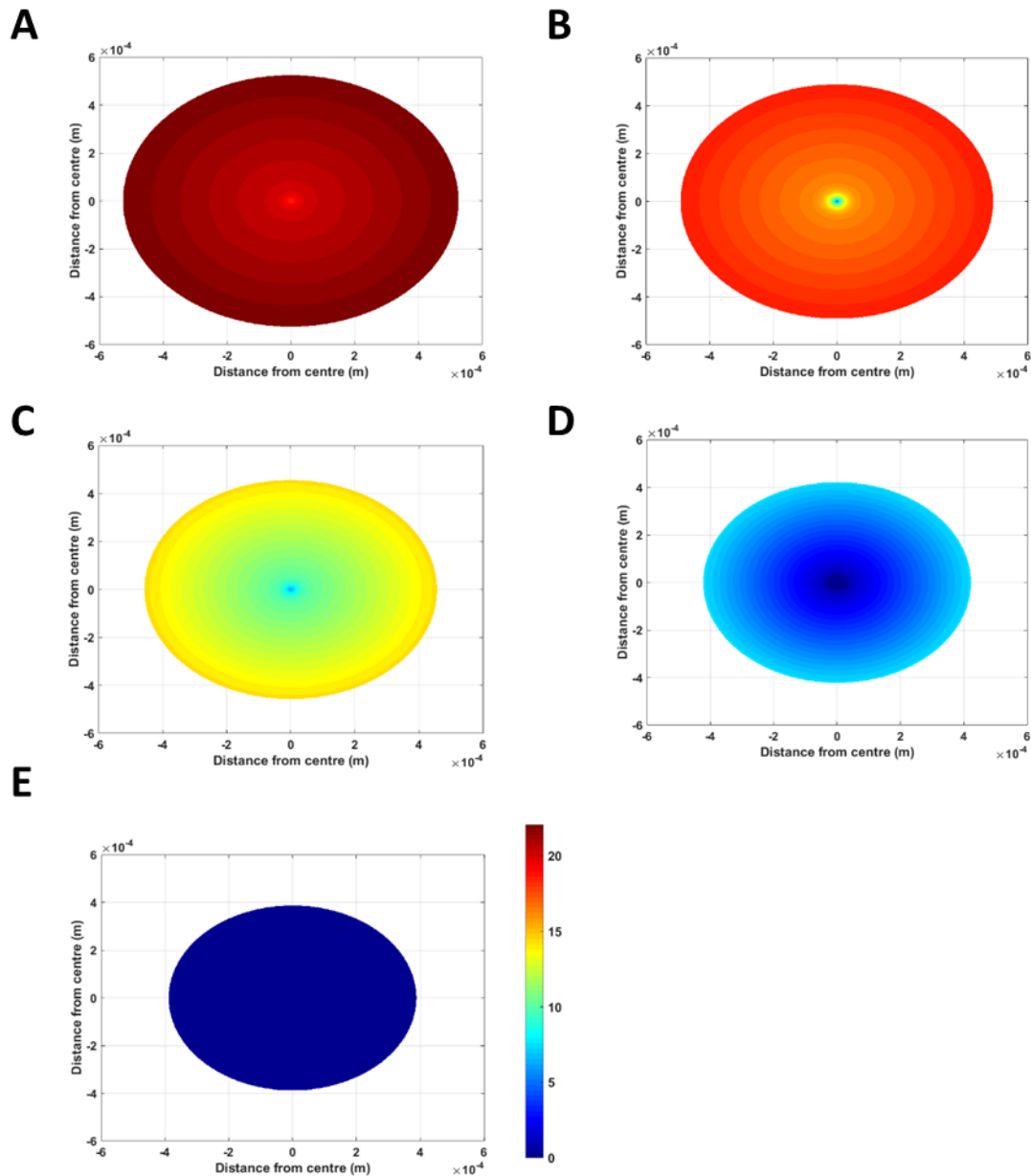


Figure 5-12 – Predicted glucose concentrations throughout the MSC spheroid with no media change during the culture. Calculated using mass transfer equations derived from Fick’s law. A – Day 1, B – Day 2, C – Day 3, D – Day 4, E – Day 5. Colour scale represents the glucose concentration set to the same scale for each graph.

As expected the glucose concentrations when no media changes are performed (Figure 5-12) are lower than when the media is changed 2/3 on days 3 and 6 (Figure 5-11). The concentrations until day 4 are the same as when the media is changed as the media change takes place after the concentrations on day 3 are predicted, the concentration on day 4 is lower without the media change than it is when the media has been changed and is completely depleted by day 5 which is a day earlier than when media changed.

The concentration throughout Y201, Y202 and HDF spheroids was calculated at various distances through the spheroids and is shown in Figure 5-13.

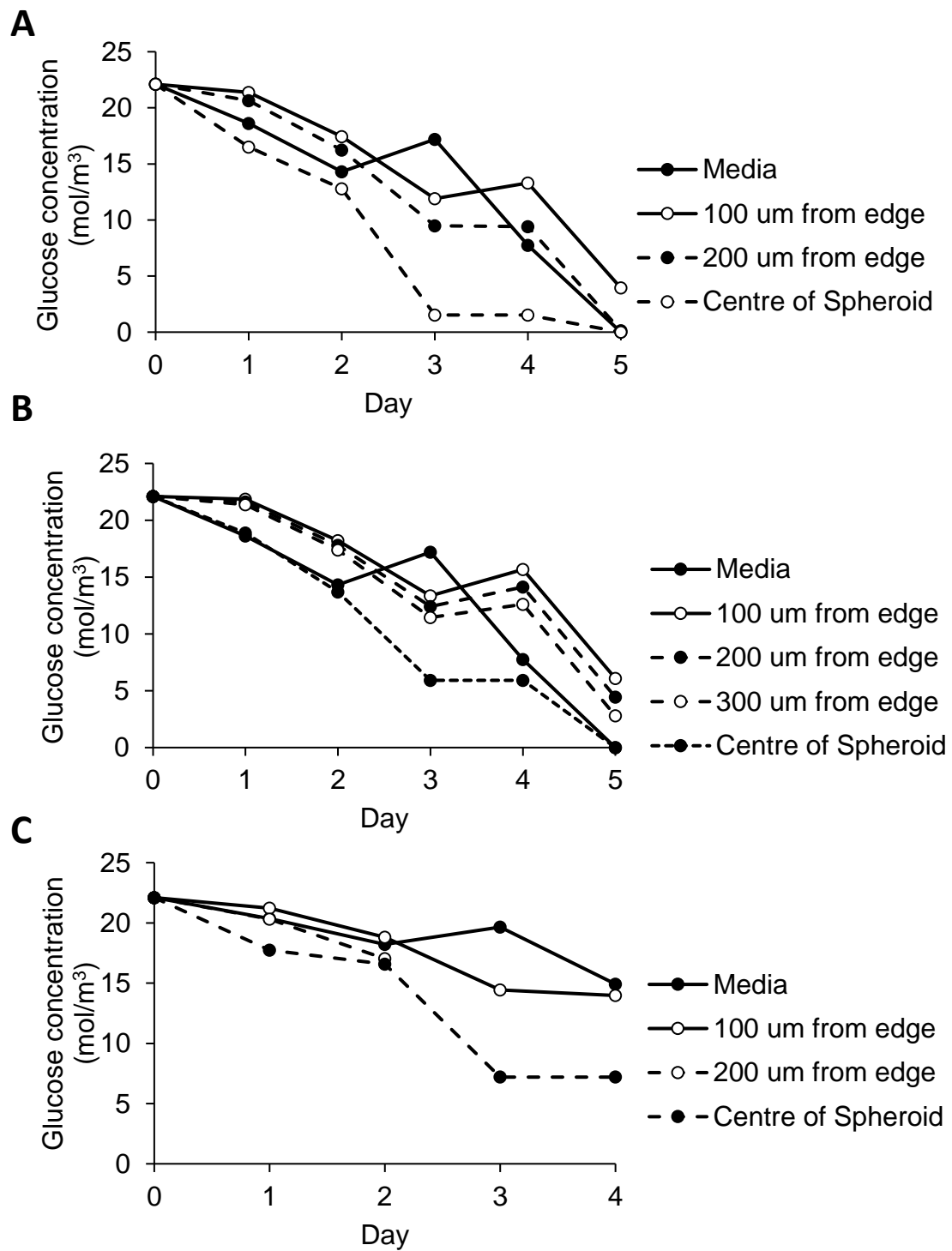


Figure 5-13 – Glucose concentrations throughout Y201, Y202 and HDF spheroids with a 2/3 media change on day 3. Calculated using mass transfer equations derived from Fick's law. A – Y201, B – Y202, C – HDF.

The concentrations within the Y201 spheroids are closest to the concentration in the MSC spheroids resulting in depletion in the centre on day 5, whereas the concentrations in the Y202 and HDF spheroids are higher, the concentration in the centre of Y202 spheroids still depletes on day 5 whereas the Y201 spheroids are depleted at greater than 100µm from the edge of the spheroid. The concentration in the HDF spheroids show no depletion throughout the culture and are the smallest spheroids. MSC and Y201 spheroids have similar oxygen and glucose concentration profiles, this is largely due to the size change also being similar over the culture.

The glucose concentration at the centre of Y201, Y202 and HDF spheroids under different media change conditions is shown in Figure 5-14.

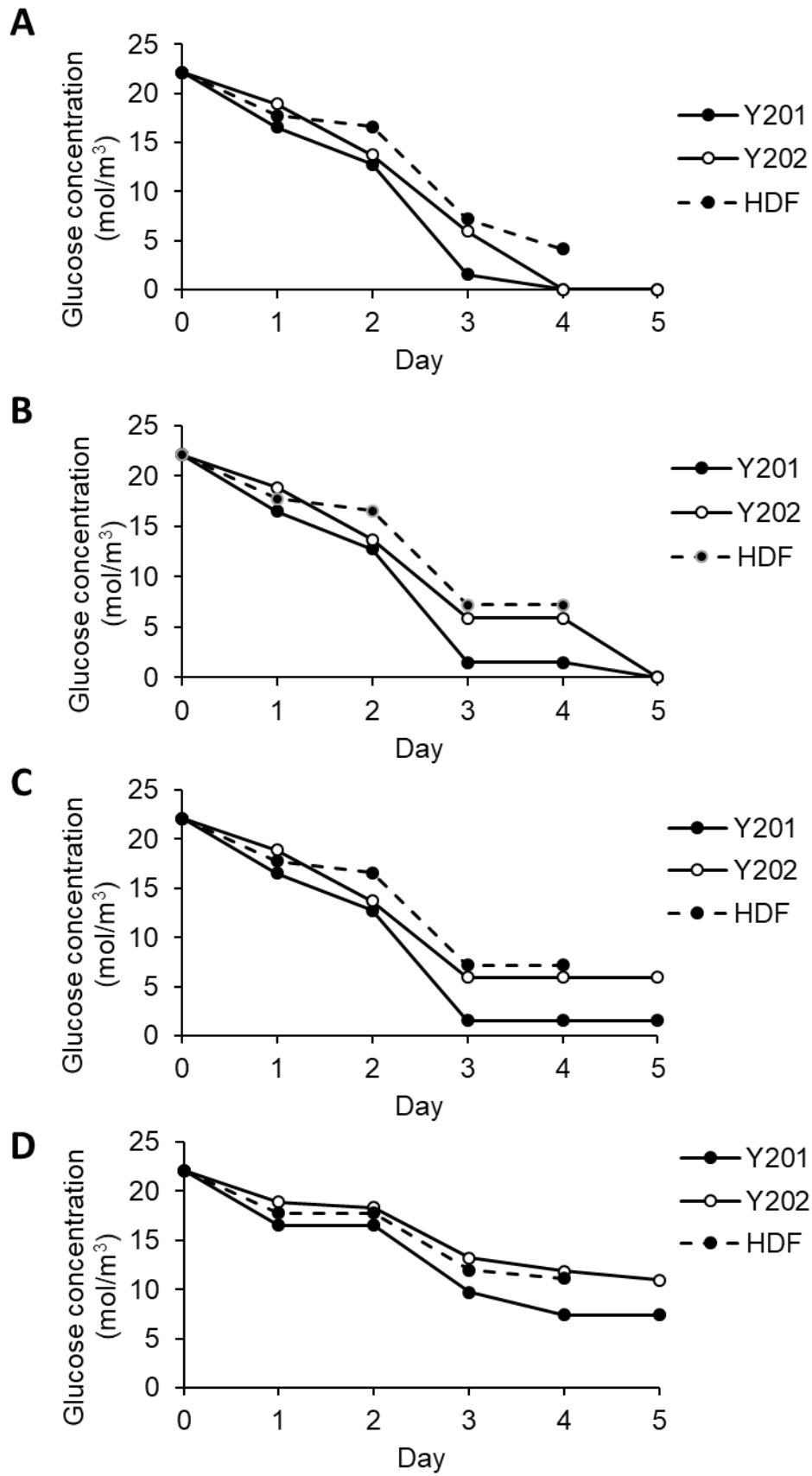


Figure continues next page.

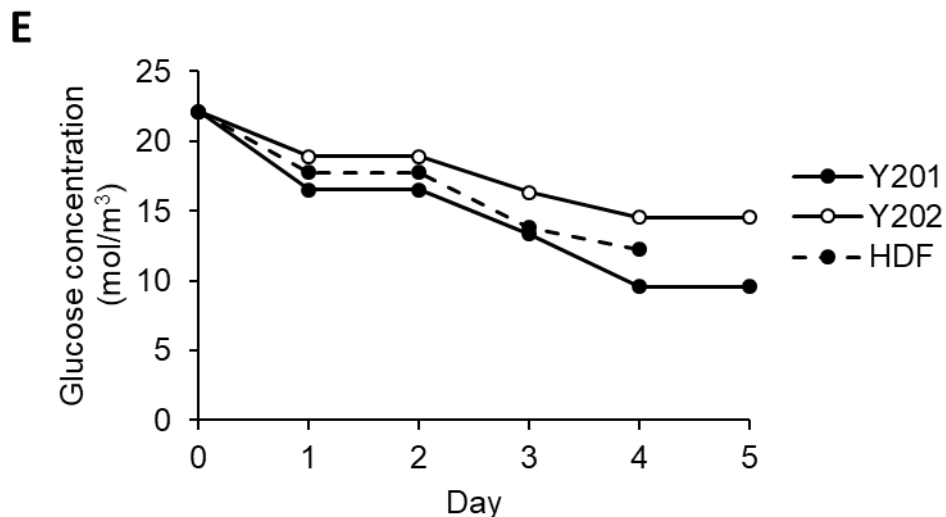


Figure 5-14 – Predicted glucose concentrations in Y201, Y202 and HDF spheroids. Calculated using mass balances and Fick’s law. A – Centre of Y201, Y202 and HDF spheroids with no media change, B – Centre of Y201, Y202 and HDF spheroids with 2/3 media change on day 3, C – Centre of Y201, Y202 and HDF spheroids with a full media change day 3, D – Centre of Y201, Y202 and HDF spheroids with a 2/3 media change every day, E – Centre of Y201, Y202 and HDF spheroids with a full media change every day.

The glucose concentrations under different media change routines as shown in Figure 5-14 differs for the different spheroids. Graph A shows that if no media change is performed the HDF spheroids are the only spheroids which do not experience glucose depletion whereas the Y201 and Y202 spheroids experience depletion in the centre from day 4. Graph B shows the concentrations when media is changed on day 3 with a 2/3 media change (normal culture procedure) as also shown in Figure 5-13 where only the Y201 spheroids experience depletion of glucose. Full media changes on day 3 (graph C) just about manage to keep the concentration above zero whereas graphs D and E show that media changes every day of either 2/3 (graph D) or full changes (graph E) keep the concentration high enough to avoid deprivation.

5.5 Experimental Glucose Concentration Studies in 2D and Suspension Cultures

In order to understand the effects of the predicted glucose levels in spheroid culture, a series of experiments was undertaken to vary glucose concentrations in 2D and suspension cultures. The effect of glucose over the range of concentrations predicted to be experienced in spheroid culture was assessed for metabolic activity and colony forming unit ability as shown in Figure 5-15 and Figure 5-16. In combination with the effect of glucose the effect of FBS concentrations was also assessed.

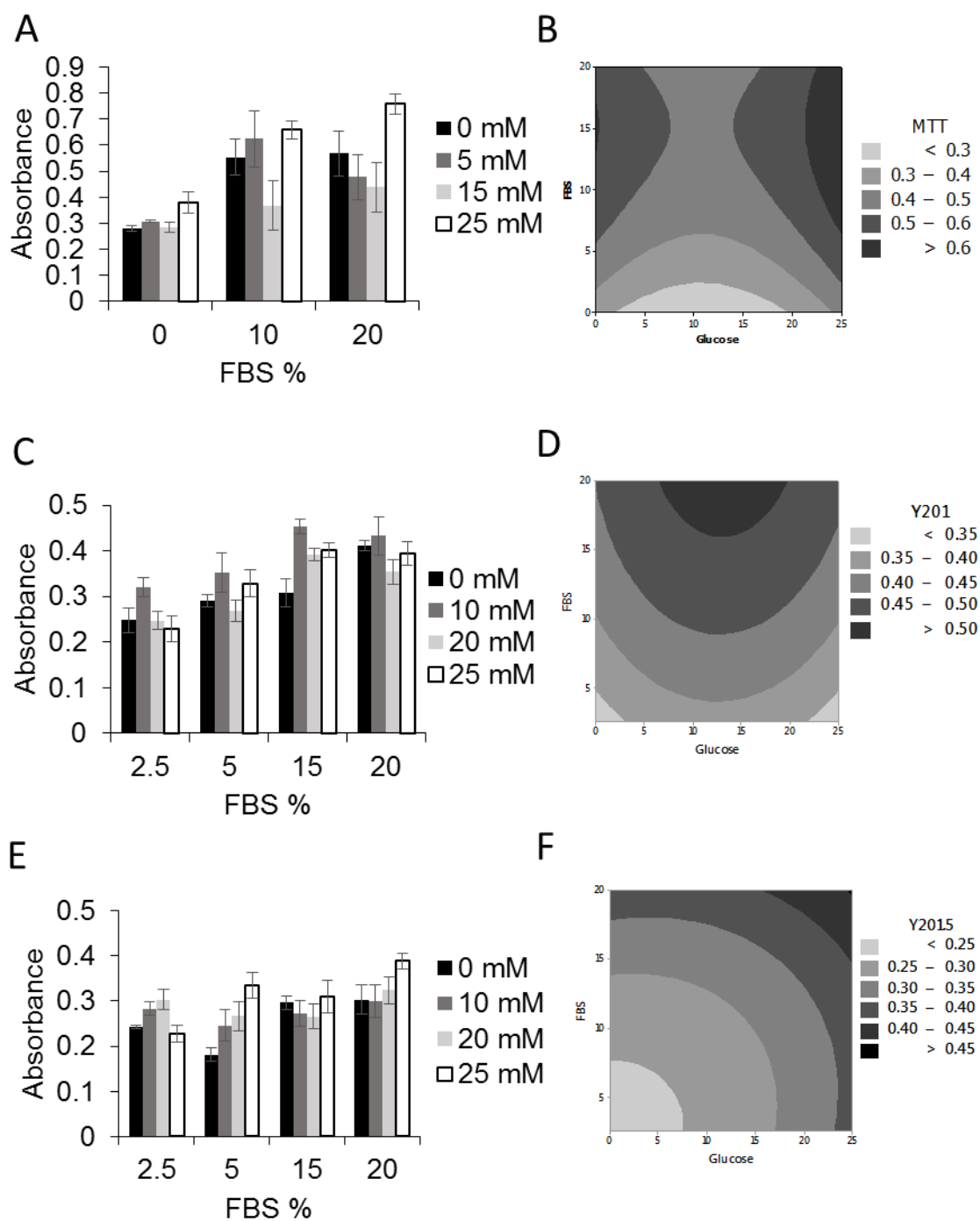


Figure 5-15 – Effect of glucose and FBS concentrations on the growth of Y201 and Y201.5 cells.

A – 72hr MTT Y201 n=6, B – Contour plot of absorbance for 72 hr Y201 MTT, C – 5 day MTT Y201 n=18, D – Contour plot of absorbance for Y201, E – 5 day MTT Y201.5 n=18, F – Contour plot of absorbance for Y201.5.

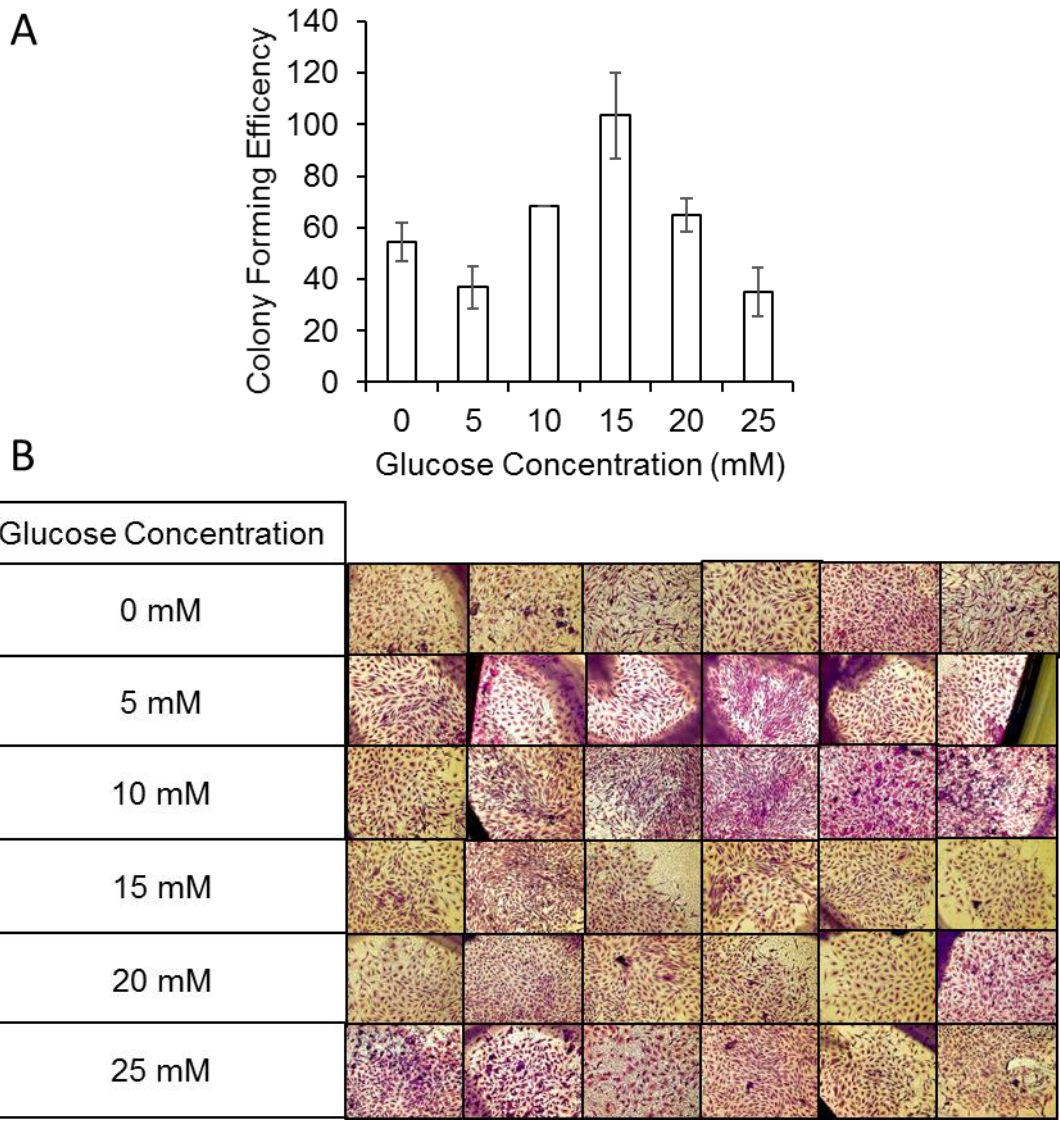


Figure 5-16 – Effect of glucose concentrations on the colony forming ability of primary MSCs.

A – Colony forming unit assay using MSCs and different glucose concentrations, B – colonies formed in colony forming unit assay.

The effect of glucose and FBS concentrations on the metabolic activity and colony forming ability is not linear. The 72-hour MTT with Y201s (Figure 5-15 Graphs A and B) showed both the effect of glucose and FBS were significant with high glucose and high FBS yielding the highest absorbance, when this was extended to a 5 day MTT (Graphs C and D) high FBS still yielded the highest absorbance however the glucose peaked between the 10 and 15 mM glucose. For the Y201.5 cell line (Graphs E and F) which has been acclimatised to 0.5% FBS conditions the peak after 5 days was high glucose and high FBS. The Y201.5 cell line was introduced at this point to investigate whether the response to the different conditions was dependent on the

conditions the cells were acclimatised to. The colony forming unit capability was assessed using only different glucose concentrations and using primary MSCs Figure 5-16, this experiment showed the peak colony forming efficiency at 15mM with glucose as a significant effect. The colony forming unit assay is performed over two weeks which along with the 5-day MTT compared to the 72-hour MTT suggests that long term effects of glucose concentration are different to the short-term effects.

The effects of glucose and FBS on the osteogenic potential of Y201s was also assessed and the results shown in Figure 5-17, Figure 5-18 and Figure 5-19.

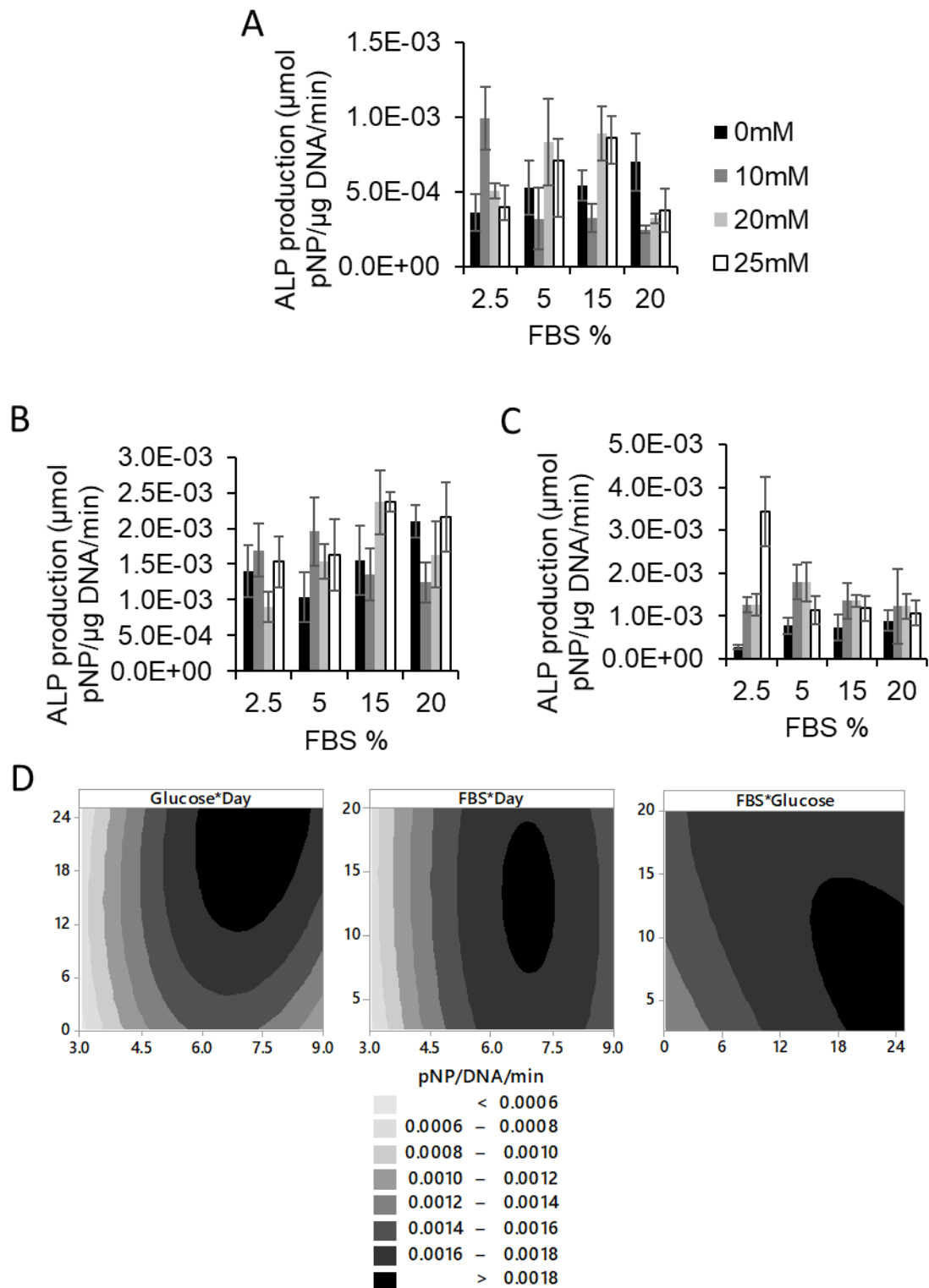


Figure 5-17 – Optimisation of glucose and FBS for osteogenic differentiation of Y201s. Measured by ALP production using pNPP assay and normalised to DNA content by picogreen assay. A – ALP production at Day 3, B – ALP production at Day 6, C - ALP production at Day 9, D contour plots of ALP production. Error shown as SEM.

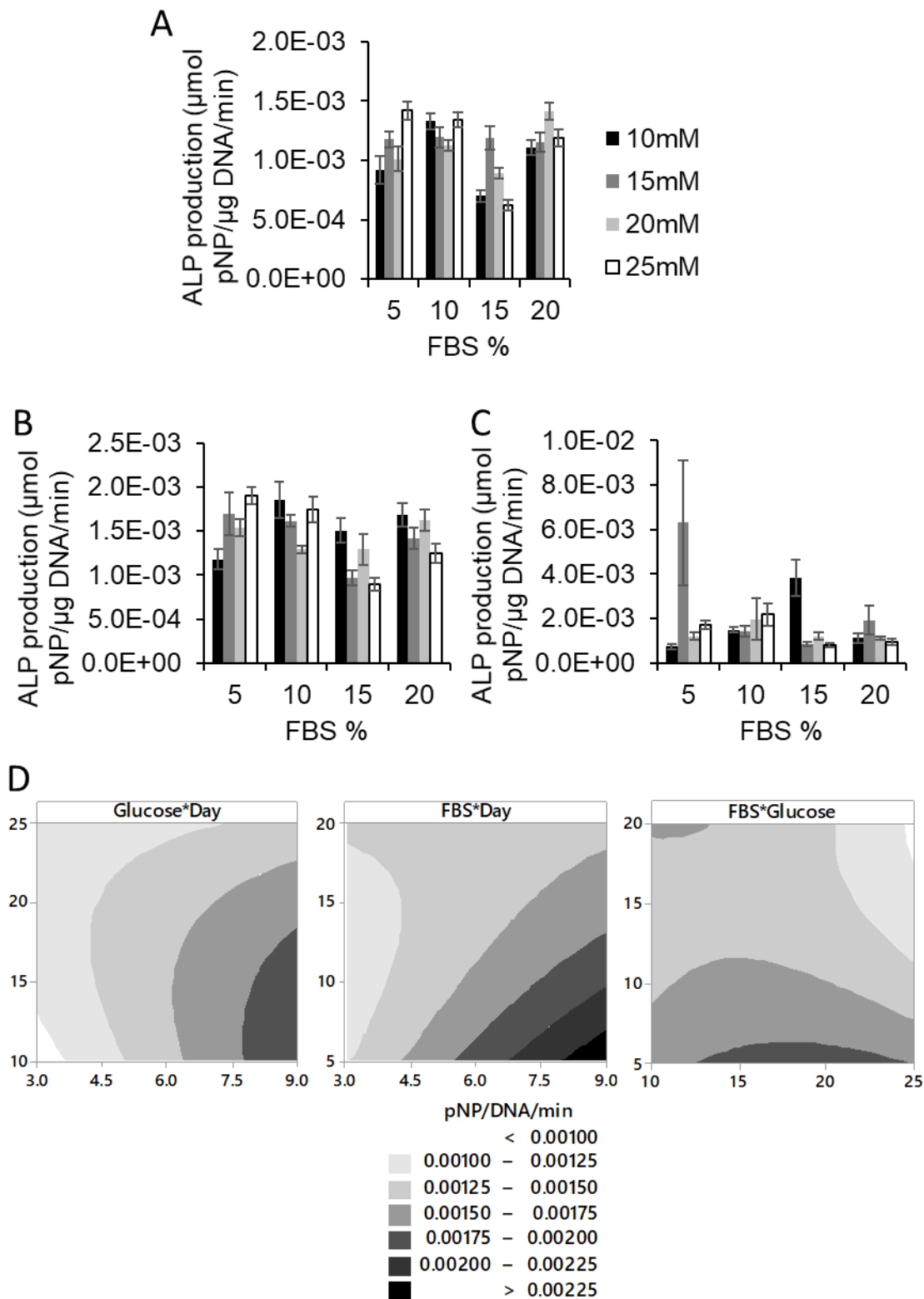


Figure 5-18 – Optimisation of glucose and FBS for osteogenic differentiation of Y201 with a narrowed down glucose range. Measured by ALP production using pNPP assay and normalised to DNA content by picogreen assay. A – ALP production at Day 3, B – ALP production at Day 6, C - ALP production at Day 9, D – Contour plots of ALP production. Error shown as SEM.

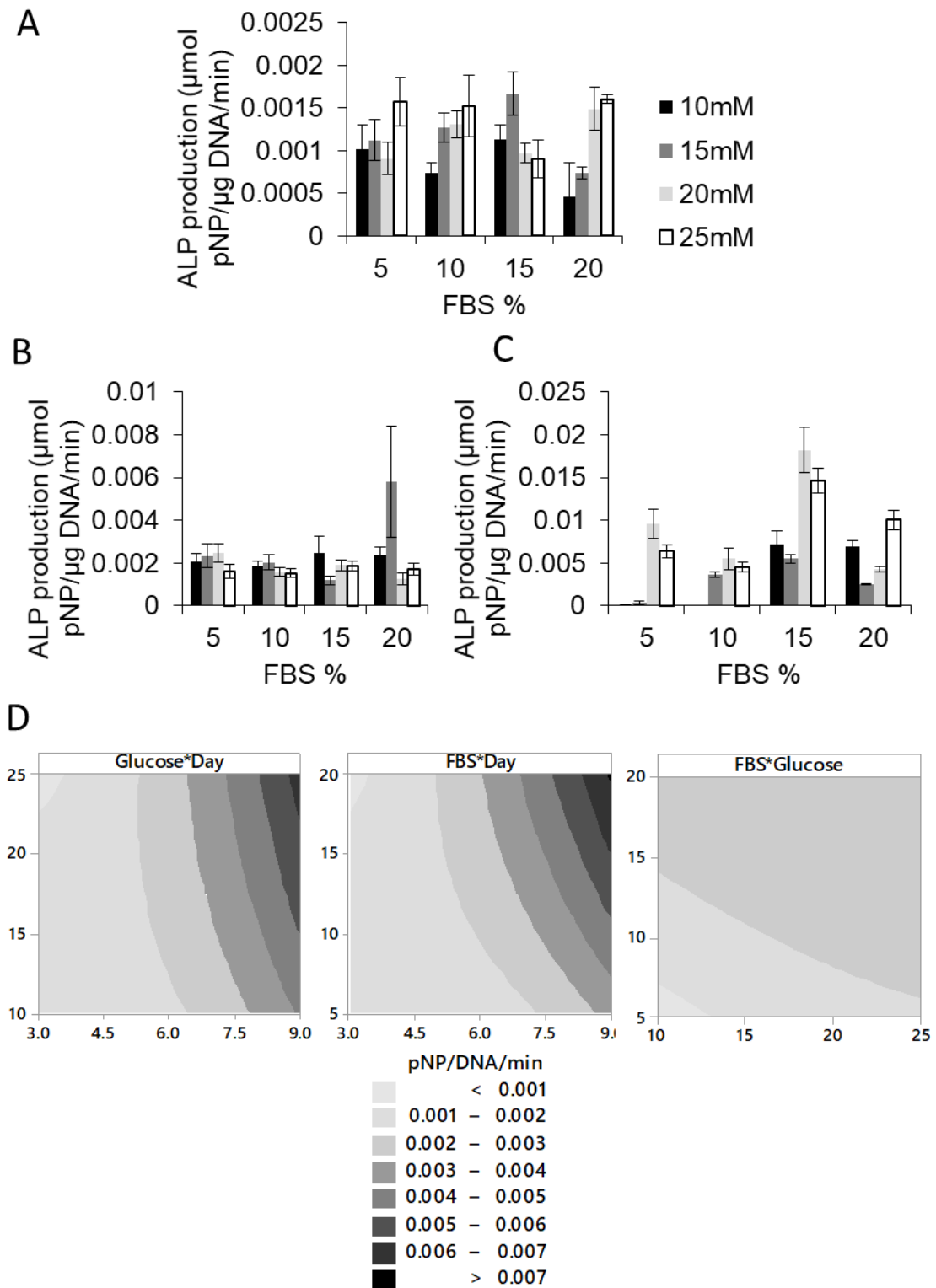


Figure 5-19 – Optimisation of glucose and FBS using smaller range of glucose and FBS concentrations for osteogenic differentiation of Y201.5s. Measured by ALP production using pNPP assay and normalised to DNA content by picogreen assay. A – ALP production at Day 3, B – ALP production at Day 6, C - ALP production at Day 9, D contour plots of ALP production. Error shown as SEM.

Osteogenic potential in Y201s peaked using high glucose and high FBS which were both significant. The range of concentrations was narrowed down for the experiments in Figure 5-19 to try and identify a clearer optimum which was not found. The effect of glucose and concentrations on adipogenic potential was also assessed in Y201s and shown in Figure 5-20.

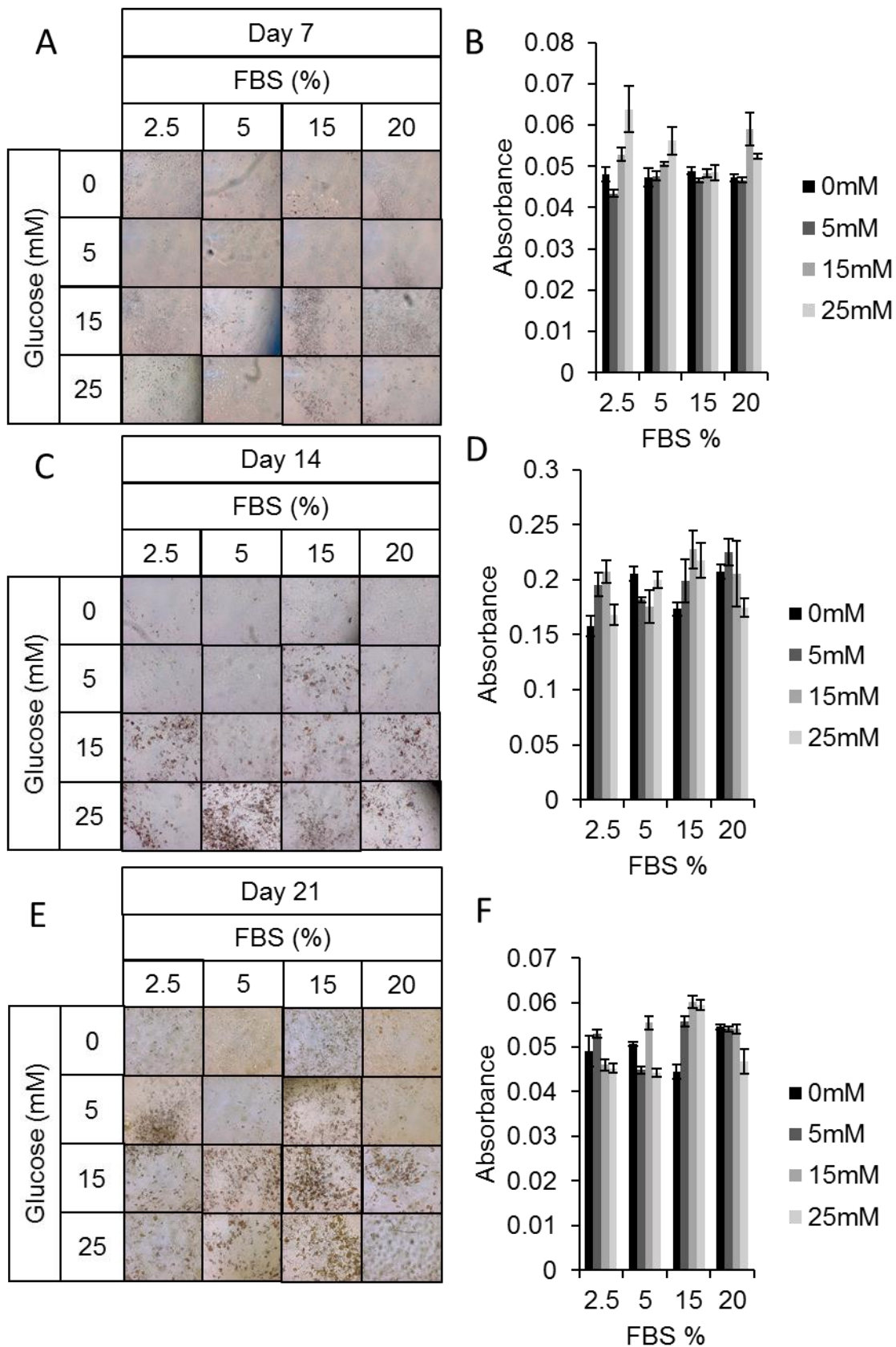


Figure 5-20 – Optimisation of glucose and FBS for adipogenic differentiation of Y201s.

Measured by lipid droplet storage stained by oil red O. A – Imaging of staining on day 7, B – Elution of stain on day 7, C – Imaging of staining on day 14, D – Elution of

stain on day 14, E – Imaging of staining on day 21, F – Elution of stain on day 21. Error shown as SEM.

Images of lipid staining in Figure 5-20 shows increased staining in and around 15mM glucose and 15% FBS, the elution of this staining was unable to detect any significance.

Suspension cultures were used to investigate whether the shrinkage seen in spheroid culture could be replicated with change in glucose concentration as in adherent cultures the size change was not achieved. The results are shown Figure 5-21, the glucose and FBS concentrations were also varied to see the effect of these in suspension culture along with the effect of suspension culture on the osteogenic potential of Y201s.

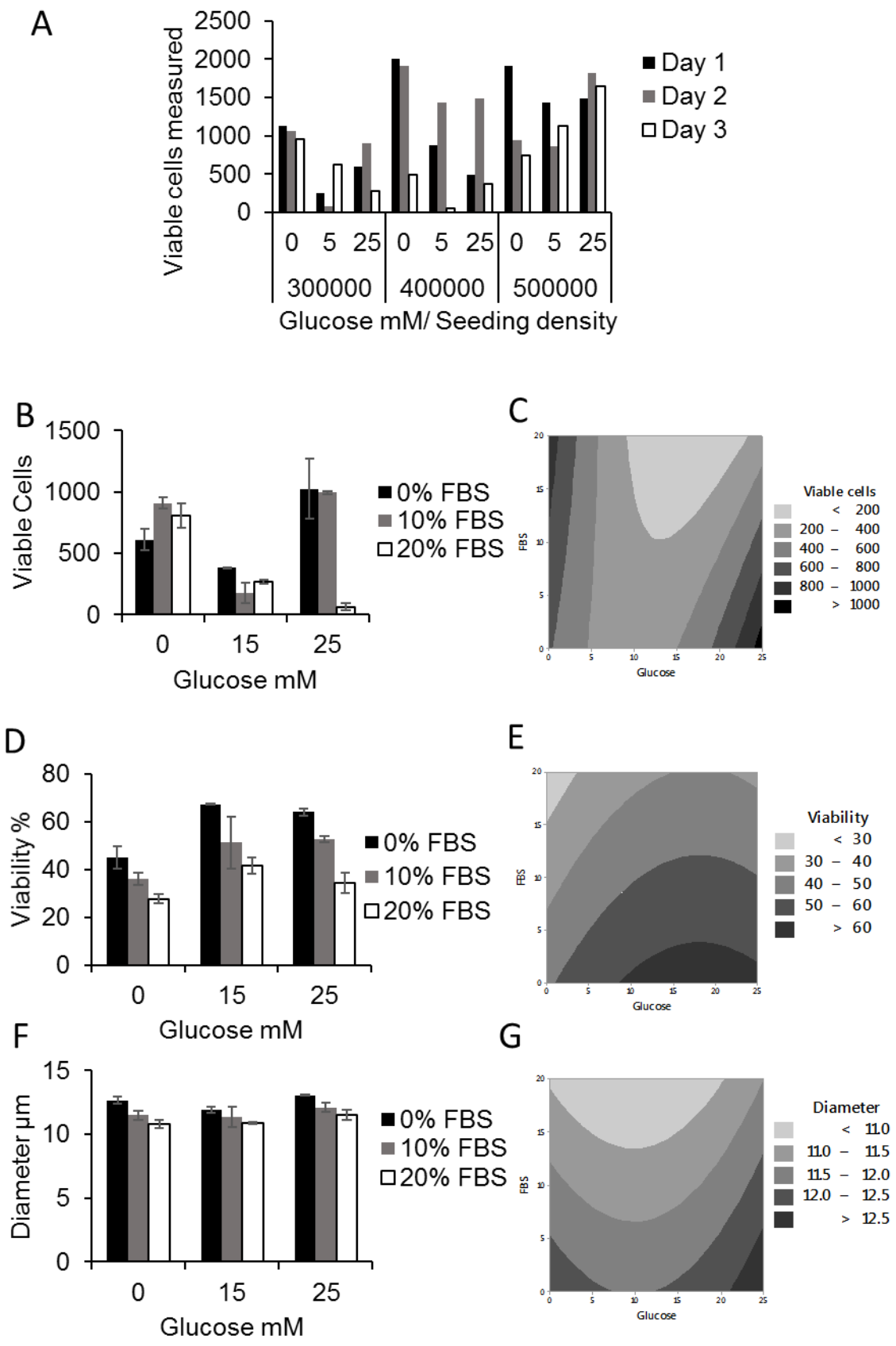


Figure continues next page.

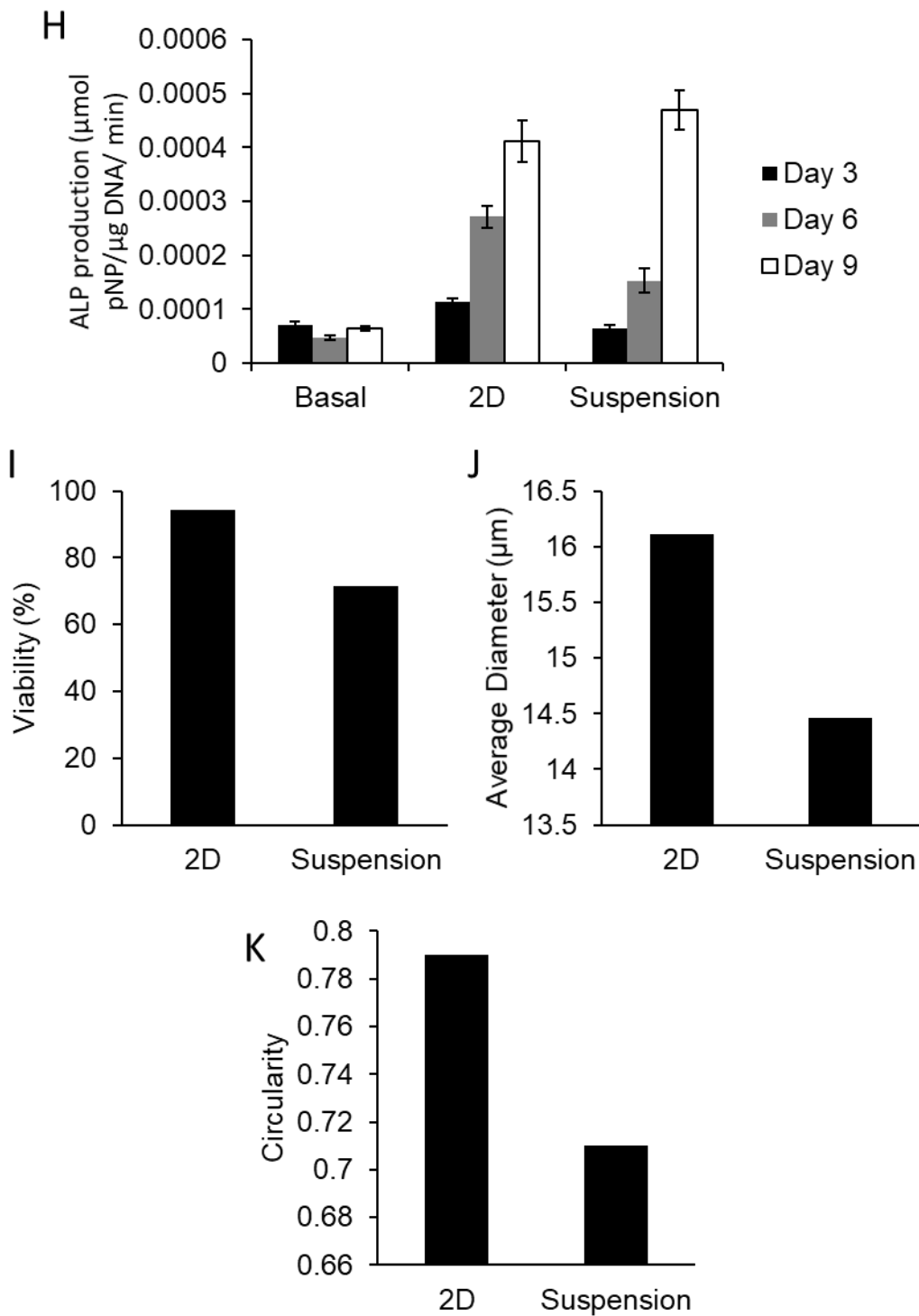


Figure 5-21 – Optimisation of seeding density, glucose and FBS in suspension cultures with Y201s, osteogenic differentiation post suspension culture in Y201s and size change analysis following suspension cultures of primary MSCs.

A – Seeding density, glucose and day optimisation using Vi-cell coulter counter, B – G glucose and FBS optimisation using seeding of 500,000 cells/ml for 2 days, analysis by Vi-cell coulter counter, B – Viable cells, C – Contour plot of viable cells D – Viability, E – Contour plot of viability, F – Diameter G – Contour plot of diameter, H – osteogenic differentiation potential following 2 days pre-treatment in suspension

culture in Y201s, error shown as SEM, I – K Vicell analysis of primary MSCs in 2D and suspension culture. I – Viability, J – Average diameter, K – Circularity.

Seeding density experiments were conducted to determine the best seeding density to collect cells for further experiments (Figure 5-21, A). The best seeding density was determined to be 500,000 cells/ml and using 25mM glucose yielded the consistent high number of cells at all three time points.

Using the seeding density of 500,000 cells/ml the effect of glucose and FBS concentrations on the number of viable cells, viability and diameter was determined in Y201 cells after 2 days (Figure 5-21). The number of viable cells in the suspension culture was significantly altered by the glucose and FBS concentrations, the highest number of viable cells was achieved with 25 mM glucose and 0% FBS. The effect of glucose and FBS was not linear and another peak is present at 0 mM glucose and 20% FBS, the effect of FBS was determined to have a significant effect linearly ($P=0.025$), the effect of glucose was significant as a quadratic term ($P<0.000$) which is shown in the curves on the contour plot (Figure 5-21, C), the effect of glucose and FBS was also significant ($P<0.000$). The viability of the sample was found to be significantly affected by glucose ($P=0.006$) and FBS ($P<0.000$) both with a linear effect where increasing the glucose concentration increased the viability and increasing the FBS concentration decreased the viability. The differences in the effects on viable cells and viability could be due to differences in the effect of glucose and FBS on cell proliferation and effects on cell survival.

The effect of glucose and FBS on the diameter of Y201 cells after 2 days in suspension culture (Figure 5-21, F and G) was determined and while the diameters look very similar FBS had a significant effect ($P<0.000$) with higher FBS concentrations resulting in smaller cells. Glucose also has a significant effect on the diameter ($P=0.013$) with 15mM yielding the smallest diameter, both 0 and 25mM glucose result in larger diameters with 25mM glucose giving the highest diameters.

Culturing Y201 cells in suspension prior to osteogenic differentiation did not significantly affect the ALP production (Figure 5-21, H).

Following 2 days in suspension culture primary MSCs were observed to have decreased in diameter (16 μ m in 2D, 14.5 μ m after suspension), this decrease is not as much as the observed decrease in spheroid culture (just below 10 μ m). the circularity of the cells is also reduced after suspension culture. The viability of the

MSCs drops in suspension culture and carries on dropping the longer the cells are in suspension (data not shown) therefore the size decrease after 5 days (length of spheroid culture) was not measured.

The process of spheroid culture has previously been shown in (Pennock, et al., 2015) to enhance differentiation potential, Y202s do not have the same differentiation potential as MSCs or Y201s and therefore spheroid culture was used to try and encourage differentiation (Figure 5-22).

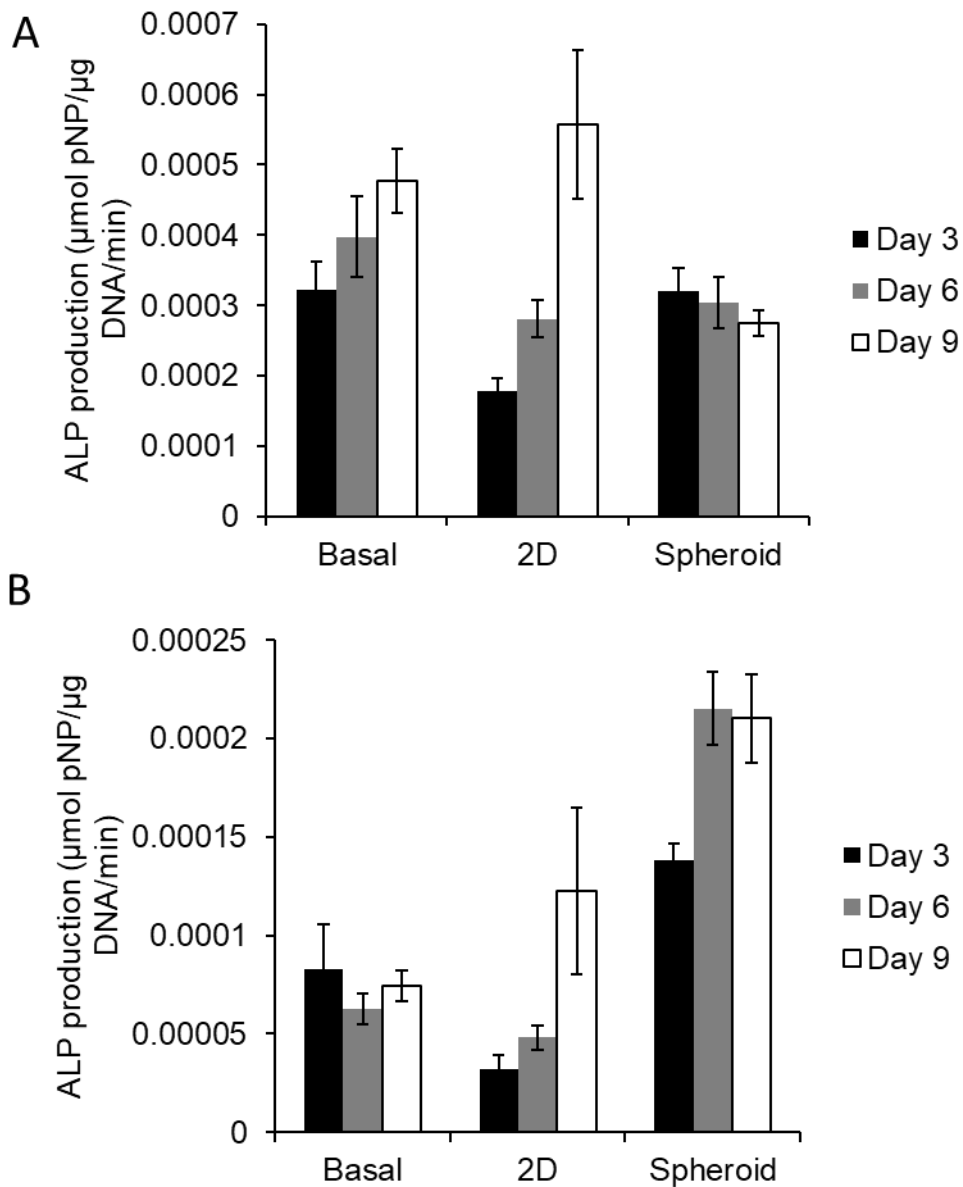


Figure 5-22 – Osteogenic differentiation of Y201s and Y202s after pre - treatment in spheroid culture.

A – Y201s, B- Y202s. Error shown as SEM.

Osteogenic differentiation following spheroid culture (Figure 5-22) shows no increase in osteogenic potential for Y201 cells following spheroid culture pre-treatment, Y202 cells also did not have their osteogenic potential increased by spheroid pre-treatment.

5.6 Qualitative Evaluation of Model Predictions from Experimental Studies

The mathematical modelling of oxygen through the spheroids predicts no oxygen depletion, which correlates with previous investigations within the lab that found the hypoxia marker HIF1 α to be absent from the spheroids (Pennock, et al., 2015). HIF1 α staining has however been found in hepatocyte spheroids of a similar size to the MSC spheroids (Anada, et al., 2012), these spheroids contain fewer cells than the MSC spheroids however the oxygen consumption rate for hepatocytes is higher than the consumption rate for MSCs which results in the uptake of oxygen being greater than the rate of diffusion of oxygen into the spheroid. Modelling of embryonic bodies cultured in spinner flasks (Winkle, et al., 2012) also predicted and found oxygen deprivation in bodies of 400 μm diameter while the ESCs have a lower oxygen consumption rate than MSCs these bodies are more dense than the MSC spheroids, 0.37 voidage for the ESCs compared to a range of 0.54-0.63 for MSC spheroids, in this paper they use Thieles modulus to assess the ratio of diffusion to uptake applying this to the MSC spheroids shows the rate of diffusion into the spheroid is greater than the uptake rate for all sizes and uptake rates in the time course whereas the balance is shifted in embryonic bodies over 500 μm . The MSC spheroids are less compact than the other spheroids investigated and therefore the mass transfer is less limited which enables adequate transport of oxygen into the spheroid.

Both oxygen and glucose concentrations have been measured and modelled in fibroblast spheroids (Barisam, et al., 2017), in this paper it was found that neither oxygen or glucose depletion occurred in 600 μm spheroids which are smaller than the spheroids used in this thesis. Further work by the same authors has subsequently found glucose depletion occurring in spheroids when media is not replenished (Barisam, et al., 2018), this paper did also find oxygen depletion however due to the culture system the oxygen concentration in the media was lower in the first place, if the MSC spheroids were cultured in this lower oxygen concentration (0.1 –

0.15 mM compared to 0.214 mM) then they are also predicted to experience oxygen depletion.

5.7 Extension of Model to Idealised Bone Tissue Geometry

MSCs reside in the bone marrow, to compare how close monolayer and spheroid cultures are to the *in vivo* conditions in terms of oxygen and glucose concentrations, models were also developed of mass transfer in bone marrow. Within bone marrow, the source of oxygen and glucose is from the blood, diffusion will then occur to deliver oxygen and glucose to the cells.

2-Dimensional sections of bone marrow were modelled containing multiple blood vessels. Within bone marrow, blood is supplied by a network of sinusoids and arterioles, the size and spatial arrangement of these vessels is important to understand the natural MSC environment; stained sections are shown in Figure 5-23 (Kunisaki, et al., 2013). Analysis of bone marrow structure (Kunisaki, et al., 2013) found that sinusoids occupied 30% of the bone marrow volume and arterioles were closer to the bone and occupied 1.2% of the volume, these arterioles were 10-20 μ m diameter when measured in mouse bone marrow. Using (Spencer, et al., 2014) for mice bone marrow the average vascular diameter was 27 μ m at 20-40 μ m from the bone. In the endosteal region (0-20 μ m from bone) the average vascular diameter was 15 μ m, at >40 μ m from the bone the average vascular diameter was 28 μ m.

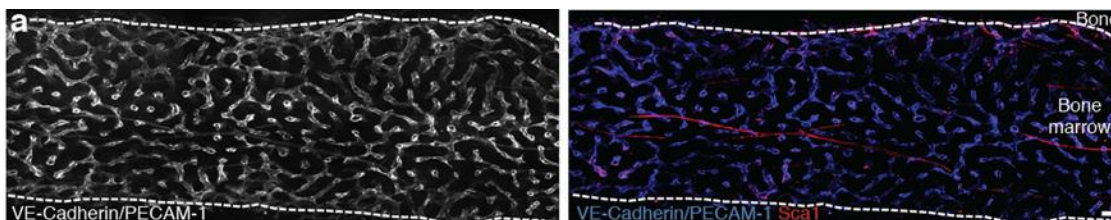


Figure 5-23 – Stained bone marrow section.

Femoral mouse bone marrow stained with anti-PECAM1, anti-vascular endothelial (VE) - cadherin and anti-Sca-1 antibodies. Scale bar, 100 μ m. Images taken from (Kunisaki, et al., 2013).

To formulate a representative geometric model for analysis, the findings of these papers were combined to establish an idealised geometry which was considered representative of bone marrow. This was necessary as the findings in these two papers as the average distances between vessels would require a larger volume fraction most likely caused by natural variation. Average distances and diameters (Spencer, et al., 2014) give a different volume fraction than the observed values.

Using the 10 μm diameter (Kunisaki, et al., 2013) the required distance between 10 μm sinusoids to achieve the 30% volume is 24 μm however using their larger estimate of 20 μm diameter the required distance to achieve 30% is 50 μm which is much closer to their measured 46 μm . Using the 28 μm (Spencer, et al., 2014) the required distance is 77 μm . A sinusoid diameter of 20 μm , arteriole diameter of 10 μm and distance between sinusoids of 50 μm provides a reasonably close approximation to the dimensions and volume fraction from the two papers. A schematic of the idealised bone marrow model is Figure 5-24.

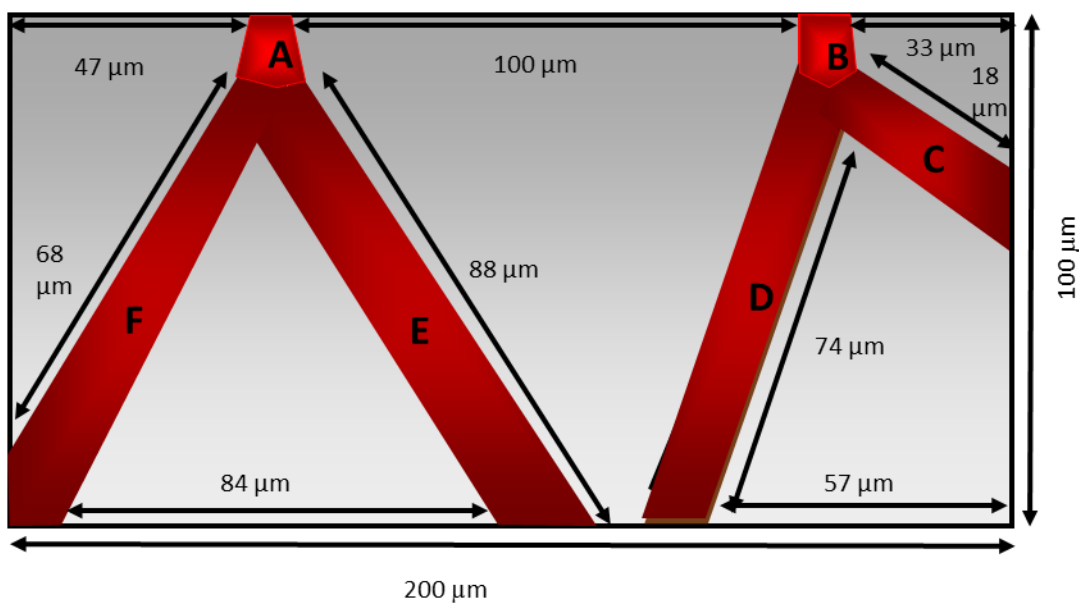


Figure 5-24 – Idealised 2D bone marrow schematic

Therefore, models needed to be developed to predict concentrations using one vessel, two vessels, three vessels and four vessels. The two-vessel model was derived from the schematic shown in Figure 5-25.

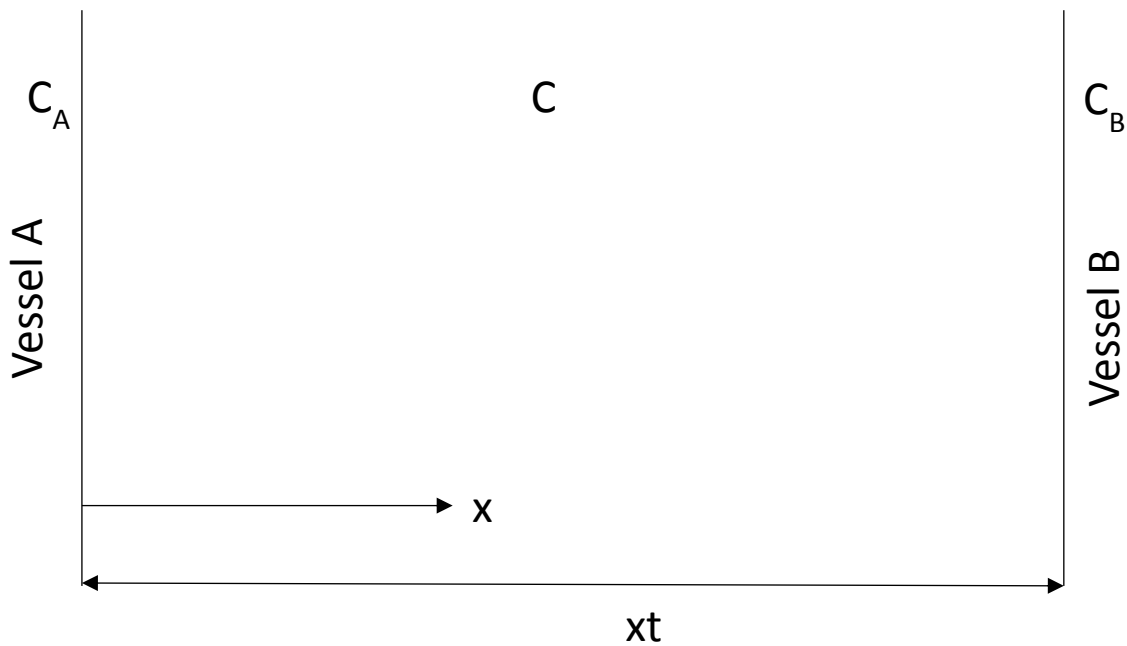


Figure 5-25 – Schematic of diffusion between two vessels

Transfer from vessel A (N_A , mol/s) is shown in equation 5.3.

$$N_A = \frac{D_c S_A (C_A - C_x)}{x} \quad (5.3)$$

Where;

D_c = Diffusion coefficient (m^2/s)

S_A = Surface area of vessel A (m^2)

C_A = Concentration in vessel A (mol/m^3)

C_x = Concentration at point x (mol/m^3)

x = Distance from vessel A (m)

Transfer from vessel B (N_B , mol/s) is shown in equation 5.4.

$$N_B = \frac{D_c S_B (C_B - C_x)}{(xt-x)} \quad (5.4)$$

Where;

S_B = Surface area of vessel B (m^2)

C_B = Concentration in vessel B (mol/m^3)

xt = Distance between vessels A and B (m)

Uptake from cells on route from vessel A (U_A , mol/s).

$$U_A = \frac{U_{cell} S_A x}{V_{cell}}$$

Where;

U_{cell} = Uptake rate per cell (mol/s)

V_{cell} = Volume of one cell (m^3)

Uptake from cells on route from vessel B (U_B , mol/s)

$$U_B = \frac{U_{cell} S_B(xt - x)}{V_{cell}}$$

Utilising the same principle as used previously, starting with a mass balance equation 4.2 which is expanded to equation 5.5.

$$\text{Oxygen in} - \text{Uptake} \pm \text{Accumulation} = 0 \quad (4.2)$$

$$(N_A - U_A) + (N_B - U_B) = \frac{dC_x}{dt} \quad (5.5)$$

$$\frac{D_c S_A (C_A - C_x)}{x} - \frac{U_{cell} S_A x}{V_{cell}} + \frac{D_c S_B (C_B - C_x)}{(xt - x)} - \frac{U_{cell} S_B (xt - x)}{V_{cell}} = \frac{dC_x}{dt}$$

As C_x is not present in U_A or U_B these can be combined as U .

$$\frac{D_c S_A (C_A - C_x)}{x} + \frac{D_c S_B (C_B - C_x)}{(xt - x)} - U = \frac{dC_x}{dt}$$

Apart from C_x all the other components are constants and can therefore be combined to allow for simplification without effecting the integration of the equation.

Let;

$$G = \frac{D_c S_A C_A}{x} + \frac{D_c S_B C_B}{(xt - x)} - U$$

Therefore,

$$G - \frac{D_c S_A C_x}{x} - \frac{D_c S_B C_x}{(xt - x)} = \frac{dC_x}{dt}$$

Let;

$$J = \frac{D_c S_A}{x} + \frac{D_c S_B}{(xt - x)}$$

Therefore,

$$G - JC_x = \frac{dC_x}{dt}$$

$$\int \frac{dC_x}{G - JC_x} = \int dt$$

$$\frac{\ln(G - JC_x)}{-J} = t + K$$

Integration constant K can again be calculated using initial conditions.

$$C_x = \frac{G - e^{-J(t+K)}}{J} \quad (5.6)$$

Expanding equation 4.14 gives a final equation of equation 4.15.

$$C_x = \frac{\frac{D_c S_A C_A}{x} + \frac{D_c S_B C_B}{(xt-x)} - \frac{U_{cell} S_A x}{V_{cell}} - \frac{U_{cell} S_B (xt-x)}{V_{cell}} e^{-\left(\frac{D_c S_A}{x} + \frac{D_c S_B}{(xt-x)}\right)(t+K)}}{\frac{D_c S_A}{x} + \frac{D_c S_B}{(xt-x)}} \quad (5.7)$$

At the edges of the model and in cases of high vessel loss it is necessary to calculate the diffusion from a single vessel.

$$\begin{aligned} N_A - U_A &= \frac{dC_x}{dt} \\ \frac{D_c S_A (C_A - C_x)}{x} - U_A &= \frac{dC_x}{dt} \\ \alpha &= \frac{D_c S_A}{x} \\ \alpha C_A - \alpha C_x - U_A &= \frac{dC_x}{dt} \\ \beta &= \alpha C_A - U_A \\ \beta - \alpha C_x &= \frac{dC_x}{dt} \\ \int \frac{dC_x}{\beta - \alpha C_x} &= \int dt \\ \frac{\ln(\beta - \alpha C_x)}{-\alpha} &= t + K \end{aligned}$$

Integration constant K can be calculated at initial conditions.

$$\begin{aligned} C_x &= \frac{\beta - e^{-\alpha(t+K)}}{\alpha} \\ C_x &= \frac{\frac{D_c S_A C_A}{x} - \frac{U_{cell} S_A x}{V_{cell}} - e^{-\frac{D_c S_A}{x}(t+K)}}{\frac{D_c S_A}{x}} \quad (5.8) \end{aligned}$$

In some models the concentration in the arterioles is not the same as the concentration in the sinusoids, this will therefore create a gradient down the model as well as across. In the model the arterioles are situated at the top and the sinusoids further down, in the case of two vessels the model is similar to the two-vessel model above, however the distance from the arteriole needs to be calculated differently.

Below is a schematic of this system Figure 5-26.

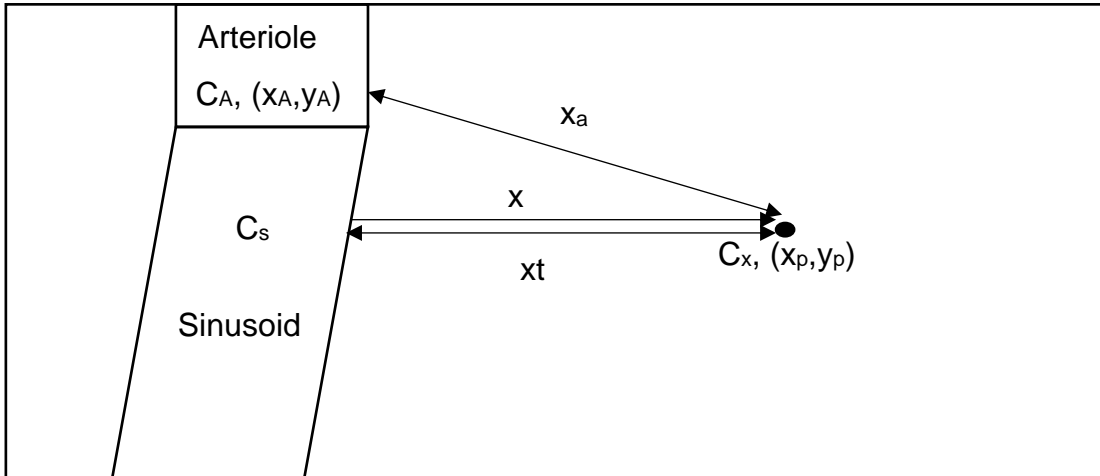


Figure 5-26 – Schematic of arteriole and sinusoid model

The distance (x_a) from point x to the arteriole is calculated using the equation below

$$x_a = \sqrt{(x_p - x_A)^2 + (y_p - y_A)^2}$$

Diffusion from arteriole

$$N_A = \frac{D_c S_A}{x_a} (C_A - C_x)$$

Diffusion from sinusoid

$$N_a = \frac{D_c S_A}{x} (C_s - C_x)$$

Uptake between x_p and arteriole

$$U_A = \frac{U_{cell} S_A x_a}{V_{cell}}$$

Uptake between x_p and sinusoid

$$U_a = \frac{U_{cell} S_A x}{V_{cell}}$$

Mass transfer is therefore represented as

$$\frac{D_c S_A}{x_a} (C_A - C_x) + \frac{D_c S_A}{x} (C_s - C_x) - \frac{U_{cell} S_A x_a}{V_{cell}} - \frac{U_{cell} S_A x}{V_{cell}} = \frac{dC_x}{dt}$$

Let;

$$U = U_A - U_a$$

Therefore;

$$\frac{D_c S_A C_A}{x_a} - \frac{D_c S_A C_x}{x_a} + \frac{D_c S_A C_s}{x} - \frac{D_c S_A C_x}{x} - U = \frac{dC_x}{dt}$$

Let;

$$E = \frac{D_c S_A C_S}{x}$$

$$F = \frac{D_c S_A C_A}{x_a}$$

$$G = E + F - U$$

Therefore;

$$G - \frac{D_c S_A C_x}{x_a} - \frac{D_c S_A C_x}{x} = \frac{dC_x}{dt}$$

Let;

$$H = \frac{D_c S_A}{x}$$

$$I = \frac{D_c S_A}{x_a}$$

Therefore;

$$G - IC_x - HC_x = \frac{dC_x}{dt}$$

Let;

$$J = H + I$$

Therefore;

$$G - JC_x = \frac{dC_x}{dt}$$

$$\int dt = \int \frac{dC_x}{G - JC_x}$$

$$\frac{\ln(G - JC_x)}{-J} = t + K$$

Integration constant K can be calculated at initial conditions

$$C_x = \frac{G - e^{-J(t+K)}}{J}$$

$$C_x = \frac{\frac{D_c S_A C_S}{x} + \frac{D_c S_A C_A}{x_a} - \frac{U_{cell} S_A x_a}{V_{cell}} - \frac{U_{cell} S_A x}{V_{cell}} - e^{-\left(\frac{D_c S_A}{x} + \frac{D_c S_A}{x_a}\right)(t+K)}}{\frac{D_c S_A}{x} + \frac{D_c S_A}{x_a}} \quad (5.9)$$

For sections between two sinusoids there will be diffusion from both sinusoids and from two arterioles as shown below in Figure 5-27.

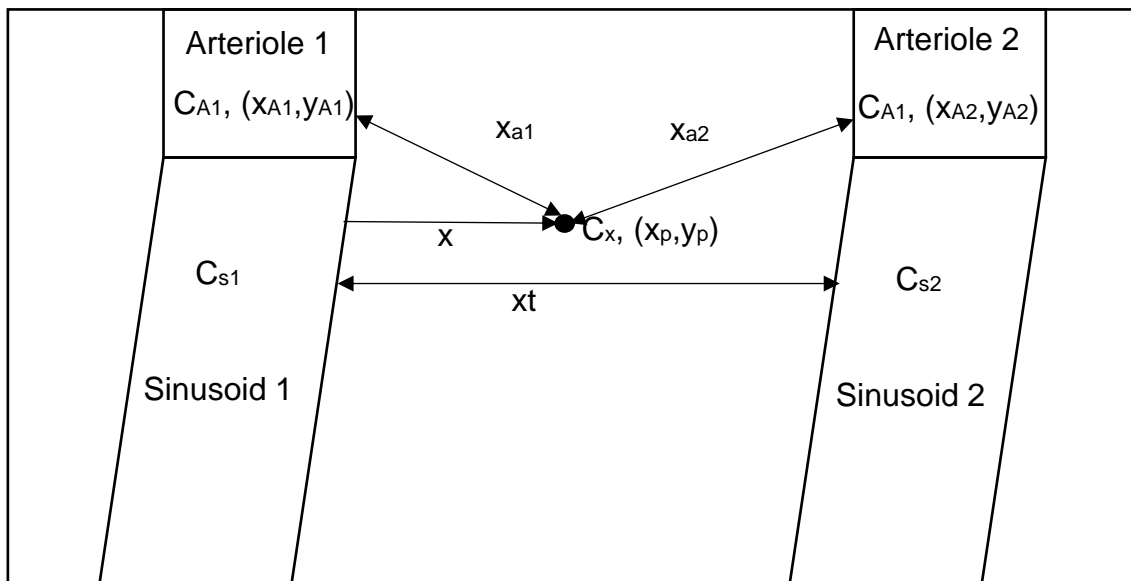


Figure 5-27 – Schematic of diffusion between two arterioles and two sinusoids

The distance (x_{a1}) from point x to the arteriole 1 is calculated using the equation below.

$$x_{a1} = \sqrt{(x_p - x_{A1})^2 + (y_p - y_{A1})^2}$$

The distance (x_{a2}) from point x to the arteriole 2 is calculated using the equation below

$$x_{a2} = \sqrt{(x_p - x_{A2})^2 + (y_p - y_{A2})^2}$$

Diffusion from arteriole 1

$$N_{A1} = \frac{D_c S_A (C_{A1} - C_x)}{x_{a1}}$$

Diffusion from arteriole 2

$$N_{A2} = \frac{D_c S_A (C_{A2} - C_x)}{x_{a2}}$$

Diffusion from sinusoid 1

$$N_{S1} = \frac{D_c S_A (C_{S1} - C_x)}{x}$$

Diffusion from sinusoid 2

$$N_{S2} = \frac{D_c S_A (C_{S2} - C_x)}{xt - x}$$

Uptake between arteriole 1 and point x

$$U_{A1} = \frac{U_{cell} S_A x_{a1}}{V_{cell}}$$

Uptake between arteriole 2 and point x

$$U_{A2} = \frac{U_{cell} S_A x_{a2}}{V_{cell}}$$

Uptake between sinusoid 1 and point x

$$U_{s1} = \frac{U_{cell} S_A x}{V_{cell}}$$

Uptake between sinusoid 2 and point x

$$U_{s2} = \frac{U_{cell} S_A (xt - x)}{V_{cell}}$$

Mass transfer can therefore be represented by

$$\frac{D_c S_A (C_{A1} - C_x)}{x_{a1}} + \frac{D_c S_A (C_{A2} - C_x)}{x_{a2}} + \frac{D_c S_A (C_{s1} - C_x)}{x} + \frac{D_c S_A (C_{s2} - C_x)}{xt - x} - \frac{U_{cell} S_A x_{a1}}{V_{cell}} - \frac{U_{cell} S_A x_{a2}}{V_{cell}} - \frac{U_{cell} S_A x}{V_{cell}} - \frac{U_{cell} S_A (xt - x)}{V_{cell}} = \frac{dC_x}{dt}$$

Let;

$$U = \frac{U_{cell} S_A}{V_{cell}} (x_{A1} + x_{A2} + x + (xt - x))$$

$$H = \frac{D_c S_A C_{A1}}{x_{A1}} + \frac{D_c S_A C_{A2}}{x_{A2}} + \frac{D_c S_A C_{s1}}{x} + \frac{D_c S_A C_{s2}}{xt - x}$$

Therefore;

$$H - \frac{D_c S_A C_x}{x_{A1}} - \frac{D_c S_A C_x}{x_{A2}} - \frac{D_c S_A C_x}{x} - \frac{D_c S_A C_x}{xt - x} - U = \frac{dC_x}{dt}$$

$$H - C_x \left(\frac{D_c S_A}{x_{a1}} + \frac{D_c S_A}{x_{a2}} + \frac{D_c S_A}{x} + \frac{D_c S_A}{xt - x} \right) - U = \frac{dC_x}{dt}$$

Let;

$$J = \frac{D_c S_A}{x_{a1}} + \frac{D_c S_A}{x_{a2}} + \frac{D_c S_A}{x} + \frac{D_c S_A}{xt - x}$$

Therefore;

$$H - JC_x - U = \frac{dC_x}{dt}$$

Let;

$$G = H - U$$

Therefore;

$$G - JC_x = \frac{dC_x}{dt}$$

$$\int dt = \int \frac{dC_x}{G - JC_x}$$

$$t + K = \frac{\ln(G - JC_x)}{-J}$$

Integration constant K can be found by setting initial conditions.

$$C_x = \frac{G - e^{-J(t+K)}}{J}$$

Which expands to;

$$C_x = \frac{\left(D_c S_A \left(\frac{C_{A1}}{x_{A1}} + \frac{C_{A2}}{x_{A2}} + \frac{C_{S1}}{x} + \frac{C_{S2}}{xt-x} \right) - \frac{U_{cell} S_A}{V_{cell}} (x_{A1} + x_{A2} + x + (xt-x)) \right)}{D_c S_A \left(\frac{1}{x_{A1}} + \frac{1}{x_{A2}} + \frac{1}{x} + \frac{1}{xt-x} \right)} - \frac{-e^{-D_c S_A \left(\frac{1}{x_{A1}} + \frac{1}{x_{A2}} + \frac{1}{x} + \frac{1}{xt-x} \right) (t+K)}}{D_c S_A \left(\frac{1}{x_{A1}} + \frac{1}{x_{A2}} + \frac{1}{x} + \frac{1}{xt-x} \right)} \quad (5.10)$$

In the case of high vascular loss models there is also a need to calculate the mass transfer from two arterioles and one sinusoid as shown in Figure 5-28.

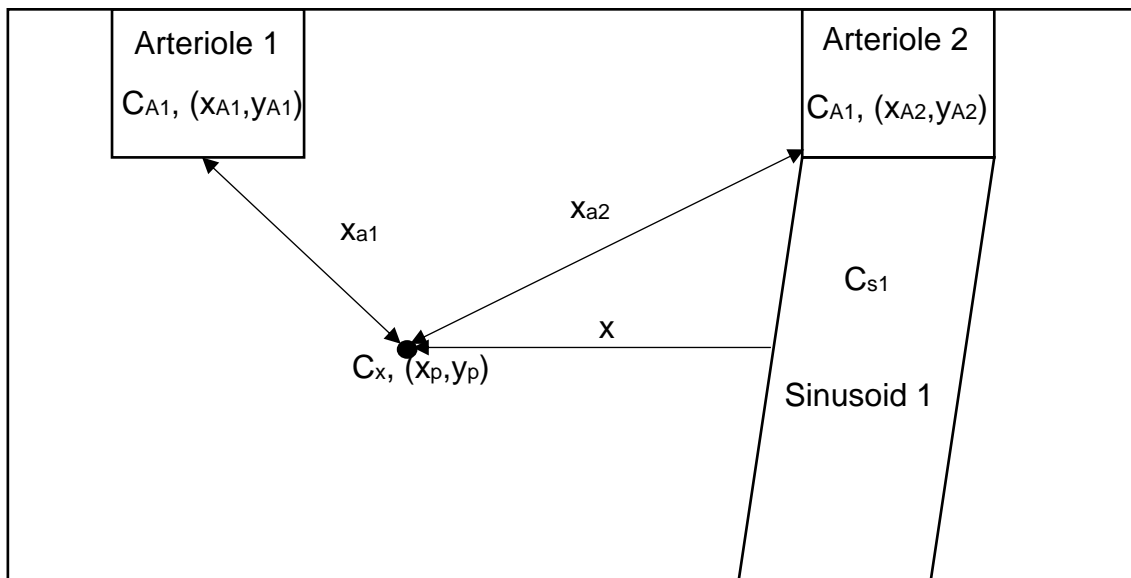


Figure 5-28 – Schematic of diffusion from two arterioles and one sinusoid

The distance (x_{a1}) from point x to the arteriole 1 is calculated using the equation below.

$$x_{a1} = \sqrt{(x_p - x_{A1})^2 + (y_p - y_{A1})^2}$$

The distance (x_{a2}) from point x to the arteriole 2 is calculated using the equation below

$$x_{a2} = \sqrt{(x_p - x_{A2})^2 + (y_p - y_{A2})^2}$$

Diffusion from arteriole 1

$$N_{A1} = \frac{D_c S_A (C_{A1} - C_x)}{x_{a1}}$$

Diffusion from arteriole 2

$$N_{A2} = \frac{D_c S_A (C_{A2} - C_x)}{x_{a2}}$$

Diffusion from sinusoid 1

$$N_{s1} = \frac{D_c S_A (C_{s1} - C_x)}{x}$$

Uptake between arteriole 1 and point x

$$U_{A1} = \frac{U_{cell} S_A x_{a1}}{V_{cell}}$$

Uptake between arteriole 2 and point x

$$U_{A2} = \frac{U_{cell} S_A x_{a2}}{V_{cell}}$$

Uptake between sinusoid 1 and point x

$$U_{s1} = \frac{U_{cell} S_A x}{V_{cell}}$$

Mass transfer can therefore be represented by;

$$\frac{D_c S_A (C_{A1} - C_x)}{x_{a1}} + \frac{D_c S_A (C_{A2} - C_x)}{x_{a2}} + \frac{D_c S_A (C_{s1} - C_x)}{x} - \frac{U_{cell} S_A x_{a1}}{V_{cell}} - \frac{U_{cell} S_A x_{a2}}{V_{cell}} - \frac{U_{cell} S_A x}{V_{cell}} = \frac{dC_x}{dt}$$

Let;

$$H = \frac{D_c S_A C_{A1}}{x_{a1}} + \frac{D_c S_A C_{A2}}{x_{a2}} + \frac{D_c S_A C_{s1}}{x}$$

$$U = \frac{U_{cell} S_A (x_{a1} + x_{a2} + x)}{V_{cell}}$$

Therefore;

$$H - \frac{D_c S_A C_x}{x_{a1}} - \frac{D_c S_A C_x}{x_{a2}} - \frac{D_c S_A C_x}{x} - U = \frac{dC_x}{dt}$$

Let;

$$J = \frac{D_c S_A}{x_{a1}} + \frac{D_c S_A}{x_{a2}} + \frac{D_c S_A}{x}$$

Therefore;

$$H - JC_x - U = \frac{dC_x}{dt}$$

Let;

$$G = H - U$$

Therefore;

$$G - JC_x = \frac{dC_x}{dt}$$

$$\int dt = \int \frac{dC_x}{G - JC_x}$$

$$t + K = \frac{\ln(G - JC_x)}{-J}$$

Integration constant K can be found at initial conditions.

$$C_x = \frac{G - e^{-J(t+K)}}{J}$$

$$C_x = \frac{\left(D_c S_A \left(\frac{C_{A1}}{x_{a1}} + \frac{C_{A2}}{x_{a2}} + \frac{C_{S1}}{x} \right) - \frac{U_{cell} S_A (x_{a1} + x_{a2} + x)}{V_{cell}} \right) - e^{-D_c S_A \left(\frac{1}{x_{a1}} + \frac{1}{x_{a2}} + \frac{1}{x} \right) (t+K)}}{D_c S_A \left(\frac{1}{x_{a1}} + \frac{1}{x_{a2}} + \frac{1}{x} \right)} \quad (5.11)$$

5.8 Idealised Bone Tissue Model Input Data

The oxygen consumption rate within the bone marrow was calculated by collecting cell fraction and oxygen consumption data for the cell types. The data for the cell fraction was found in (Posel, et al., 2012, Jang, et al., 2015 and Verma, et al., 2002).

Table 5-1 – Oxygen consumption rates for cells within bone marrow

Cell type	Cell fraction (%)	OCR (mol/cell.s)	Proportional OCR (mol/cell.s)
Erythroid (Browne, et al., 2014)	60	1.17E-18	7.02E-19
Leukocyte (Reiss & Roos, 1978)	20.19	1.66E-18	3.35E-19
Polymorphonuclear cells (Parker, et al., 1985)	12	4.58E-16	5.50E-17
Endothelial Cell (EC) (Liu, et al., 2014)	4.81	5.83E-17	2.80E-18
Hematopoietic stem cell (HSC) (Piccoli, et al., 2005)	2.58	1.40E-19	3.61E-21
Mesenchymal stroma cell (MSC)	0.18	2.16E-18	3.92E-21
Vascular smooth muscle cell (VSMC)/pericyte (Lu, et al., 2015)	0.15	1.69E-16	2.46E-19
Adipose tissue derived stromal cell (ASC) (Ferng, et al., 2016)	0.06	7.64E-19	4.65E-22
Total	99.97		5.91E-17

The overall oxygen consumption rate for bone marrow is higher than the oxygen consumption rate for MSCs (5.9×10^{-17} mol/cell.s compared to 2.16×10^{-18} mol/cell.s). Polymorphonuclear cells have the highest oxygen consumption rate (4.58×10^{-16} mol/cell.s) and are the third most abundant cell type which means this consumption rate greatly influences the overall oxygen consumption rate. The cell type with the lowest oxygen consumption rate is the haematopoietic stem cell (1.4×10^{-19} mol/cell.s) but as these are less abundant than most other cell types the influence on the overall consumption rate is much smaller than the high consumption rate of the polymorphonuclear cells.

The oxygen concentration in vessels within the bone marrow used in this model were sourced from (Spencer, et al., 2014) as 1.17 mol/m^3 (22.7mmHg / 3%) for vessels less than $15 \mu\text{m}$ diameter (Vessels A and B in model) and 1.01 mol/m^3 (19.5mmHg / 2.6%) for vessels greater than $15 \mu\text{m}$ diameter (Vessels C, D, E and F in model). A gradient was used to transition between the concentrations in different vessels.

The glucose concentration in vessels used was 5mM which is the average blood glucose level (Tankasala & Linnes, 2019) and the glucose consumption rate used was $8.11 \times 10^{-12} \text{ mol/s}$ which is the same value used in the monolayer culture.

5.9 Idealised Bone Tissue Model Predictions

The models derived in section 5.7 were used together with Figure 5-24 to predict the oxygen and glucose concentrations across the bone marrow section. The oxygen concentrations are shown in Figure 5-29 and the glucose concentrations are shown in Figure 5-30.

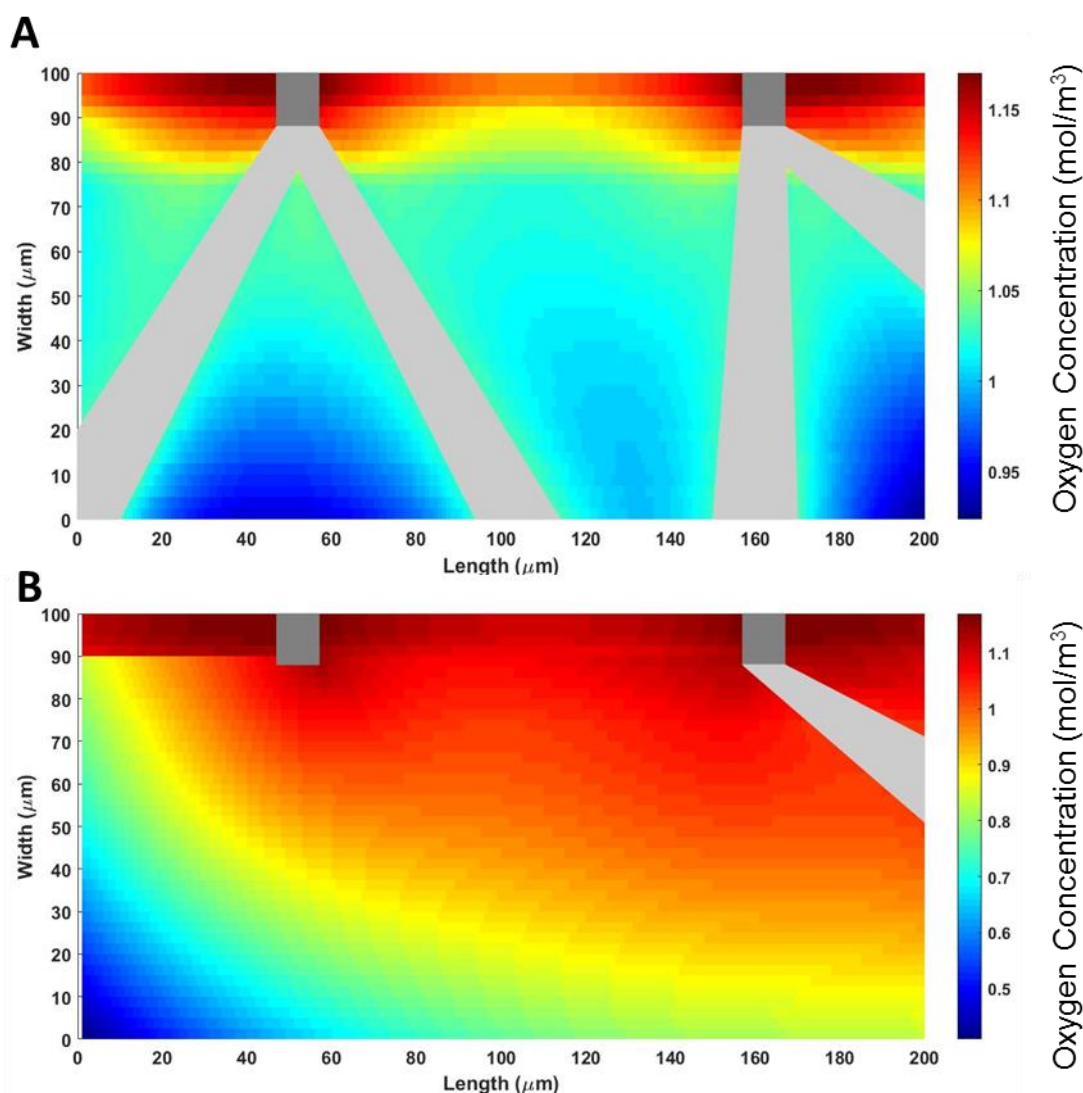


Figure 5-29 – Model of bone marrow for oxygen transport.

A – Full model with oxygen concentration shown using a colourmap. B – Model representing 85% loss of vasculature with oxygen concentration represented as a colourmap.

As shown in Figure 5-29 with full vasculature the oxygen concentration is not depleted and is higher than in monolayer, MSC spheroids and Y201 spheroid cultures, on average oxygen levels in culture are one fifth of *in vivo* conditions. With full vasculature the oxygen concentrations stay within 80% of the highest vascular concentration. Loss of 85% of the vasculature results in oxygen deprivation in a small area of the section which is close to 200 μm from the nearest vessel, this distance is smaller than the size a spheroid needs to be to encounter the same problems despite the starting concentration being higher in bone marrow as the average oxygen

consumption rate in bone marrow is higher in bone marrow than in MSCs on their own.

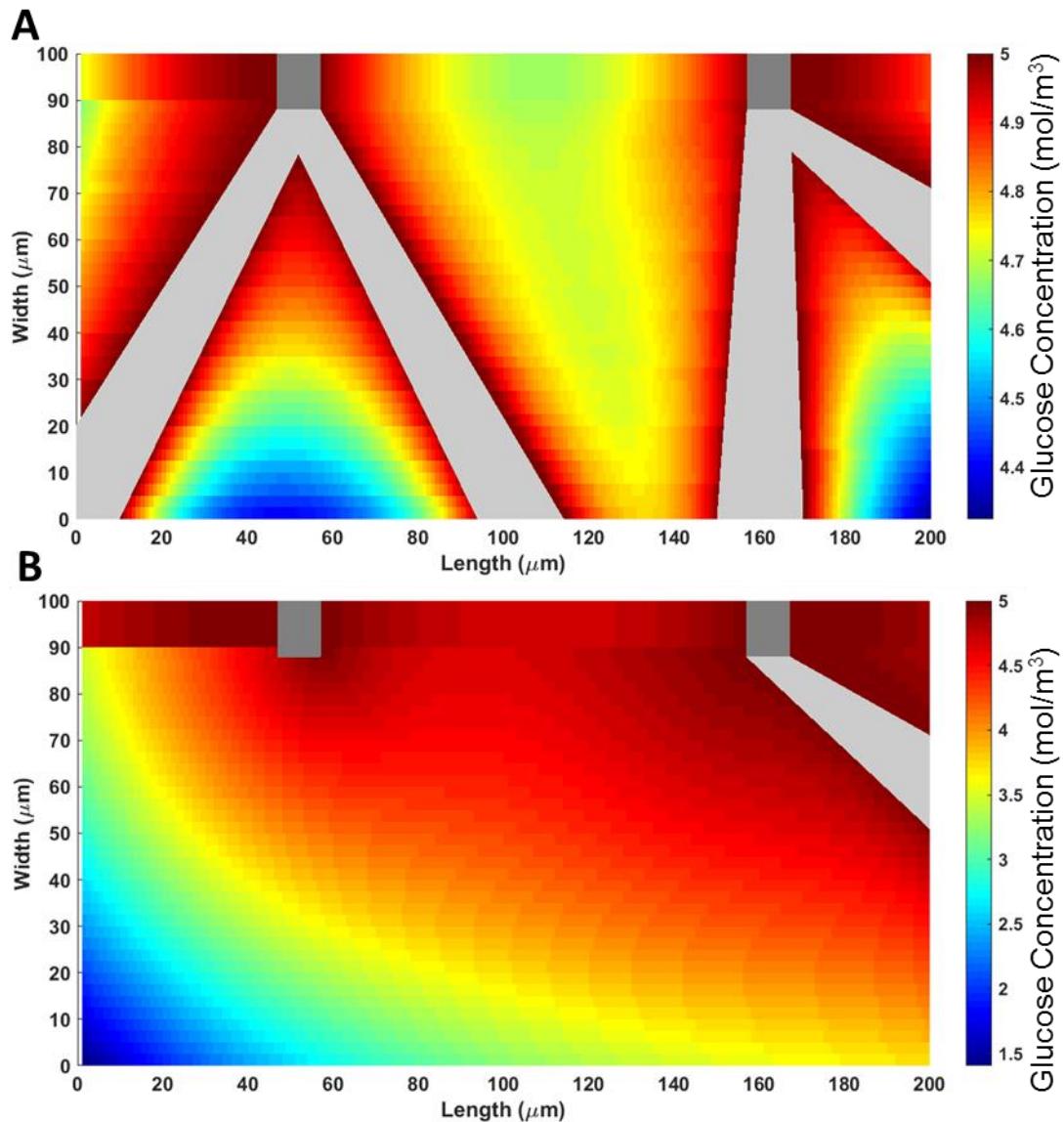


Figure 5-30 – Model of bone marrow for glucose transport.

A – Full model with glucose concentration shown using a colourmap. B – Model representing 85% loss of vasculature with glucose concentration represented as a colourmap.

As with the oxygen concentration the glucose concentration in the full vasculature model (Figure 5-30) does not result in glucose depletion. The glucose concentration stays relatively stable as the lowest concentration is 4.4 mM compared to 5mM a drop of 12% in some small areas, most of the section is above 4.7 mM which equates to most of the section experiencing less than a 6% drop. In the 85% loss model the glucose concentration doesn't drop to the level of depletion (unlike the oxygen

model) but does result in much lower glucose concentrations than in the full vasculature model with a drop of 70% to 1.5 mM.

5.10 Recreation of Bone Marrow Conditions

The comparison between the oxygen and glucose concentrations in monolayer culture and the concentrations in bone marrow shows that the oxygen concentrations are higher in bone marrow and the glucose concentrations are lower than they are in laboratory culture. Therefore, oxygen carriers were used to raise the oxygen concentration in media and functional tests on cell function were carried out, this was also done with glucose concentrations used normally in culture and physiologically relevant concentrations.

Viability of culture in perfluoro-octane (PFO) was assessed at different time points during culture, the results after 24 hours are shown in Figure 5-31, after 72 hours in Figure 5-32, and after 7 days in Figure 5-33.

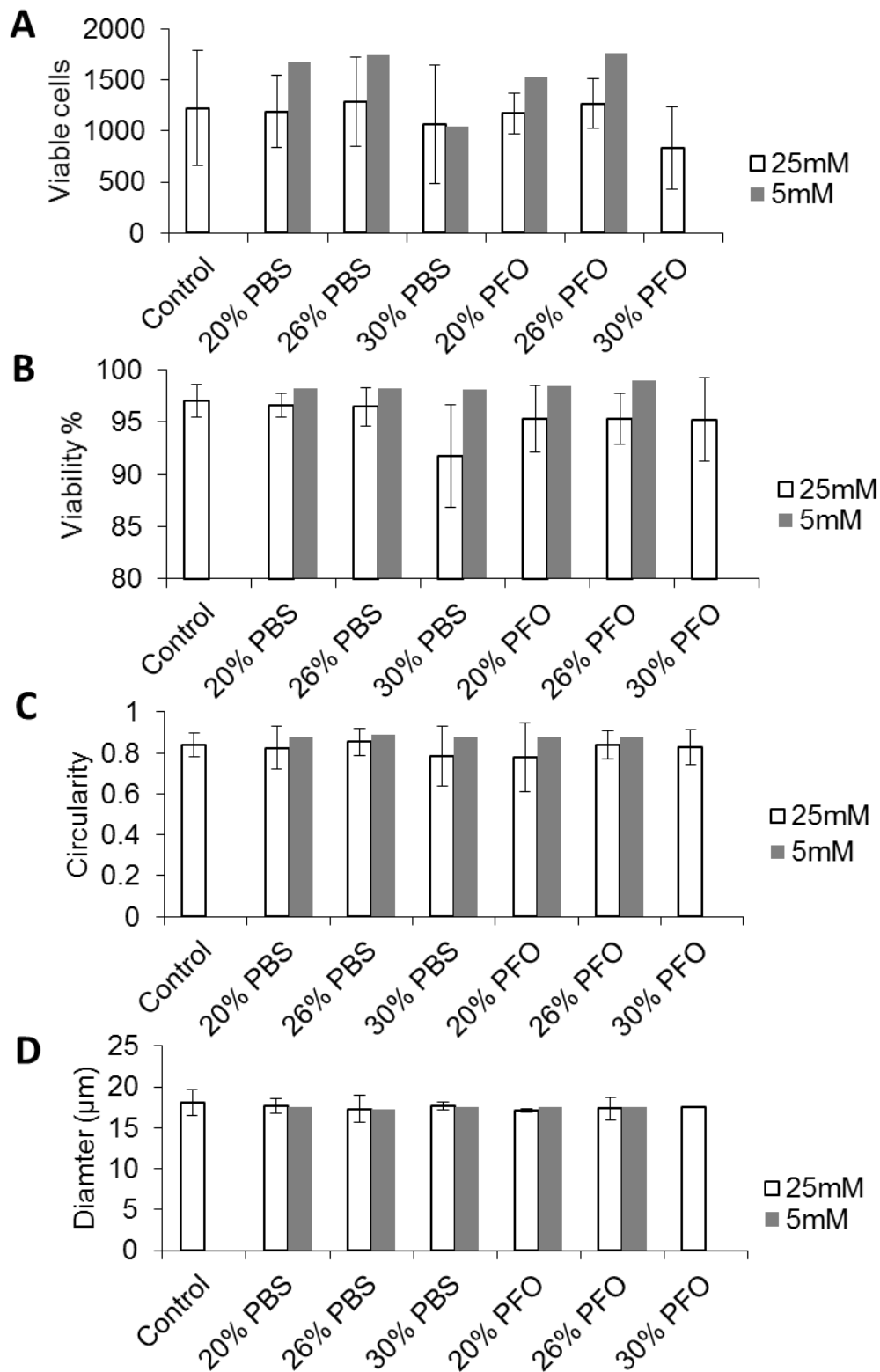


Figure 5-31 – 24-hour viability analysis of Y201s exposed to perfluoro-octane. Various concentrations of PFO with diluted PBS controls and at 5 and 25mM glucose concentrations. Cultures all analysed using VI cell coulter counter. A – Viable cells measured, B – Viability of cells within the sample, C – Circularity of cells, D – Diameter of cells. Error shown as SD.

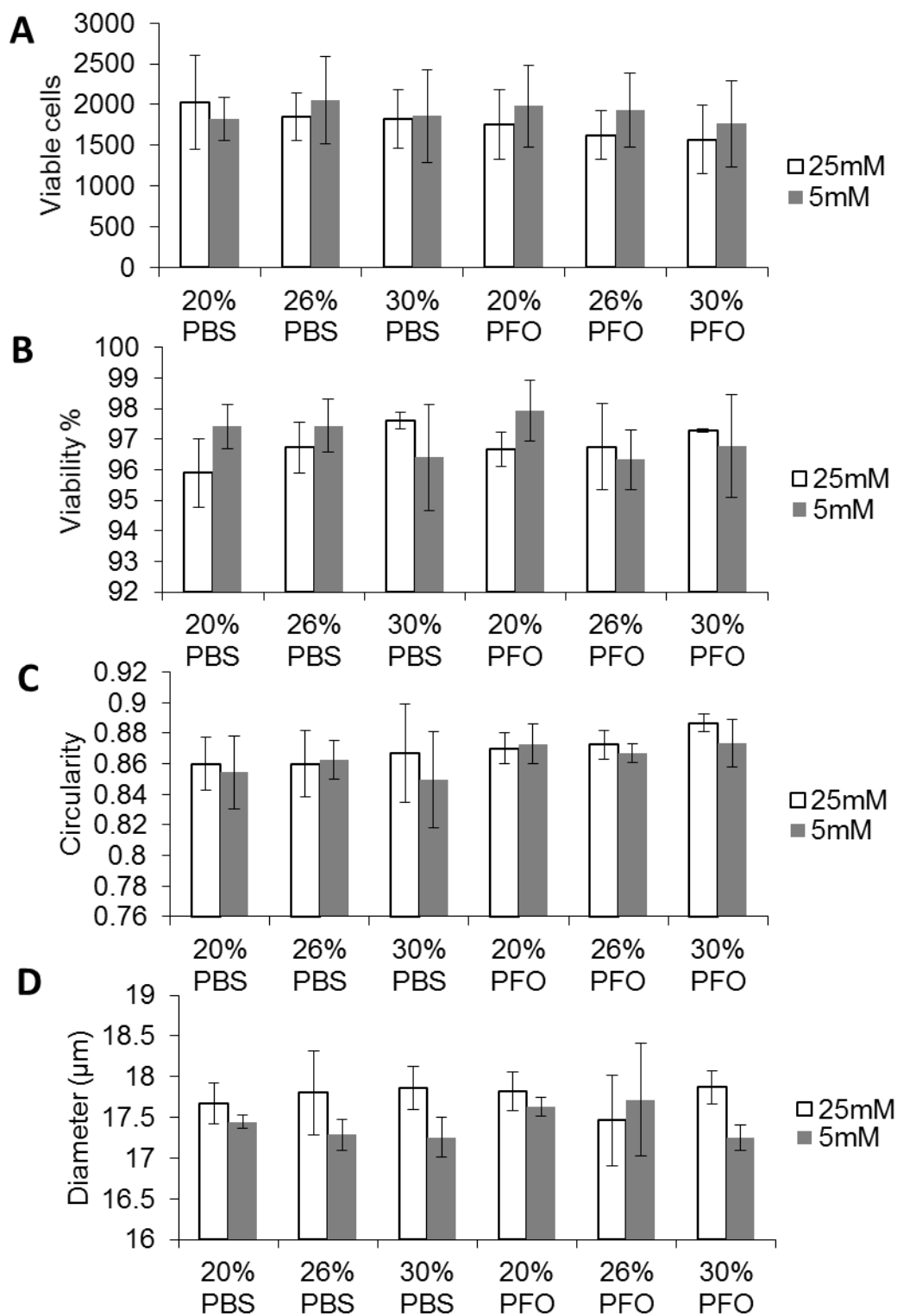


Figure 5-32 – 72-hour viability analysis of Y201s exposed to perfluoro-octane. Various concentrations of PFO with diluted PBS controls and at 5 and 25mM glucose concentrations. Cultures all analysed using VI cell coulter counter. A – Viable cells measured, B – Viability of cells within the sample, C – Circularity of cells, D – Diameter of cells. Error shown as SD.

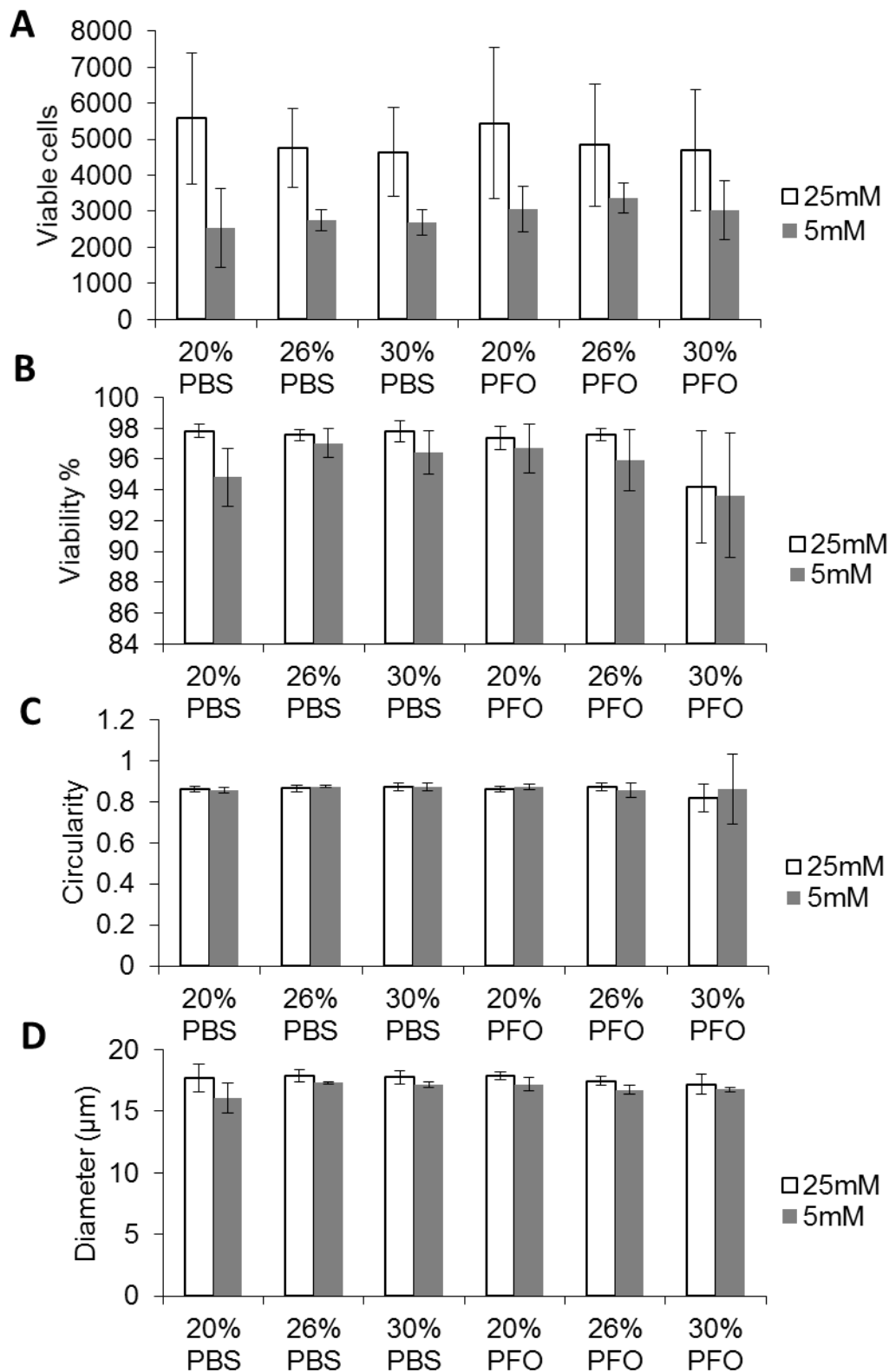


Figure 5-33 – 7-day viability analysis of Y201s exposed to perfluoro-octane. Various concentrations of PFO with diluted PBS controls and at 5 and 25mM glucose concentrations. Cultures all analysed using VI cell coulter counter. A – Viable cells measured, B – Viability of cells within the sample, C – Circularity of cells, D – Diameter of cells. Error shown as SD.

Across all three timescales there were no consistent significant effects on any of the measured parameters. No significant changes were seen after 24 hours, after 72 hours 5mM glucose did significantly reduce the diameter of the cells but this was not seen after 7 days. After 7 days the only significant change was in the number of viable cells which was lower in 5mM glucose. Viability was not changed by the glucose concentration, so it is more likely that the lower glucose concentration affected the proliferation of the cells.

Further experiments were carried out to assess the metabolic activity and the osteogenic potential using perfluoro-octane and high and low glucose media shown in Figure 5-34.

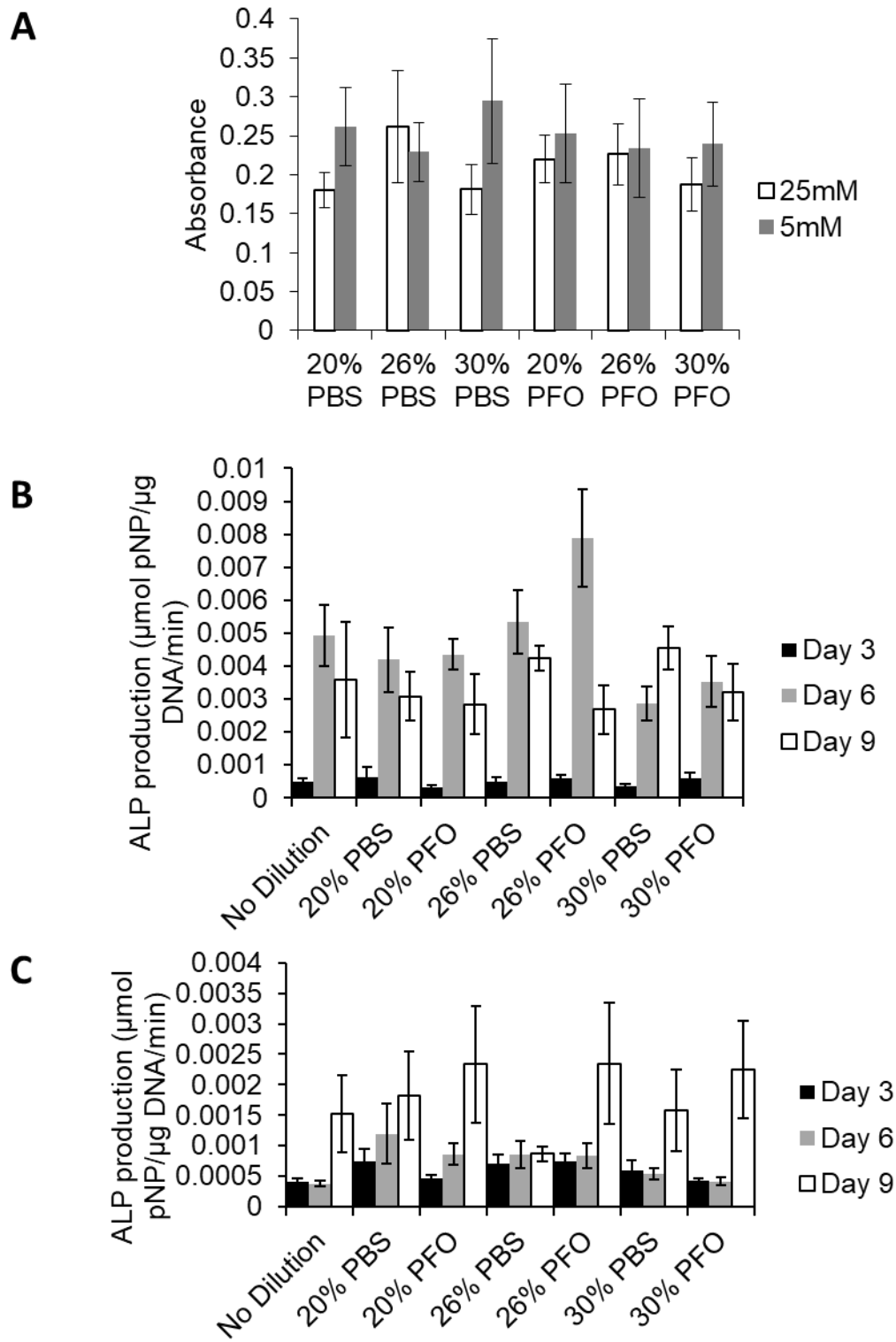


Figure 5-34 – Metabolic activity and osteogenic differentiation in Y201s with various concentrations of perfluoro-octane with PBS controls. A – MTT absorbance after 72 hours with perfluoro-octane, B – ALP production with low glucose media (5mM), C – ALP production with high glucose media (25mM). error shown as SEM.

The metabolic activity was assessed by MTT absorbance as shown in Figure 5-34 graph A, overall glucose did have a statistically significant effect with the lower (5mM) glucose level causing higher absorbances. The effect of both PFO and PBS was also significant with the lowest concentrations causing the highest absorbance therefore the dilution of media with PFO or PBS reduces the metabolic activity. Osteogenic potential was assessed using a pNPP assay where ALP activity was measured, the results in graphs B and C were combined to analyse the effect of glucose and oxygen concentrations. There was no significant effect of culture with PFO or PBS, ALP production is expected to increase during the course of the experiment, and this was found to be significant. The effect of glucose was again found to be significant with the 5mM glucose yielding higher ALP production.

5.11 Discussion

During spheroid culture the size of the spheroids decreases for all cell types used, the cell size also decreases during the culture. Dependent on cell type, the spheroids either condense and become denser over the culture or become less dense. Y202 and HDF spheroids become denser and Y201 and K139 spheroids become less dense (Figure 5-2). The coupling of cell types which condense and those which decrease in size without condensing is also the same pairing relationship between cells that differentiate and those that do not differentiate. The size change of the spheroids and the change in voidage within the spheroid effects the mass transfer, the surface area available for mass transfer into the spheroid reduces which impedes mass transfer, the distance reduces which aids mass transfer, condensing spheroids increases resistance to mass transfer and non-condensing spheroids aid mass transfer. It is not possible to tell simply from the size data whether the mass transfer is better or worse at the end of the culture compared to the beginning prior to calculating the mass transfer models.

The current model alters the diffusion coefficient for oxygen transport through the spheroid according to the overall voidage in the spheroid, the TEM shows that the voidage is not uniform throughout the spheroid. It would be possible to add the changing voidage into the model however this is unlikely to significantly change the model results.

Oxygen and glucose transfer into the spheroid adds another layer of transfer compared to monolayer culture. In primary MSC spheroid culture the oxygen concentration is not depleted and is only slightly lower than the concentration in

monolayer culture this is also seen in Y201 spheroids, whereas in Y202 spheroids the oxygen concentration in the centre does reach depletion. Y202 spheroids are bigger and start the culture less dense than primary MSC spheroids but end the culture more dense than primary MSC spheroids (Figure 5-5 and Figure 5-7). The larger size of the Y202 spheroids combined with being denser than the primary MSCs restricts the mass transfer of oxygen into the centre of the spheroid, the majority of the Y202 spheroid does not experience oxygen depletion. HDF spheroids also experience oxygen depletion in the centre and while HDF spheroids are the smallest they are also the densest. Again, the primary MSCs and Y201s behave in a similar way and the Y202s and HDFs are similar to each other as well.

Oxygen transfer within the spheroids has been found not to be a major problem as the balance between diffusion in and uptake allows for adequate transfer. However, oxygen transfer still needs to be an important consideration in other 3D cultures. Glucose transfer within the spheroid however is limited and does result in localised deprivation followed by widespread deprivation. This highlights the need to consider mass transfer of more than one component of a system (Figure 5-11). The glucose deprivation in the centre of the spheroid at day 2 coincides with the transcription factor EB (TFEB) expression increasing which coordinates the expression of autophagy genes (Pennock, et al., 2015). Indicating that the glucose concentration could be the trigger for autophagy and de-differentiation.

Under standard media change conditions of 2/3 media change on days 3 and 6 the concentration of glucose in the media for spheroid culture will be depleted on day 5. This does not happen for 2D cells at the same seeding density as the glucose consumption in spheroid culture is higher than in 2D and peaks on days 4 and 5 causing the depletion (Figure 5-9). Glucose depletion is present in primary MSC, Y201 and Y202 spheroids but not in HDF spheroids (Figure 5-13). HDF spheroids are smaller than the other spheroids, do not get cultured for as long (4 days) and have proportionally more media (half the cells. 2/3 the media) which all contribute to the higher concentrations in HDF spheroids. Most experiments with MSC, Y201 and Y202 spheroids are ended after five days, this results in only the centre of MSC and Y202 spheroids predicted to experience depletion with the depletion in Y201 spheroids slightly more widespread. The depletion in the centre of the spheroids can be avoided by altering the media change regime. A full media change on day 3 would prevent complete glucose depletion but still result in low glucose concentrations. Full

media changes are also problematic as more damage and spheroid loss is more likely to occur, the best way to avoid the depletion would be to change 2/3 of the media every day (Figure 5-14). Currently it is not known if a change in the media change schedule would alter the behaviour of cells in terms of glucose consumption rates or induction of autophagy and other changes seen in spheroid culture.

Spheroid culture causes the cells to be exposed to a range of glucose concentrations, the effects of glucose concentration on cell behaviour in monolayer culture showed the optimal glucose concentration varied dependant on behaviour measured. The most notable was that colony forming unit ability was best using a middle glucose concentration of 15mM (Figure 5-15). The effects of glucose concentration on differentiation capability were less clear, this is most likely due to the complexity of the differentiation process.

Suspension cultures were used to try and stimulate the size change observed in spheroid culture. Shrinkage was observed however not to the extent seen in spheroid culture, possibly due to the more limited time scale used in suspension culture (Figure 5-21). Cell survival in suspension culture was not long enough to complete a comparable time course to the spheroid culture experiments,

Within bone marrow, normal vasculature creates oxygen concentrations higher than *in vitro* which are relatively stable between vessels, distance between vessels to cause deprivation is smaller than spheroid sizes due to increased oxygen consumption rates (Figure 5-29). Glucose concentration is also stable in full vasculature and requires larger vasculature loss than oxygen between vessels to reach zero, but still reaches zero at around 200 μm from nearest vessel (Figure 5-30). Oxygen concentrations are predicted to be higher *in vivo* than *in vitro*, whereas glucose concentrations are predicted to be lower *in vivo* than *in vitro*.

Oxygen concentrations within blood are raised above the concentration of oxygen dissolved in media due the binding of oxygen to haemoglobin, this ensures oxygen is supplied to all tissues *in vivo*. Glucose concentration within blood is controlled so that the supply of glucose into tissues is more stable than the intake from food consumption. In culture it is more practical to deliver glucose in media changes and therefore the concentrations are more varied *in vitro* than *in vivo* and higher concentrations are used to avoid depletion between media changes.

Perfluro-octane (PFO) was used to increase the availability of dissolved oxygen along with physiological glucose concentrations. Culturing the cells in these conditions did not significantly alter the viability, number of viable cells, diameter or the circularity of the cells (Figure 5-31, Figure 5-32 and Figure 5-33). Osteogenic potential was found to be affected by glucose concentration but not by the presence of PFO (Figure 5-34). The amount of PFO added to the cultures was calculated to try and achieve physiological concentrations however the absolute concentration was not successfully measured to validate this. Therefore, it is possible that the oxygen concentration was not increased at a cellular level.

In summary oxygen availability is not restricted in the spheroids modelled, whereas glucose availability is depleted. Under average vasculature the concentration of oxygen and glucose in bone marrow is stable, with oxygen concentrations higher than in tissue culture and glucose concentrations which are lower than standard culture conditions.

The findings presented in this chapter show that:

- A mathematical model can be successfully developed to predict nutrient concentrations in spheroid culture.
- The concentration profile can differ over similar appearing systems.
- A mathematical model has been developed to predict the nutrient concentration in bone marrow.

Chapter 6 Discussion

6.1 Novelty and Validity of the Model

The ability to predict the oxygen and glucose concentrations within 3D cell culture structures allows the assessment of nutrient availability in circumstances where measurement is not possible or practical, either due to the technology available or for comparing hypothetical potential structures for use. The design of the model presented in the thesis allows simple adjustment for cell type, structure size and the glucose model could be used for other media components provided a suitable diffusion coefficient is used. The modelling of bone marrow shows how this model can be used for complex systems and allows easy comparison to the models used for spheroids and monolayer culture.

One of the limitations of all these models is that the model is applied in a 2D plane, a 3D model would provide a more accurate assessment especially in the bone marrow model but would bring a lot more complexity. While variable oxygen and glucose consumption rates have been worked into the spheroid model these are only changed daily and the oxygen and glucose consumption rates used are averages and do not represent changes over the cell cycle. The consumption rates used in monolayer and bone marrow models are assuming that over the cell population the average consumption rates are sufficient representation. Within spheroid culture it has been previously shown that the cells are not proliferating (Pennock, et al., 2015) so therefore proliferation has not been included in the model. Other spheroid culture systems have found proliferation so applying this model to those systems would carry that limitation however this could be accounted for by adjusting the cell number and consumption rates accordingly at the time points measured in a similar way to how the changing consumption rates over the time course has been incorporated. In the current model the cultures are all in static media, the models could directly be used on dynamic cultures with fluid flow or circulation systems, a model could be developed using the same derivation process, but would be more complex and bare more resemblance to the bone marrow model than the other culture models.

Validation of these models has largely been done comparatively with other findings and previous work. Application of the monolayer model to other systems found in literature shows good correlation to measured oxygen concentrations including systems with different oxygen consumptions and cell density, this model would

however be limited in situations with high proliferative rates and highly variable oxygen consumption rates. In situations with high proliferation and highly variable oxygen consumption rates these could be adapted into the model.

The results of the oxygen profile in spheroid culture did correlate to the HIF- α staining in (Pennock, et al., 2015) which also found no evidence of hypoxia in the spheroids. The model also correctly predicts oxygen depletion in the hepatocyte spheroids in (Anada, et al., 2012) even though these spheroids are the same size as the MSC spheroids the oxygen consumption rate is higher in the hepatocyte spheroids which has a greater effect than the smaller cell density. The oxygen concentration is correctly predicted in embryoid bodies (Winkle, et al., 2012) which are more dense than the MSC spheroids and also in fibroblast spheroids (Barisam, et al., 2018) where the ambient oxygen concentration is lower than standard. The spheroid model is very sensitive to error or changes in the diameter of the spheroid as this is used to calculate various parameters, in particular the voidage of the spheroid as this uses the cube of the diameter. As with the monolayer culture this model does not account for proliferation and has not been validated with any spheroid systems which include proliferating cells for a sustained period of time even though it does work at assessing the snapshot.

Validation of the glucose spheroid model is less explored as this area has less prevalence in literature. Glucose concentration was measured in (Barisam, et al., 2017) which found no depletion in spheroids smaller than the MSC spheroids and then found depletion in these smaller spheroids (Barisam, et al., 2018) when media changes were not performed, the results in (Barisam, et al., 2018) do correlate to the results of the model but direct comparisons were not possible due to the information available. The glucose consumption rates used in the model are calculated from lactate and pyruvate production, it would be more accurate to measure the consumption rate directly however this was not achieved successfully during this project. Direct measurement of glucose consumption was attempted by fluorescent enzyme digestion, but this was unsuccessful.

The recreation of the conditions from 3D in monolayer and suspension culture were not conclusive in validating the effects of the 3D glucose profile, this was then also investigated in suspension cultures to assess if the lack of adherence made a difference, these investigations are incomplete.

Predicted oxygen concentrations in the bone marrow show that under average conditions no relative depletion would occur, hypoxia has been found in several publications (Nombela-Arrieta & Silberstien, 2014, Parmar, et al., 2007) by HIF-1 α and pimonidazole staining, it is unclear at what absolute concentrations this occurs. Within cell culture HIF-1 α is usually undetectable in normal conditions, the presence of HIF-1 α has been found to increase as the atmospheric oxygen concentration was lowered to 0.5% (Maxwell, 2003). Correlating HIF- α and pimonidazole staining with the localisation of HSCs showed distribution evenly throughout the bone marrow and was not influenced by proximity to vessels (Nombela-Arrieta, et al., 2013) which indicates that they may not be the best choice for assessing oxygen concentrations in this range; the oxygen concentration will be highest directly next to blood vessels and lower further away. Localised areas of hypoxia which are not predicted by the model could be caused by the localisation of cell populations. The model uses an averaged oxygen consumption rate calculated from the oxygen consumption rates of the cell types and the abundance of these cell types. Areas with more cells with relatively high oxygen consumption would have a higher consumption rate in this area which would then result in a lower concentration of oxygen present. The oxygen consumption rates are also measured *in vitro*, cells may have a different consumption rate *in vivo* which is a limitation of this analysis. Utilising a bone marrow section stained for vasculature and the highest oxygen consuming cells and modelling that would be one way to help validate the model and provide more accuracy.

Very little work has been done on measuring glucose concentration anywhere *in vivo* except blood, which impedes analysis with literature. There has been a study which examined glucose concentration in the brain using two-photon fluorescence lifetime imaging microscopy (Diaz-Garcia, et al., 2019), two-photon phosphorescence microscopy has also been used to measure oxygen concentration in bone marrow (Spencer, et al., 2014), therefore there is the potential to use this approach to measure glucose concentration in bone marrow.

6.2 Implications of Results

In the spheroid MSC culture the oxygen availability is not significantly different to the concentrations experienced in monolayer culture, oxygen concentrations are however affected in the centre Y202 and HDF spheroids. This shows how close the balance is and how important it is to assess the oxygen availability in 3D culture systems, as it could easily be assumed that the oxygen availability in the Y202 spheroids would be the same as the MSCs and Y201s. It also could have been reasonably assumed that as the HDF spheroids contain less cells that the mass transfer would be less restricted than the MSC spheroid however mass transfer is more restricted. With the increasing use of 3D cultures for tissue regeneration the evaluation of oxygen availability is important. The oxygen concentration is maintained in MSC spheroids however this is only possible because the oxygen consumption rate drops in spheroid culture, what is not known is if the oxygen consumption rate drops as a result of the unsustainability of the oxygen supply or whether the drop in consumption rate has a different cause. The oxygen consumption rates used in the Y201, Y202 and HDF models are the rates measured for the primary MSCs, the accuracy of these models could be improved by measuring the change in consumption rates for these cell types. What using the same consumption rate does show however is how much of an effect density and size does have even at this relatively small scale.

In vitro conditions do not match *in vivo* conditions, the effects of using *in vivo* conditions *in vitro* could give a better insight into the behaviour of MSCs and other cell types. There is the potential that cells could behave completely differently at physiological conditions and it is not possible to be sure the behaviour currently observed *in vitro* is relevant to equivalent behaviour *in vivo*. If the cells are able to respire at the rate required in conventional cell culture conditions then the effect could be minimal especially if this is not the limiting factor in cellular processes, however if the respiration rate is a limiting factor then cellular processes could change significantly.

Culturing at *in vivo* oxygen concentrations requires increasing the oxygen availability not decreasing it, more work is required on this. Increasing the oxygen concentration using perfluoro-octane in this project did not show significant changes in cell behaviour. The oxygen concentration achieved was not successfully measured and

the distribution of perfluoro-octane within the culture media was not uniform. To achieve a uniform distribution of perfluoro-octane gentle stirring could be used, alternative oxygen carriers could potentially mix with media more successfully. Increasing the partial pressure of oxygen in the incubator would raise the concentration of oxygen dissolved in the media however this creates an explosive atmosphere and therefore is not a practical solution to do safely. Replicating a stable glucose concentration could be achieved using flowing media to replenish media automatically.

Spheroid culture of MSCs results in glucose deprivation which coincides with the expression of TFEB (transcription factor EB) which manages the expression of autophagy genes and lysosomal biogenesis (Pennock, et al., 2015)) which indicates the possibility that glucose deprivation triggers the autophagy response in the spheroids, this was tested by using the glucose concentration at day 2 in the spheroids in monolayer and suspension culture. Some size change was observed but the effects of this glucose concentration needs investigating further, assessing the comparable markers by QPCR and TEM of cells cultured this way would be a good starting point.

The change in cell size during spheroid culture originally was thought to be an effect of the autophagic dedifferentiation, in monolayer culture the size change has not been replicated when autophagy has been induced (other work within the lab). Size change is observed in suspension cultures regardless of the glucose concentration which could mean that the size change is driven by the lack of adherence in spheroid and suspension culture. The process of autophagy does involve the removal of cellular matter which likely does contribute to the cell shrinkage in spheroid culture however it appears that autophagy and lack of plastic adherence combine to result in the magnitude of the size changes seen. Induction of autophagy by addition of rapamycin in Jurkat cells found a cell volume reduction of 50%, these cells were cultured in suspension (control and treated cells) (Fumarola, et al., 2005), the combination of autophagy and lack of adherence appears to allow the reduction in cell size as also seen in the MSC spheroids.

The oxygen availability in bone marrow is lower than many other areas of the body, atmospheric oxygen is 21% which drops to 14.5% by the time it reaches the alveoli, the brain has an average of 4.4%, 5.4% in the liver (Carreau, et al., 2011) but bone marrow is 2.6-3% (Spencer, et al., 2014) however it is higher than the availability in

standard tissue culture (media 0.54%). Average vasculature distribution also provides small gradients which is expected as nutrient availability is needed to support the cells within the bone marrow. The results of this modelling also show the extent of vasculature loss required to deplete the oxygen and glucose supply which could be useful in the assessment of diseases, for example it could be used in research for diseases such as avascular necrosis.

The glucose availability in bone marrow is relatively stable in normal vasculature conditions however as with oxygen the glucose availability is subject to the distribution of blood vessels at a similar scale. Glucose diffusion is slower than the diffusion of oxygen as glucose is a much larger molecule but the similarity in distance between vessels to cause deprivation shows the balance within the body and also suggests other nutrients are likely to be depleted at these distances too. The results of the bone marrow model show the range of distances between vessels that allow for sufficient transfer, this information could be used to set the parameters in 3D scaffold design to provide channels for mass transfer to occur. The change in consumption rates in spheroid culture compared to monolayer culture also suggest that the consumption rates within bone marrow may also be different which would then affect the predictions accuracy however the consumption rates for glucose and oxygen within bone marrow are currently unknown.

The availability of oxygen, glucose and other nutrients are paramount for cell survival especially in 3D culture systems. Understanding how the mass transfer of these substances in different systems (monolayer, 3D and *in vivo*) effects the concentration available at a cellular level can lead to better understanding of cell behaviour and survival in these systems.

6.3 Recommendations for Future Work

Further work for this project would be to continue the investigations into the use of applying the spheroid glucose profiles in 2D and suspension culture to induce de-differentiation on a larger scale. This would include testing whether the same markers elevated in spheroid culture are elevated in suspension culture.

Spheroid models could be expanded to incorporate proliferation for use in cell types where proliferation continues in 3D culture. The accuracy of the glucose model could also be improved by gaining direct glucose consumption rates.

In vivo model for bone marrow could be improved by including the localisation of cell types so that the oxygen consumption rate can be varied to reflect the differences in oxygen consumption rate for the different cell types within bone marrow. This model could also be used for other tissues to improve the understanding of how the oxygen and glucose concentrations vary in different tissues. This knowledge could also then be applied to *in vitro* culture to observe cell behaviour in more physiological conditions.

References

- Alvarez, C. et al., 2012. Defining stem cell types: understanding the therapeutic value of ESCs, ASCs and IPS cells. *Journal of Molecular Endocrinology*, Volume 49, pp. 89-111.
- Anada, T., Fukuda, J., Sai, Y. & Suzuki, O., 2012. An oxygen permeable spheroid culture system for the prevention of central hypoxia and necrosis of spheroids. *Biomaterials*, Volume 33, pp. 8430-8441.
- Ardakani, A., Cheema, U., Brown, R. & Shipley, R., 2014. Quantifying the correlation between spatially defined oxygen gradients and cell fate in an engineered three dimensional culture model. *Journal of the Royal Society Interface*, Volume 11, p. 20140501.
- Arthritis Research UK, 2014. *General News: Arthritis Research UK*. [Online] Available at: <http://www.arthritisresearchuk.org/news/general-news/2014/july/new-stem-cell-based-knee-operations-could-help-prevent-arthritis.aspx> [Accessed June 2016].
- Ayhan, E., Kesmezacar, H. & Akgun, I., 2014. Intraarticular injections (corticosteroid, hyaluronic acid, platelet rich plasma) for knee osteoarthritis. *World Journal of Orthopaedics*, Volume 5, pp. 351-361.
- Bai, Q. et al., 2013. Embryonic stem cells or induced pluripotent stem cells? A DNA integrity perspective. *Current Gene Therapy*, 4(12), pp. 878-886.
- Barisam, et al., 2017. Numerical simulation of the behaviour of torodial and spheroidal multicellular aggregates in microfluidic devices with microwell and U shaped barrier. *Micromachines*, Volume 8, pp. 358-374.
- Barisam, et al., 2018. Prediction of necrotic core and hypoxic zone of multicellular spheroids in a microbio reactor with U shaped barrier. *Micromachines*, 9(3), pp. 94-113.
- Benson Ham III, P. & Raju, R., 2017. Mitochondrial function in hypoxic ischemic injury and influence of aging. *Progress in Neurobiology*, Volume 157, pp. 92-116.
- Berg, J., Tymoczko, J. & Stryler, L., 2002. *Biochemistry*. s.l.:WH Freeman.
- Bianco, P. et al., 2013. The meaning, the sense and the significance: translating the science of mesenchymal stem cells into medicine. *Nature Medicine*, Volume 19, pp. 35-42.
- Biazzo, A. et al., 2020. Autologous adipose stem cell therapy for knee osteoarthritis: Where are we now?. *The Physician and Sportsmedicine*, Volume 48, pp. 392-399.
- Browne, S. M., Daud, H., Murphy, W. G. & Al-Rubeai, M., 2014. Measuring dissolved oxygen to track erythroid differentiation of hematopoietic progenitor cells in culture. *Journal of biotechnology*, Volume 187, pp. 135-138.
- Carreau, A., Hafmy-Rahbi, B., Matejuk, A. & Grillon, C. K. C., 2011. Why is the partial oxygen pressure of human tissues considered a crucial parameter? Small molecules and hypoxia. *Journal of Cellular Molecular Medicine*, Volume 15, pp. 1239-1253.

- Carstairs, A. & Genever, P., 2014. Stem cell treatment for musculoskeletal disease. *Opinion in Pharmacology*, Volume 16, pp. 1-6.
- Chen, C., Wang, Y. & Yang, G. Y., 2013. Stem cell mediated gene delivering for the treatment of cerebral ischemia: progress and prospectives. *Current Drug Targets*, Volume 14, pp. 81-89.
- Chen, W. & Blurton-Jones, M., 2012. Concise Review: Can stem cells be used to treat or model alzheimers's disease. *Stem Cells*, Volume 30, pp. 2612-2618.
- Choudhry, H. & Harris, A., 2018. Advances in hypoxia inducible factor biology. *Cell Metabolism*, 27(2), pp. 281-298.
- Costa Gomes, M., Deschamps, J. & Menz, D., 2014. Solubility of dissolved oxygen in seven fluorinated liquids. *Journal of Florine Chemistry*, Volume 125, pp. 1325-1329.
- Coulson, J. M., Richardson, J. F., Backhurst, J. R. & Harker, J. H., 2008. *Coulson and Riochardson's Chemical Engineering Volume 1*. s.l.:Elsevier.
- Crane, A. T., Rossignol, J. & Dunbar, G. L., 2014. Use of genetically altered stem cells for the treatment of huntingtons disease. *Brain Science*, Volume 4, pp. 202-219.
- Curico, E. et al., 2014. Kinetics of oxygen uptake by cells potentially used in a tissue engineered trachea. *Biomaterials*, Volume 35, pp. 6829-6837.
- Demirel, Y., 2002. *Nonequilibrium Thermodynamics*. s.l.:Elsevier.
- Diaz-Garcia, C. M. et al., 2019. Quantitative in vivo imaging of neuronal glucose concentrations with a genetically encoded lifetime sensor. *Journal of neuroscience reasearch*, 97(8), pp. 946-960.
- Diekman, B. & Guilak, F., 2013. Stem cell based therapies for osteoarthritis: Challenges and opportunities. *Current Opinion Rheumatology*, Volume 25, pp. 119-126.
- Edwards, J. J. et al., 2015. Quality indicators for the primary care of osteoarthritis: a systematic review. *Annals of the Rheumatic Diseases*, Volume 74, pp. 490-498.
- Engineering Toolbox, 2005. *Oxygen - solubility in fresh and sea water*. [Online] Available at: https://www.engineeringtoolbox.com/oxygen-solubility-water-d_841.html [Accessed February 2021].
- Ferng, A. S. et al., 2016. Adipose derived human stem/stromal cells: comparative organ specific mitochondrial bioenergy profiles. *Springer plus*, Volume 5, pp. 2057-2066.
- Frith, J. & Genever, P., 2008. Transcriptional control of mesenchymal stem cell differentiation. *Transfusion Medicine and Hemotherapy*, Volume 35, pp. 216-227.
- Fumarola, C. et al., 2005. Cell size reduction induced by inhibition of the mTOR/S6K-signalling pathway protects Jurkat cells from apoptosis. *Cell death and differentiation*, Volume 12, pp. 1344-1357.
- Glick, D., Barth, S. & Macleod, K., 2010. Autophagy: Cellular and molecular mechanisms. *Journal of Pathology*, Volume 221, pp. 3-12.

- Glicklis, R., Merchuk, J. & Cohen, S., 2004. Modelling mass transfer in hepatocyte spheroids via cell viability, spheroid size and hepatocellular functions. *Wiley InterScience*, Volume 86, pp. 672-681.
- Gupta, S. et al., 2005. The economic burden of disabling hip and knee arthritis (OA) from the perspective of individuals living with this condition. *Rheumatology*, Volume 44, pp. 1531-1537.
- Heimburg, D. et al., 2005. Oxygen consumption in undifferentiated versus differentiated adipogenic mesenchymal precursor cells. *Respiratory Physiology and Neurobiology*, Volume 146, pp. 107-116.
- Hipp, J. & Atala, A., 2008. Sources of stem cells for regenerative medicine. *Stem Cell Reviews*, Volume 4, pp. 3-18.
- Ito, K. I. K., 2016. Metabolism and control of cell fate decisions and stem cell renewal. *Annual Review of Cell and Developmental Biology*, Volume 32, pp. 399-409.
- James, J. L., Srinivasan, S., Alexander, M. & Chamley, L. W., 2014. Can we fix it? Evaluating the potential of placental stem cells for the treatment of pregnancy disorders. *Placenta*, Volume 35, pp. 77-84.
- James, S. et al., 2015. Multiparameter Analysis of Human Bone Marrow Stromal Cells Identifies Distinct Immunomodulatory and Differentiation- Competent Subtypes. *Stem Cell Reports*, Volume 4, pp. 1004-1015.
- Jang, Y. et al., 2015. Characterisation of adipose tissue derived stromal vascular fraction for clinical application to cartilage regeneration. *In vitro cellular and developmental biology - Animal*, Volume 51, pp. 142-150.
- Kagawa, Y., Matsuura, K., Shimizu, T. & Tsuneda, S., 2015. Direct measurement of local dissolved oxygen concentration spatial profiles in a cell culture environment. *Biotechnology and bioengineering*, Volume 112, pp. 1263-1274.
- Kunisaki, Y. et al., 2013. Articular niches maintain haematopoietic stem cell quiescence. *Nature*, Volume 502, pp. 637-658.
- Leardini, G. et al., 2004. Direct and indirect costs of osteoarthritis of the knee. *Clinical and Experimental Rheumatology*, Volume 22, pp. 699-706.
- Liu, K. et al., 2014. Mesenchymal stem cells rescue injured endothelial cells in an in vitro ischemia reperfusion model via tunneling nanotube like structure mediated mitochondrial transfer. *Microvascular Research*, Volume 92, pp. 10-18.
- Lopa, S., Coloumbini, A., Moretti, M. & Girolamo, L. d., 2019. Injective mesenchymal stem cell based treatments for knee osteoarthritis from mechanisms of action to clinical evidences. *Knee Surgery, Sports Traumatology, Arthroscopy*, Volume 27, pp. 2003-2020.
- Losina, E. et al., 2015. Lifetime medical costs of knee osteoarthritis manemant in the united states: impact of extending indications for total knee arthroplasty. *Arthritis Care Research*, Volume 62, pp. 203-215.

- Lu, Y. et al., 2015. Beneficial effects of astragaloside IV against angiotensin II induced mitochondrial dysfunction in rat vascular smooth muscle cells. *international journal of molecular medicine*, Volume 36, pp. 1223-1232.
- Main, H., Munsie, M. & O'Connor, M., 2014. Managing the potential and pitfalls during clinical translation of emerging stem cell therapies. *Clinical and Transational Medicine*, Volume 3, pp. 10-20.
- Maxwell, P., 2003. HIF-1: An oxygen response system with special relevance to the kidney. *Journal of the american society of nephrology*, Volume 14, pp. 2712-2722.
- Mizushima, K., 2007. Autophagy: Process and function. *Genes and Development*, Volume 21, pp. 2861-2873.
- Molder, E., Mashirin, A. & Tenno, T., 2005. Measurement of the oxygen mass transfer through the air water interface. *Environmental Science and Pollution Research*, Volume 12, pp. 66-70.
- Moore J, S. C. P. P., 2010. *Principles of Chemistry: The Molecular Science*. s.l.:Cengage Learning.
- Murphy, M. J. et al., 2002. Reduced chondrogenic and adipogenic activity of mesenchymal stem cells from patients with advanced osteoarthritis. *Arthritis and Rheumatism*, Volume 46, pp. 701-713.
- Muscari, C. et al., 2013. Priming adult stem cells by hypoxic pretreatments for applications in regenerative medicine. *Journal of Biomedical Science*, Volume 20, pp. 63-76.
- National Joint Registry, 2013. [Online]
Available at:
http://www.njrcentre.org.uk/njrcentre/Portals/0/Documents/England/Reports/10th_annual_report/NJR%2010th%20Annual%20Report%202013%20B.pdf
[Accessed February 2021].
- National Joint Registry, 2015. [Online]
Available at:
<http://www.njrcentre.org.uk/njrcentre/Portals/0/Documents/England/Reports/12th%20annual%20report/NJR%20Online%20Annual%20Report%202015.pdf>
[Accessed February 2021].
- National Joint Registry, 2018. *15th Annual Report 2018*. [Online]
Available at: <https://www.hqip.org.uk/resource/national-joint-registry-15th-annual-report-2018/#.YBmlrOj7T0M>
[Accessed February 2021].
- NHS, 2019. *Knee Replacement*. [Online]
Available at: <http://www.nhs.uk/Conditions/Knee-replacement/Pages/Kneereplacementexplained.aspx>
[Accessed February 2021].
- Nombela-Arrieta, C. et al., 2013. Quantitative imaging of haematopoietic stem and progenitor cell localisation and hypoxic status in the bone marrow microenvironment. *Nature Cell Biology*, 15(5), pp. 533-554.

- Nombela-Arrieta, C. & Silberstien, L. E., 2014. The science behind the hypoxic niche of hematopoietic stem and progenitors. *Hematology*, pp. 542-548.
- Ntwambe, S., Williams, C. & Sheldon, M., 2010. Water-immiscible dissolved oxygen carriers in combination with pluronic F68 in bioreactors. *African Journal of Biotechnology*, 9(8), pp. 1106-1114.
- Parker, A. V., Williams, R. N. & Paterson, C. A., 1985. The effect of sodium citrate on the stimulation of polymorphonuclear leukocytes. *Investigative ophthalmology and visual science*, Volume 26, pp. 1257-1262.
- Parmar, K. et al., 2007. Distribution of hematopoietic stem cells in the bone marrow according to regional hypoxia. *PNAS*, 104(13), pp. 5431-5436.
- Pennock, R. et al., 2015. Human cell dedifferentiation in mesenchymal condensates through controlled autophagy. *Scientific Reports*, Volume 5.
- Pentz, M. & Shott, M., 1989. *Handling experimental data*. s.l.:Open University Press.
- Petek, D., Hannouch, D. & Suva, D., 2019. Osteonecrosis of the femoral head: pathophysiology and current concepts of treatment. *EFORT open review*, Volume 4, pp. 85-97.
- Piccoli, C. et al., 2005. Characterization of mitochondrial and extra mitochondrial oxygen consuming reactions in human hematopoietic stem cells. *The journal of biological chemistry*, 280(28), pp. 26467-26476.
- Place, T., Domann, F. & Case, A., 2017. Limitations of oxygen delivery to cells in culture: An underappreciated problem in basic and translational research. *Free Radical Biology and Medicine*, Volume 113, pp. 311-322.
- Posel, C. et al., 2012. Density gradient centrifugation compromises bone marrow mononuclear yield. *Plos one*, 7(12), p. e50293.
- Reed, D., Foldes, G., Harding, S. & Mitchell, J., 2013. Stem cell derived endothelial cells for cardiovascular disease: a therapeutic perspective. *British Journal of Clinical Pharmacology*, 75(4), pp. 897-906.
- Reiss, M. & Roos, D., 1978. Differences in oxygen metabolism of phagocytosing monocytes and neutrophils. *The journal of clinical investigation*, Volume 61, pp. 480-488.
- Richardson, J. et al., 2017. Efficacy and safety of autologous cell therapies for knee cartilage defects (autologous stem cells, chondrocytes or the two): randomized controlled trial design. *Regenerative Medicine*, 12(5), pp. 493-501.
- Roberts, S., Genever, P., McCaskie, A. & De Bari, C., 2011. Prospects of stem cell therapy in osteoarthritis. *Regenerative Medicine*, 6(3), pp. 351-366.
- Romeo, F., Costanzo, F. & Agostini, M., 2012. Embryonic stem cells and inducible pluripotent stem cells: two faces of the same coin?. *Aging*, 4(12), pp. 877-886.
- Salem, O. et al., 2014. Naproxen affects osteogenesis of human mesenchymal stem cells via regulation of indian hedgehog signaling molecules. *Arthritis Research and Therapy*, 16(4), p. R152.

Sanders R, 2014. Compilation of Henry's law Constants. *Atmospheric Chemistry and Physics*, Volume 14, pp. 29615-30521.

Sato, Y. et al., 2011. Cellular hypoxia of pancreatic b cells due to high levels of oxygen consumption for insulin secretion in vitro. *The journal of biological chemistry*, 286(14), pp. 12524-12533.

Singh, R. et al., 2009. Autophagy regulates lipid metabolism. *Nature*, Volume 458, pp. 1131-1135.

Spencer, J. et al., 2014. Direct measurement of local oxygen concentration in bone marrow of live animals. *Nature*, Volume 508, pp. 269-285.

Subczynski, W. K., Hopwood, L. E. & Hyde, J. S., 1992. Is the mammalian cell plasma membrane a barrier to oxygen transport. *Journal of general physiology*, Volume 100, pp. 69-87.

Swijnenburg, R.-J. et al., 2008. In vivo imaging of embryonic stem cells reveals patterns of survival and immune rejection following transplantation. *Stem Cells and Development*, Volume 17, pp. 1023-1030.

Takahashi, K. et al., 2007. Induction of pluripotent stem cells for adult human fibroblasts by defined factors. *Cell*, 131(5), pp. 861-872.

Tankasala, D. & Linnes, J. C., 2019. Noninvasive glucose detection in exhaled breath condensates. *Translational Research*, Volume 213, pp. 1-22.

The Robert Jones and Agnes Hunt Orthopaedic Hospital NHS Foundation Trust, 2019. *ASCOT Trial*. [Online]
Available at: <https://www.rjah.nhs.uk/Research/ASCOT-Trial.aspx>
[Accessed 6th November 2019].

Verma, S. et al., 2002. Adipocytic proportion of bone marrow is inversely related to bone formation in osteoporosis. *Journal of clinical pathology*, Volume 55, pp. 693-698.

Wilson, A., Webster, A. & Genever, P., 2019. Nomenclature and heterogeneity: consequences for the use of mesenchymal stem cells in regenerative medicine. *Regenerative Medicine*, 14(6), pp. 595-611.

Winkle, A., Gates, I. & Kallos, M., 2012. Mass transfer limitations in embryonic bodies during human embryonic stem cell differentiation. *Cells Tissues Organs*, Volume 196, pp. 34-47.

Woolf, A. D. & Pfleger, B., 2003. Burden of major musculoskeletal conditions. *Bulletin of the World Health Organisation*, 81(9), pp. 646-657.

Xian, L. C. & Jevnikar, A. M., 2015. *Transplant Immunology*. s.l.:John Wiley and Sons.